Journal of Science & Technology in the Tropics

Volume 1 Number 1 June 2005

COSTAM

Journal of Science & Technology in the Tropics

JOSTT

DEDICATED TO THE ADVANCEMENT OF SCIENCE AND TECHNOLOGY RELATED TO THE TROPICS

Volume 1 Number 1
June 2005
ISSN 1823-5034

Journal of
Science & Technology
in the Tropics Volume 1 Number 1 June 2005

CONTENTS

the shape of pleats differs from those in *D. chattoni*. The host frog is always seen near forest streams.

Diamondtrypanum katak new species
(Figs. 11, 36-64)

Description: Longest diameter of body 26.4~94.7μm (52.87±11.55μm); shortest diameter of body 19.8~48.8μm (37.71±6.19μm); longest diameter of nucleus 3.6~8.3μm (5.94±0.88μm); shortest diameter of nucleus 2.6~8.3μm (4.94±1.0μm); flagellum 3.0~10.2μm (5.93±1.51μm); shortest distance of kinetoplast to nuclear membrane -2.0~1.0μm (-0.10±0.51μm). Measurements from other hosts are shown in Figure 102.

Type host – *Rana hosii* (Amphibia: Ranidae).

Type locality – Gombak Field Study Centre of University of Malaya, Selangor.

Other locality – Selangor: Gombak Field Study Centre

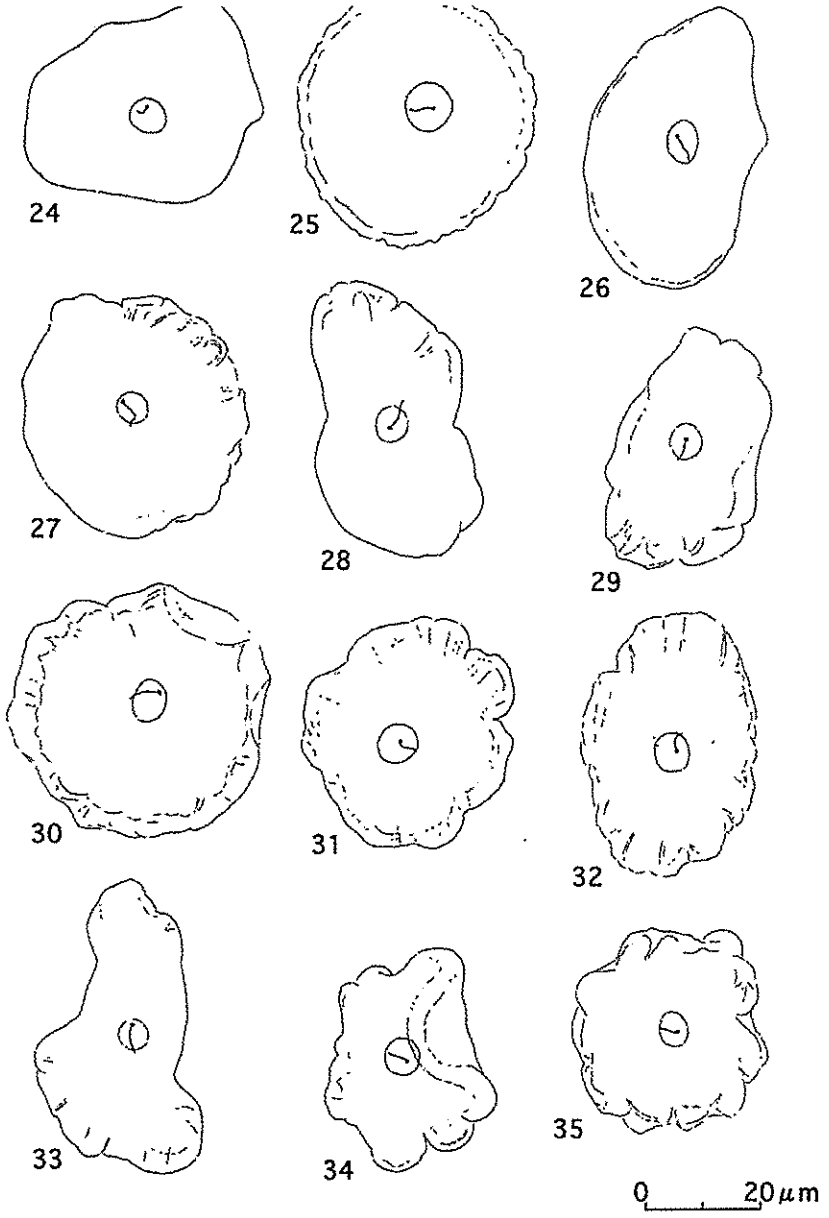

Figures 24-35. 24-25: *Diamondtrypanum kodok* new spcies, in *Bufo asper*.
26-35: *Diamondtrypanum bungateratai* new species in *Rana blythi*.

of University of Malaya; Ampang Forest Park; Templer Park; Ulu Langat. Pahang: Bukit Rengit; Cameron Highland. Johor: Kota Tinggi. Sarawak: Sematang.

Type smears – Holotype slide: No. 89-08-30-07 from Gombak Field Study Centre of University of Malaya, Selangor. Paratype slides: No. 89-09-01-02 from the type locality; No. 90-05-26-08 from Bukit Rengit, Pahang.

Other hosts and their localities – (1) *Rana erythraea* (Figs. 5, 36-40): Kuala Lumpur – University of Malaya (No. 89-09-08-02); Desa Pahlawan (No. 89-09-06-10). Selangor – Gombak; Sementa; Templer Park (No. 89-09-27-02). Penang – Rice Field; Botanical Garden. Sarawak – Sematang; Kuching. (2) *Rana chalconota* (Figs. 4, 41-48): Selangor – Ampang Forest Park; Gombak; Templer Park; Bukit Gasing (No. 91-10-10-22). Pahang – Bukit Rengit. Penang – Botanical Garden. Sarawak – Sematang (No. 90-04-20-38); Matang. (3) *Rana nicobariensis* (Figs. 58-64): Selangor – Templer Park (No. 89-10-20-05).

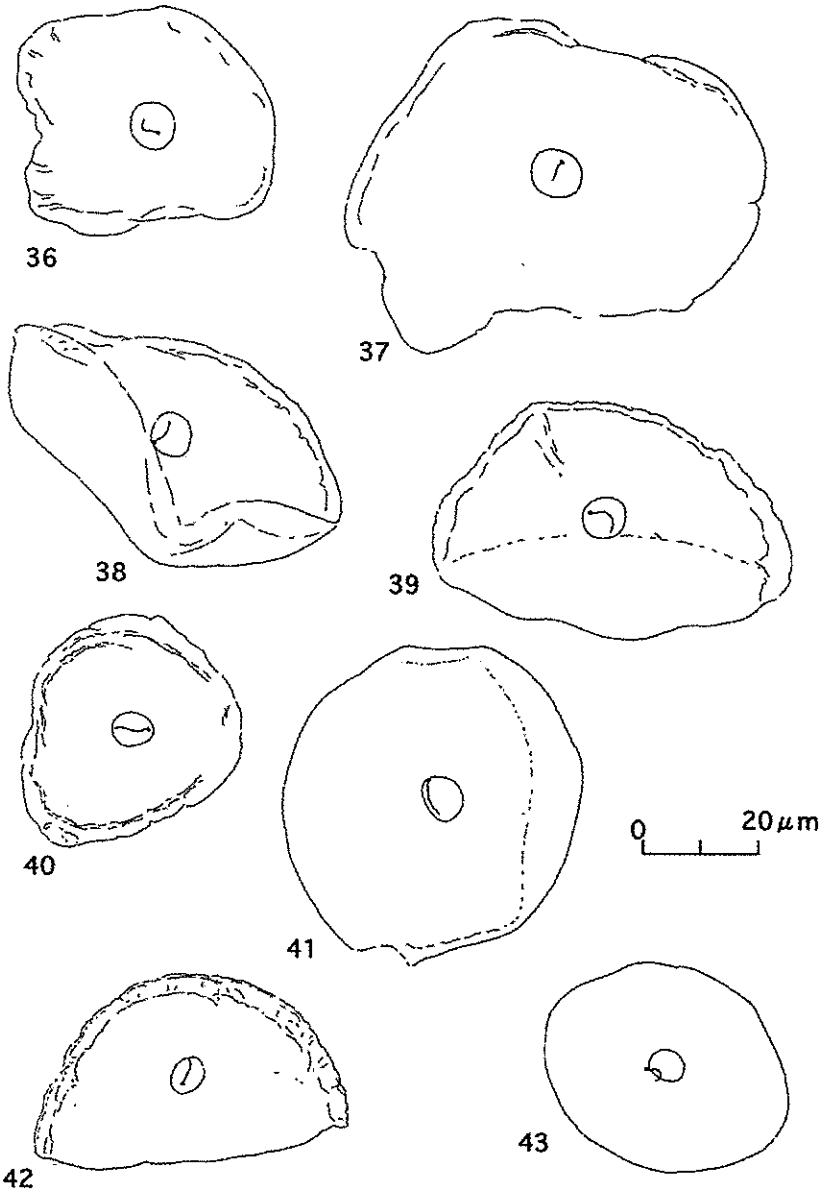

Figures 36-43. 36-40: *Diamondtrypanum katak* new species, in *Rana erythraea*.
41-43: *Diamondtrypanum katak* new species, in *Rana chalconota*.

Etymology – The word '*katak*' means frog in Malay.
Remarks – *D. katak* is apparently different from previously described species in its large body size and the position of the kinetoplast that is always situated very close to the nuclear membrane. The narrowly brimmed body is usually very clear and often forms a characteristic shallow hollow in the middle like a soup plate (Figs. 47-48, 52, 62-63).

Among the four hosts, *D. katak* of *R. nicobariensis* has the smallest body compared with those of the other three hosts. Each *D. katak* detected in the three other frogs is slightly different from each other in body size, nuclear size, and the distance of the kinetoplast to the nuclear membrane. *D. katak* of *R. erythraea* is the largest; that of *R. chalconota* is the smallest. The nuclear size of *D. katak* of *R. chalconota* is the smallest, while that of *R. erythraea* is the largest. The position of the kinetoplast is very different in each species. In about 80% of *D. katak* in *R. hosii*, the kinetoplast is situated very close to the nuclear membrane; in *R. erythraea*, the incidence came down to 55%, and in *R. chalconota* to 35%. However, it is impossible to separate them as

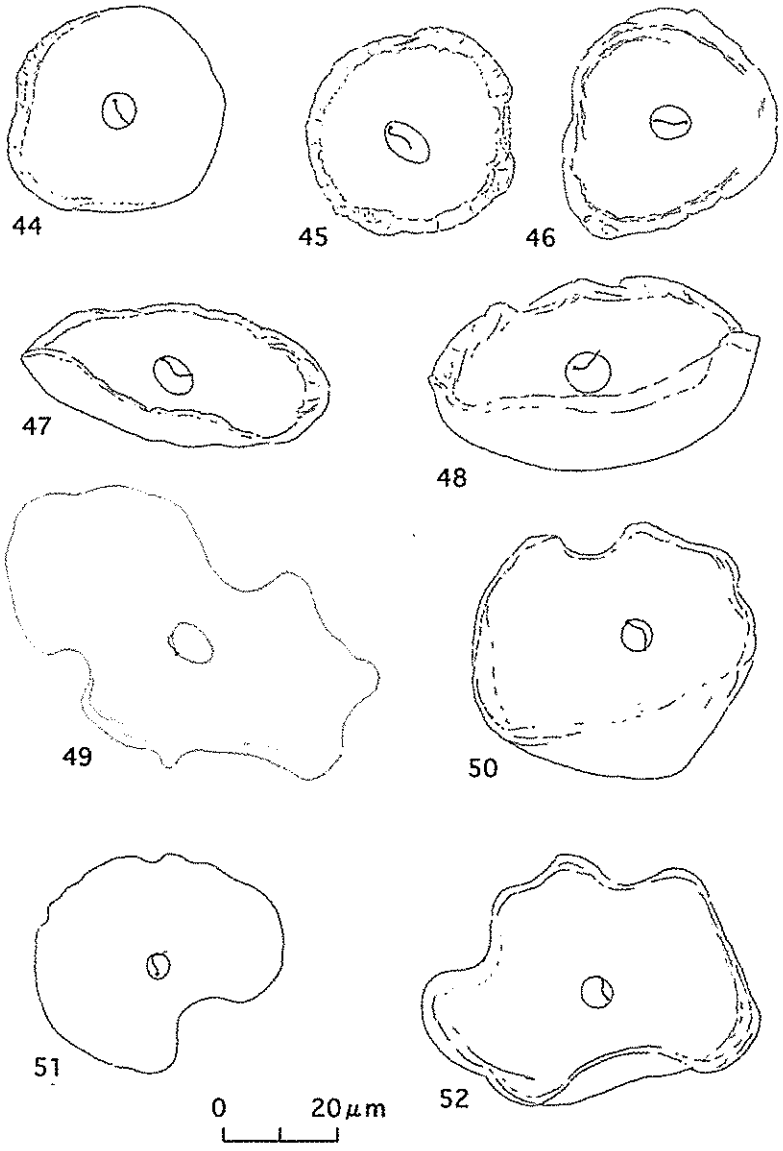

Figures 44-52. 44-48: *Diamondtrypanum katak* new species, in *Rana chalconota*.
49-52: *Diamondtrypanum katak* new species, in *Rana hosii*.

distinct species at present because the morphological differences in these trypanosomes from the four frog species are very slight. The host frog species of *D. katak* prefer very different ecological habitats. *Rana nicobariensis* is a rather uncommon frog among the four hosts in Malaysia. *Rana hosii* is a forest dwelling species; *R. chalconota* is usually seen with *R. hosii* near forest streams, while *R. erythraea* is strictly an open land species. Presumably *D. katak* is still undergoing cospeciation.

Diamondtrypanum tsunezomiyatai (Miyata, 1978), new combination

Trypanosoma tsunezomiyatai Miyata, 1978

Redescription – (1) Malaysian Material (Figs. 7-8, 65-75): Longest diameter of body 22.1~44.9μm (28.57±4.24μm); shortest diameter of body 16.8~31.4μm (23.06±3.25μm); longest diameter of nucleus 5.9~8.9μm (7.38±0.78μm); shortest diameter of nucleus 2.3~7.3μm

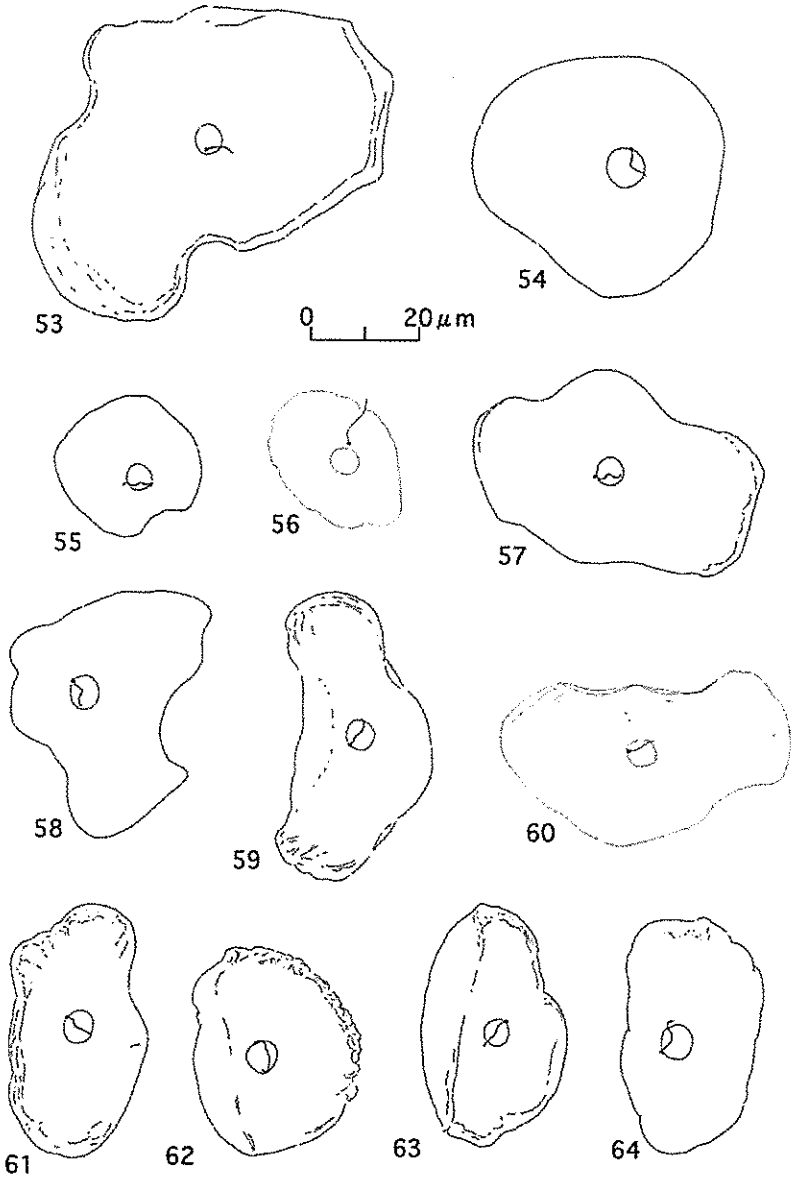

Figures 53-64. 53-57: *Diamondtrypanum katak* new species, in *Rana hosii*. **58-64**: *Diamondtrypanum katak* new species, in *Rana nicobariensis*.

(5.96±0.87μm); flagellum 3.0~8.3μm (5.32±1.22μm); shortest distance of kinetoplast to nuclear membrane -3.6~0.7μm (-0.96±1.03μm).

(2) Japanese Material: Longest diameter of body 22.1~31.0μm (25.84±2.48μm); shortest diameter of body 17.5~25.4μm (21.63±2.19μm); longest diameter of nucleus 4.6~10.2μm (6.44±1.11μm); shortest diameter of nucleus 4.3~6.6μm (5.19±0.63μm); length of free flagellum 1.7~5.9μm (3.68±1.30μm); shortest distance of kinetoplast to nuclear membrane -2.3~0μm (-0.72±0.79μm).

Host – *Rana limnocharis* (Amphibia: Ranidae).
Smears – Slides Nos. 90-01-05-43 and 89-11-22-38 from Templer Park, Selangor, and No. 90-04-23-03 from Kampung Plaman Bantang, Sarawak; Nos. 96-05-11-33 and 92-05-08-35 from Oita, Kyushu, Japan.
Remarks – *D. tsunezomiyatai* was originally described as *Trypanosoma tsunezomiyatai* in the blood smears of *Rana rugosa* (type host) taken in Mogi, Nagasaki, Japan, but later it was often detected in the blood of *Rana limnocharis* in Japan and Malaysia. Werner [10] also reported this species in a Chinese frog, *R.*

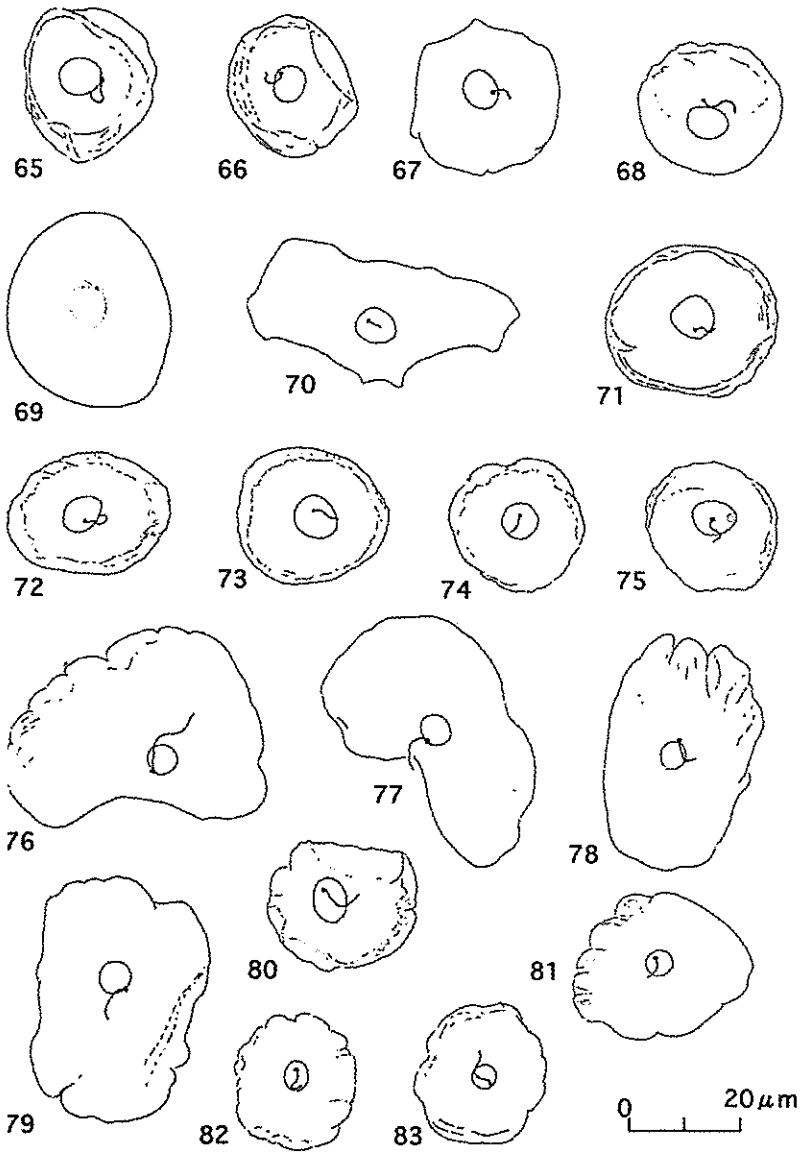

Figures 65-83. 65-75: *Diamondtrypanum tsunezomiyatai* (Miyata, 1978), new combination, in Malaysian *Rana limnocharis*. **76-83**. *Diamondtrypanum katakpadi* new species in *Rana cancrivora*.

limnocharis. Apparently *R. rugosa* is an exceptional host for this species. Therefore, the above redescription was made based on the new materials obtained from *R. limnocharis* from Malaysia and Japan. *D. tsunezomiyatai* in *R. limnocharis* and *R. rugosa* is the smallest species in the genus *Diamondtrypanum*, and is characterized by the position of the kinetoplast that is usually situated inside the nuclear outline, and by narrow brimmed body with a round nucleus.

***Diamondtrypanum katakpadi* new species**
(Figs. 76-83)

Description – Longest diameter of body 22.7~47.9μm (33.79±7.58μm); shortest diameter of body 15.2~36.0μm (25.76±4.89μm); longest diameter of nucleus 4.6~7.6μm (5.86±0.88μm); shortest diameter of nucleus 3.0~5.9μm (4.64±0.74μm); flagellum

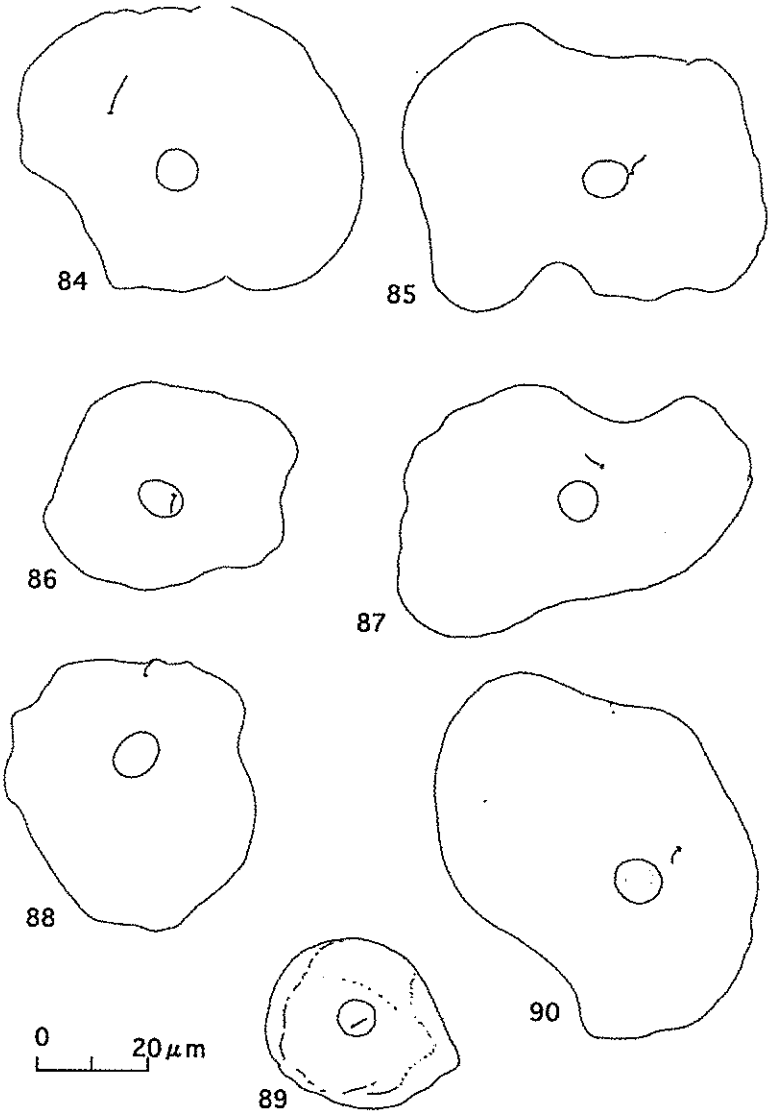

Figures 84-90. *Diamondtrypanum amolops* new species, in *Amolops larutensis*.

3.6~14.2μm (6.93±2.68μm); shortest distance of kinetoplast to nuclear membrane -2.3~1.3μm (-0.33±0.80μm).

Type host – *Rana cancrivora* (Amphibia: Ranidae).

Type locality – Ampang Forest Park, Selangor.

Type smears – Holotype slide: No. 89-11-08-13 from Ampang Forest Park, Selangor. Paratype slides: No. 89-11-08-14 and No. 89-11-08-15 from Type Locality, and No. 89-09-27-01 from Sementa, Selangor.

Etymology – '*katakpadi*' is derived from Malay words meaning 'a rice field frog'.

Remarks – *D. katakpadi* is also a small form like *D. tsunezomiyatai* but differs in its small nucleus, peripheral position of the kinetoplast, and the presence of lobed pleats. The type host is a common frog species in the rice field in Peninsular Malaysia.

Diamondtrypanum amolops new species
(Figs. 84-90)

Description – Longest diameter of body 33.7~74.3μm (54.21±12.94μm); shortest diameter of body 27.1~60.4μm (39.83±8.47μm); longest diameter of nucleus 6.3~8.9μm (7.51±0.79μm); shortest diameter of nucleus 4.0~7.6μm (5.84±0.86μm); flagellum 2.3~5.9μm (3.39±0.96μm); shortest distance of kinetoplast to nuclear membrane -1.0~18.2μm (2.98±5.15μm).

Type host – *Amolops larutensis* (Amphibia: Ranidae).

Type locality – Gombak area near Hindu Temple, Selangor.

Type smears – Holotype slide No. 89-10-14-01; Paratype slides Nos. 90-01-11-05 and 90-01-11-04.

Etymology – The species name '*amolops*' is taken from the generic name of the host.

Remarks – This species is easily distinguished by the position of the kinetoplast, which is often situated very far from the nucleus. In the Gombak area, there are two large streams and *A. larutensis* is very common on the rock in their upper reaches flowing through the forest. *Rana hosii* and *R. chalconota* also appear in the forest stream with *A. larutensis*. The first stream flows from north to south at the Gombak Field Study Centre, 100 meters above sea level. In this stream, *D. katak* is common in the blood of *R. hosii* and *R. chalconota*. However *Diamondtrypanum* is not detected in *A. larutensis* from this stream in spite of the examination of 36 individuals. This stream flows down to Kuala Lumpur as the Gombak River. The second stream belongs to a different water system and flows through the Gombak area near a Hindu Temple (300 meters above sea level) from east to west. *Amolops larutensis*, *R. hosii* and *R. chalconota* are very common here. In this area, *D. amolops* is often detected in the blood of *A. larutensis*.

Diamondtrypanum sarawakense new species
(Figs. 91-95)

Description – Longest diameter of body 30.0~38.6μm (33.08±3.57μm); shortest diameter of body 24.8~32.0μm (28.18±2.77μm); longest diameter of nucleus 5.6~6.9μm (6.26±0.65μm); shortest diameter of nucleus 4.3~6.3μm (5.16±0.80μm); flagellum 3.6~7.6μm (5.68±1.84μm); shortest distance of kinetoplast to nuclear membrane 0~0.3μm (0.06±0.13μm).

Type host – *Staurois natator* (Amphibia: Ranidae).

Type locality – Matang, Sarawak.

Type smear: Holotype slide: 90-05-11-37.

Etymology – The species name is derived from the type locality, Sarawak.

Remarks – *D. sarawakense* is a small species like *D. tsunezomiyatai* but it is easily distinguished by the small nucleus, peripheral situation of the kinetoplast, and unbrimmed body.

Diamondtrypanum gemuk new species
(Figs. 96-101)

Description – Longest diameter of body 22.8~42.2μm (30.21±6.15μm); shortest diameter of body 21.1~25.4μm (23.17±2.04μm); longest diameter of nucleus 4.9~6.3μm (5.74±0.44μm); shortest diameter of nucleus 4.0~5.6μm (4.73±0.53μm); flagellum 7.9~15.8μm (11.84±2.75μm); shortest distance of kinetoplast to nuclear membrane -0.7~0.3μm (-0.21±0.47μm).

Type host – *Occidozyga laevis* (Amphibia: Ranidae).

Type locality – Ampang Forest Park, Selangor.

Type smear – Holotype slide: No. 90-01-08-28.

Etymology – The species name is derived from the Malay word 'gemuk' meaning voluminous body. Used as a noun in apposition.

Remarks – The body of this species is somewhat different from all the congeners in having globular voluminous body, and peripheral nucleus. This species is tentatively included in the genus *Diamondtrypanum* because of the round body and the absence of undulating membrane.

DISCUSSION

Species of the genus *Diamondtrypanum* have been reported from various parts of the world except Australia. As far as we know, França and Athias [11] first illustrated two types of trypanosomes, "*Trypanosoma rotatorium*" and "*Trypanosoma chattoni*" types, as *Trypanosoma rotatorium*, in *Hyla arborea* var. *meridionalis* from Portugal. Those trypanosomes were named *Trypanosoma hylae* by França [12]. They apparently believed that those types were two different morphological forms belonging to one species.

Dutton *et al.* [13] figured a round trypanosome as *Trypanosoma loricatum* in the blood of "frogs" from Congo, Africa. Then Mathis and Léger [1] reported

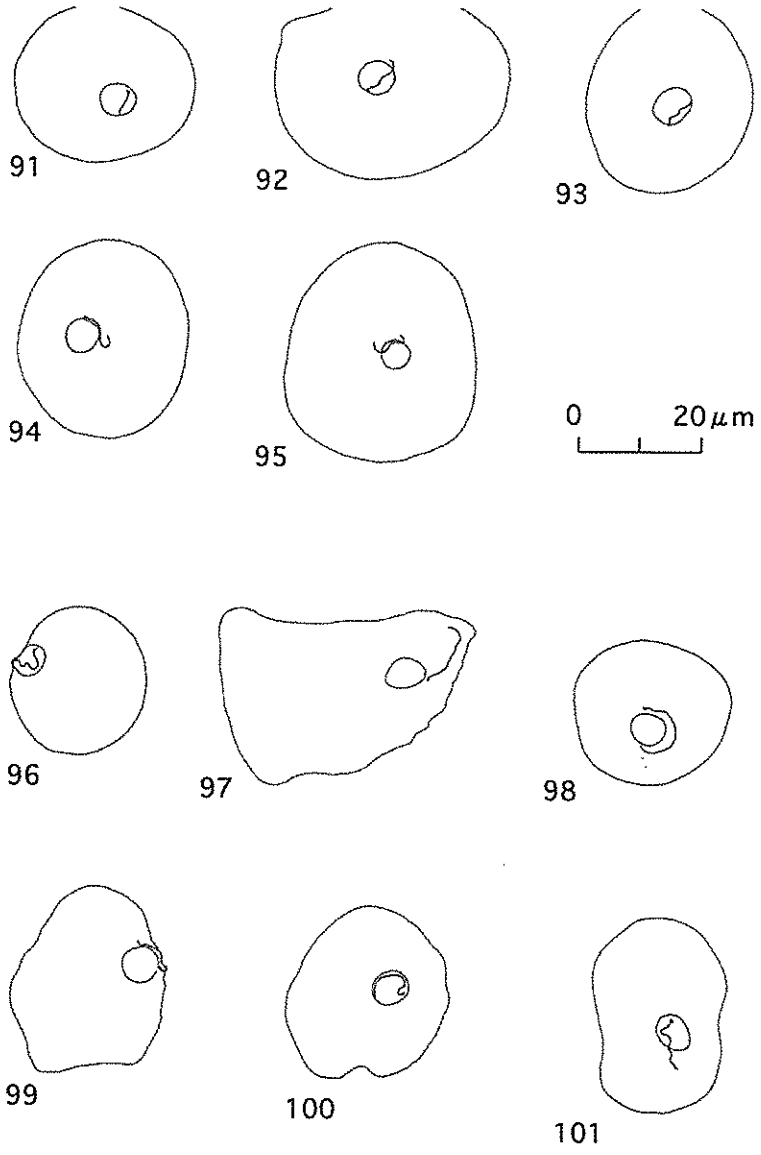

Figures 91-101. 91-95: *Diamondtrypanum sarawakense* new species, in *Staurois natator*.
96-101: *Diamondtrypanum gemuk* new species, in *Occidozyga laevis*.

round trypanosomes apparently belonging to *Diamondtrypanum* as a part of *Trypanosoma rotatorium*, which were detected in *Rana tigrina*, *R. limnocharis* and *R. guntheri* in Tonkin, Vietnam. Furthermore, as already mentioned in remarks to the diagnosis of *Diamondtrypanum*, they also described *T. chattoni* in the blood of *B. melanostictus* from the same locality.

Machado [14] reported a round trypanosome in *Leptodactylus ocellatus* as "*Trypanosoma rotatorium* Formas arredondadas" (a round form) from Brazil. Again Brumpt [8] described, perhaps the same trypanosome, as *Trypanosoma celestinai* in *L. ocellatus* from Brazil. This species apparently belongs to *Diamondtrypanum*. However, simultaneously he described another trypanosome from *L. ocellatus* as *Trypanosoma ocellati*, which was apparently a mixed species of two morphological types of trypanosomes, *T. rotatorium*- and *T. chattoni*-types. *Diamondtrypanum celastinai* (new combination) is the available scientific name for the round trypanosome of *L. ocellatus*.

Miyata [9] described *T. tsunezomiyatai* in the blood of *Rana rugosa* from Nagasaki, Japan, as the third species of *T. chattoni*-type.

Diamond [6] reviewed the amphibian trypanosomes and listed the following anurans recorded as hosts of *T. chattoni*-type: *Bufo arenarum*, *B. melanostictus*, *Ceratophrys ornata*, *Hyla arborea*, *H. raddiana*, *L. ocellatus*, *Phyllomedusa sauvagii*, *Rana catesbiana*, *R. clamitans*, *R. pipiens*, and *R. sphenocephala*. Since his monograph, many amphibians have been added as hosts of *T. chattoni* as follows: (i) *Rana erythraea*, *R. hosii*, *R. limnocharis*, *R. macrodon*, and *Bufo melanostictus* from Malaysia [15]; (ii) *Phrynobatrachus natalensis* and *Ptychadena mascarensis* from Africa [16]; (iii) *Rana holsti*, *R. narina*, *R. limnocharis*, and

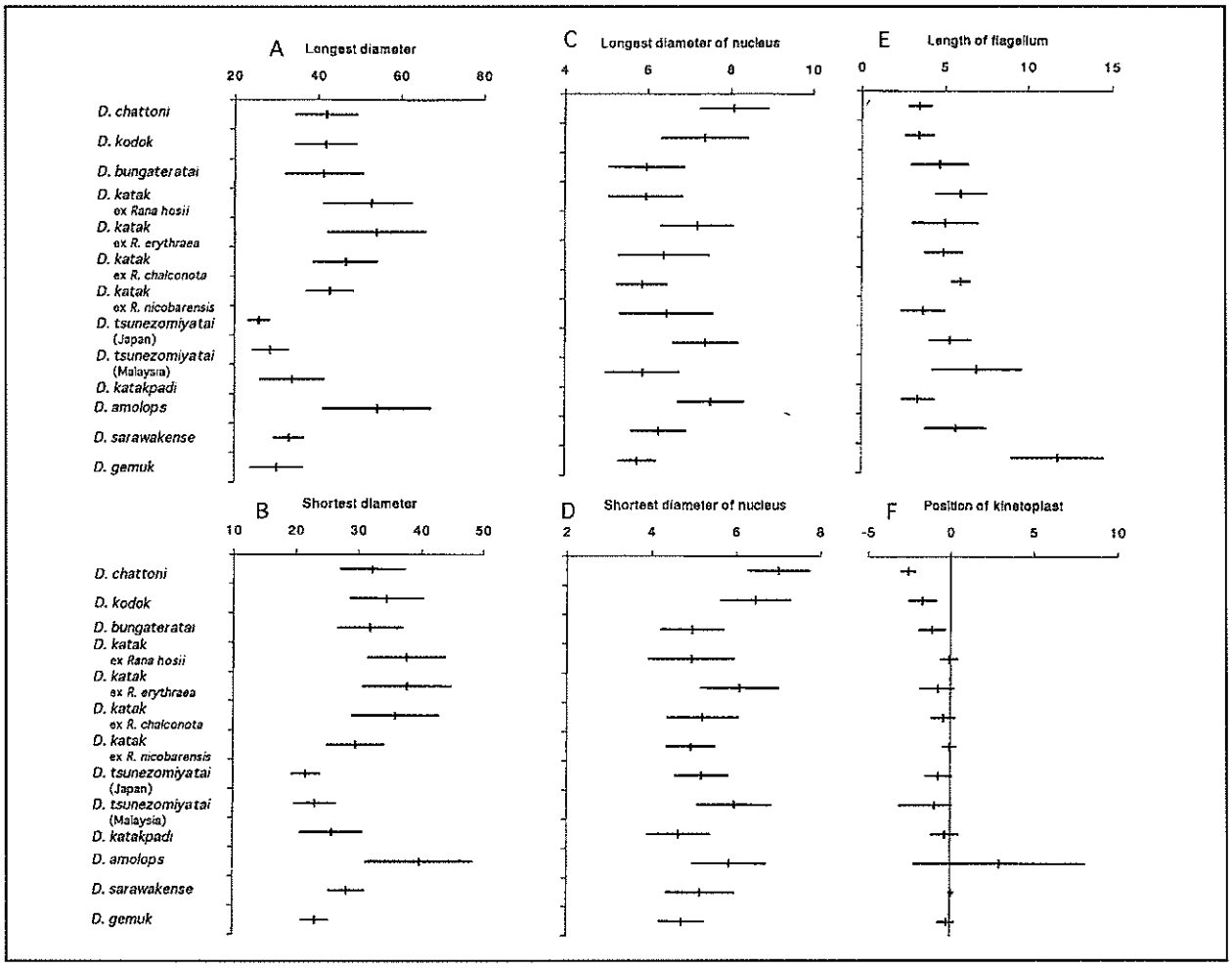

Figure 102. Comparison of various characters in *Diamondtrypanum* species.

R. namiyei from Ryukyu, Japan [9]; (iv) *Rana palmipes, Eleutherodactylus fitzingeri, E. longirrostris, Hyla boans,* and *H. rosembergi* from "Costa Pacifica de Colombia" [17] with a figure of its dividing stage; (v) *Rana limnocharis, R. tigrina, Bufo stomaticus, B. melanostictus, Microhyla ornata, Rhacophorus malabaricus,* and *R. maculatus* from India [18]; and (vi) *T. chattoni*-type in *Bufo gargarizans* and *T. tsunezomiyatai* in *R. limnocharis* from Sichuan Province of China [10]. Unfortunately most of the early descriptions are very brief and it is impossible to use them for further taxonomic discussion.

We did not observe dividing stage in *Diamondtrypanum* spp., but Diamond [6] suggested that there were two forms of reproduction in peripheral blood and visceral organs (heart, kidney, liver, lung and spleen) – binary fission and multiple fission. Jones and Woo [19] also detected the dividing forms of *Daimondtrypanum* sp. in stained kidney impressions of *Rana pipiens* in Canada. According to their report, it divides by binary fission during which daughter kinetoplasts migrate to opposite poles of the nucleus before nuclear division, and cell division follows nuclear division. During the process of binary fission, the above mentioned authors did not observe the undulating membrane.

More recently, molecular biological analyses have been applied for phylogenetic study of amphibian trypanosomes. For example, according to Clark *et al.* [20] *Trypanosoma chattoni* (ATTCC 50294) isolated in *Rana pipiens* from Minnesota, U.S.A., and *Trypanosoma* sp. (ATCC 50295) in *Rana sphenocephala* from Florida, U.S.A., were only distantly related to the other species based on the results of riboprinting. Lun and Desser [21] compared isolates within species of anuran trypanosomes using amplified polymorphic DNA. They concluded that ATCC 50294 and ATCC 50295 were the same species and, perhaps, the same isolate, and the samples could have been mistakenly identified by the ATCC. This means that the culture of *T. chattoni* (ATCC 50294) is not useful anymore for the phylogenetic study of trypanosomes.

For such an analysis, in vitro cultures of protozoa are usually necessary. However, at present, it is very difficult to culture the species of anuran trypanosomes, because mixed infection with two or three species is quite common. Furthermore, the morphology of the cultured form becomes often much simpler compared with more complicated form in the blood. It is thus necessary to distinguish species morphologically before attempting in vitro culture in order to ensure that only one species is contained in the sample. The characters for distinguishing *Diamondtrypanum* species are summarized in Figure 102.

Acknowledgements – We are deeply indebted to the Vice-Chancellor, University of Malaya, the Socio-Economic Research Unit of the Prime Minister's Department of Malaysia, and the Director of Sarawak Museum for supporting this research.

REFERENCES

1. Mathis C. and Léger M. (1911) Trypanosomes des batraciens du Tonkin. *Ann. Inst. Pasteur* **25**: 671-681, pl. V-VI.
2. Berry P.Y. (1975) *The Amphibian Fauna of Peninsular Malaysia.* Kuala Lumpur, Tropical Press.
3. Inger R.F. (1966) *The Systematics Zoogeography of the Amphibia of Borneo.* A Continuation of the Zoological Series of Field Museum of Natural History Volume 52. U.S.A., Chicago.
4. Inger R.F. and Stuebing R.B. (1989) *Frogs of Sabah.* Sabah Parks Piblication No. 10. Kota Kinabalu, Sabah Parks Trustees.
5. Inger R.F., Voris H.K. and Walker P. (1985) A key to the frogs of Sarawak. *The Sarawak Museum Journal* **34**(55) (New Seroes): 161-182.
6. Diamond L.S. (1958) *A study of the morphology, biology and taxonomy of the trypanosomes of Anura.* Doctoral Thesis, University of Minnesota.
7. Miyata A. (1979) *The Parasitic Protozoa: its Taxonomy, Ecology and Evolution.* 2 vols. Nagasaki, Inst. Trop. Med. Nagasaki, Nagasaki Univ..(in Japanese).
8. Brumpt E. (1936) *Prácis de Parasitologie.* Paris, Masson et C, Editeur.
9. Miyata A. (1978) Anuran trypanosomes in Kyushu and Ryukyu Islands, with descriptions of six new species. *Trop. Med.* **20**(1): 51-80.
10. Werner J.K. (1993) Blood parasites of amphibians from Sichuan Province, People's Republic of China. *J. Parasitol.* **79**(3): 356-363.

11. França C. and Athias,M. (1906) Recherches sur les trypanosomes des amphibiens. *Arch. R.Inst. Bact. Camara Pestana* **1**: 127-165.
12. França C. (1909) Encore sur le trypanosome do *Hyla arborea. Arch. R. Inst. Bact. Camara Pestana* **2**: 271-272.
13. Dutton J.E., Todd J.L. and Tobey E.N. (1907) Concerning certain parasitic protozoa observed in Africa. *Ann. trop. Med. Parasit.* **1**: 285-370.
14. Machado A. (1911) Pesquizas citolojicas sobre o *Trypanosoma rotatorium* Gruby. *Mem. Inst. Oswaldo Cruz* **3**: 107-135.
15. Sullivan J.S. and Sullivan J.J. (1977) Prevalence of Hematozoa in some anurans from the Malayan Peninsula. *Southeast Asian J. Trop. Med. Pub. Hlth.* **8**: 126-128.
16. Baker J. (1977) Some trypanosomes of African Anura. *Protozoology* **3**: 75 82.
17. Carvajal H. (1982) Tripanosomas de anfibios de la costa Pacífica de Colombia. *Actualidades biol. Medellin* **11**(42): 107-114, illustr.
18. Ray R. and Choudhury A. (1983) *Trypanosomes of Indian anurans*. Zoological Survey of India Technical Monograph No. 8, 1-60.
19. Jones S.R.M. and Woo P.T.K. (1986) *Trypanosoma chattoni* Mathis & Léger, 1911 in *Rana pipiens* of southern Ontario: morphometrics and a description of the division process. *Syst. Parasitol.* **9**: 57-62.
20. Clark C.G., Martin D.S. and Diamond L.S. (1995) Phylogenetic relationships among anuran trypanosomes as revealed by riboprinting. *J. Euk. Microbiol.* **42**(1): 92-96.
21. Lun Z-R. and Desser S.S. (1996) Analysis of isolates within species of anuran trypanosomes using random amplified polymorphic DNA. *Parasitol Res.* **82**: 22-27.

Journal of Science and Technology in the Tropics (2005) **1**: 19-33

Oil palm: The agricultural producer of food, fibre and fuel for global economy

Yusof Basiron and Chan Kook Weng
Malaysian Palm Oil Board, 6 Persiaran Institusi, Bandar Baru Bangi,
43000 Kajang, Selangor Darul Ehsan, Malaysia

Paper presented at the Malaysian Science and Technology Conference 18-20 April 2005

Abstract Oil palm industry has expanded from just being an agricultural producer of food comprising of oils and fats to fibre (material) and fuel (energy) for the global economy. In producing food, fibre and fuel (the 3Fs) the industry has also identified the enlarged environmental consequences it will now be involved. Arising from this, the science and technology (S&T) too for the 3Fs production now falls squarely on the type of research and development (R&D) undertaken on land use and land-use cover changes from forestry (LULUCF) with inclusion of the two latter products. Besides the best practices implemented to enhance the economic, environmental and social requirements, any change in land-use pattern is prioritized with the environmental consequences identified and minimized. The S&T development in itself is not enough and must be applied together with business. It is critical that sustainability and poverty reduction remain the guiding principles for efficient use of resources, harness of intellect, and channel knowledge to benefit the rural poor and the marginalized. As more plantations companies develop the potential to produce the 3Fs, there is greater realization that both policy and infrastructure support from the Government is important. This must be accompanied by higher participation of activities by all stakeholders over the whole value supply chain that involve the companies, industry and nation at all three levels to strengthen agricultural development to realize this 3Fs objective.

The benefits of this new 3Fs approach are three-fold: firstly, greater promotion of value addition and an accomplishment of accelerated growth of agro-businesses in the food, material (fibre) and energy (fuel) sub-sectors; secondly, creating more jobs in the rural sector with greater security for a fair standard of living for the small holders and their families; and thirdly, discourage migration of people to the urban areas when the rural populace is better able to face the challenges coming from the economic liberalization and globalization resulting from more job opportunities created by the plantations and the emerging agro-businesses. A total of 10 recommendations for policy refinement to enhance 3Fs objective is discussed. They are aimed at achieving food security, fibre and fuel production by focusing on developmental and environmental consequences, an continuing sustainable agriculture to improve the economic, social and environmental impacts of the companies in managing the 3Fs objective thereby hastening rural development when these new agro-businesses start to benefit not only the welfare of the people living in and around the plantations but along the whole- value chain.

Keywords oil palm – agricultural producer – food – fibre – fuel – global economy

INTRODUCTION

Sustainable development in any country, developed or developing, requires the people to do the things that nurture mankind's aspirations and provide society's needs while ensuring a safe and viable environment where the very ecological base people live on and in is protected. Progressive agriculture is basic to sustainable development [1]. Tree crop based agricultural production systems all around the world are basically managed by agroforesters who have developed efficient use of soil, water and air resources to enhance the productivity of the crop for the benefit of the environment and its inhabitants.

Efficient agroforestry cleans up the air by fixing large amount of CO_2 and gives out O_2, improves hydrological

cycles through the 'rain forest effect', stabilizes soil through protective and robust root systems, recycles an ample supply leaf litter, and provides a closed canopy that becomes a favourable bio-diverse habitat for many plants and animals. One such agroforest system is the advanced oil palm plantation system that is highly sustainable in producing 42% of the palm oil export for the world.

The advanced oil palm system in Malaysia, however, does not just happen. It is planned, implemented and managed for over a hundred years. The planters are agroforesters at their best. They know their basics [2]. They are well versed on what best developed practices to use, what improved genetic planting material to plant, when optimum balanced fertilizers to apply, how soils are protected by natural ground covers, what biodiversity to maintain, when integrated pest management to introduce, and all these and many more, are based on good science, technology and engineering, with documented evidence. As a result the oil palm industry moves to become more sustainable and competitive [3], year after year, with the crop ultimately benefiting both the environment and its inhabitants [4,5]. The planters are indeed truly the stewards of the earth resources.

Basically in the 21st Century, the oil palm industry has three important simultaneous challenges to meet. They are to produce (1) a steady supply of palm oil for food security, (2) material for fibre products manufacturing, and (3) renewable green fuel by conversion of excess palm oil into biodiesel for the global economy.

The call to the industry to move to the 3Fs has been made earlier [1] but there was only an outline of what was involved and this prompted us to look further into the complexity of the 3Fs objective for the industry. It has to move from the production of food [6], the first 'F' that it is doing very well, to fibre material [7], the second 'F' that has taken off, and now into fuel [8], the third 'F' that is beginning. The treble Fs (3Fs of food-, fibre- and fuel-production) objective requires the industry to re-examine the developmental and environmental impacts of the enlarged extraction of fibre and fuel in addition to food, all of which are taken out from the same land to supply the world demand. Agronomically it is possible to mine the land optimally for the 3Fs, as there are new opportunities to produce other new uses for food, fibre and fuel [9]. In other words without neglecting the world's need of palm oil for food, the industry has also to gear itself towards more value-added products from fibre and fuel if the 3 Fs objective is to be fulfilled while preserving agronomic and environmental sustainability within the plantations.

The aim of this paper is to explore ways on how to fulfill the 3Fs objective in the oil palm production system without over exploiting the land on which the oil palm is grown.

DEVELOPMENTAL AND ENVIRONMENTAL ASPECTS OF THE 3FS PRODUCTION OBJECTIVES

Developmental aspect

In the cultivation of oil palm from the developmental aspects within the context of 3Fs production objective, the potential benefits expected identified are as follows:

1. It is to enhance the employment opportunities for the benefit of the people and for rural development. There is a multiplying effect that helps to generate more economic activities that would help eventually to strengthen the local economy, particularly that in the rural areas where new industries are expected to be spawned. The agro-businesses arising from 3Fs objective are a significant source of domestic employment in the form of short- and long-term creation of jobs such as planting, cultivation, harvesting and transport of palm oil as food, fibre material from biomass, excess palm oil to be used as feedstock for fuel, and the construction and operation of food processing plants, fibre extraction plants for production of material and bioenergy conversion plants for fuel production.
2. In addition to the creation of jobs, there is in frastructure development and this is imple mented through the extension of the 3Fs services that allow the rural populace, on one hand, to produce more food, fibre and fuel energy in plantations, particularly in their small holdings and on the other hand for the Government agencies and extension teams to do their advisory work. The aim is for their income to be raised.
3. As a further benefit of the 3Fs objective, particularly on the third 'F' when the oil palm industry, as both an energy producer and user at

the same time, must demonstrate that as a result of its energy surplus situation, it is in a good position to use the excess energy to enhance the fulfillment of the other two Fs of food security and fibre material production.Very often, even with just a 2Fs objective in other agricultural systems like soyabean, rape seed and sunflower seed crops of say food and energy production, there are already potential conflicts due to the competition and need for the same limited land to grow either an energy producing crop or a food cereal crop. This conflict is however avoided in the case of the oil palm industry. This is because within the oil palm production system, palm oil forming the first 'F' is at 10% while there is about 90% of the plant biomass remaining largely untapped and is available for the second 'F' fibre material production and also the manufacturing of export 'value-added' finished fibre products, and for the third 'F' fibre material for combustion to generate the 'green' fuel energy. There is therefore synergy rather than conflict in the 3Fs objective in the oil palm system.

4. For the excess of palm oil stock particularly at year-end, efforts have begun to exploit the excess by coversion into biodiesel and turning it into an agro-energy resource to boost the supply of third 'F' fuel energy for use in food and fibre production and in the transport industry. All these again reflect the strong synergistic effect of the 3Fs objective within the oil palm industry.
5. Another benefit is for the palm oil importing countries to encourage and save the land used for their costly cultivation of oilseeds to be reserved for the cultivation of other more essential food cereal crops, thereby ensuring food security in the staple crops. As an example if soyabean oil or other oilseeds when assumed to yield 0.5t/ha oil, then for every tonne of palm oil imported, the oilseed producing countries can save about two hectares of land planted with oilseeds and reserve them for planting with the much needed cereal food crops.

The major challenge for the Malaysian palm oil industry is to ensure food security by producing additional food by using excess fibre or oil while conserving the depleting resources, particularly of land, for fibre and fuel production. This 3Fs objective indeed has spill-over effect for the palm oil importing countries where they can use their limited land resources to focus on the production of a diverse food basket by raising other essential food grains crops given that the land is freed from oilseed planting.

Environmental aspect

On the environmental aspect, there are several consequences that need to be addressed if the 3Fs objective is to benefit the industry.

1. The first benefit of the 3Fs objective is derived from the energy production function of the oil palm industry through its contribution to the climate change mitigation whereby the excess energy produced can help to reduce the use of fossil fuels. The excess fibre, over those already required for combustion in the conventional boilers, instead of being recycled to the field as mulching material, can be further combusted in the newer and more efficient boilers to generate even more heat and energy. More complete combustion pyrolysis is being investigated. The excess energy generated, besides being demonstrated to be 'green' because oil palm biomass is generally a carbon-neutral source of energy, is also renewable. For example, at each replanting of an oil palm field after every 25 years, the production of biomass, particularly of fibre and shell, is renewed in a very short time after three years of immaturity, to continue the 3Fs production for another 22 years before the whole cycle is repeated. The '25 years time span' is dictated by the economic life span of the oil palm field when the tall palm harvesting becomes a problem.
2. Though the oil palm plantation is not able to accumulate as much as the necessary biomass when compared with the natural forests over the short 25 years of each replanting cycle, there is however the benefit of producing relatively more carbon sequestered through improved land management compared with any of the short-term annual oil seed crops of soyabean, rapeseed and sunflower seed where the land is tilled every year.
3. The oil palm effluent ponds are now considered as avenues to provide the benefit, where the methane produced has been neglected in the

past, will be harnessed through the new technologies being developed to improve the capture and use the methane as a source of biogas energy to replace fossil fuels thereby further reducing the GHG emissions.

4. Not withstanding the aforementioned benefits, the oil palm provides another benefit by being a cheap means of reducing atmospheric emission of CO_2 through carbon sequestration. As the biomass from the oil palm plantation becomes continuously prized as a modern efficient energy source through its fibre production, new opportunities abound for oil palm to be planted at closer spacing for the sole purpose of growing for biomass production. Such opportunities when implemented on a larger scale will offer the industry new avenues to tap on yet another benefit of rehabilitating the steep marginal areas and abandoned degraded lands by planting them up as dense agroforests. Whereas in the past such marginal areas, blamed to be the cause of low yields that bring the national average yield down, will now consider any yield of FFB from these dense agro-forests planted for fibre production, to be a bonus.
5. The biomass production from these dense oil palm agroforests grown on marginal and steep land offer the opportunity to the industry to address yet another environmental concerns such as biodiversity. The close canopy in such dense planting will simulate the conditions of 'natural forest effects' where different flora and fauna will flourish to enhance richness of bio diversity. The areas under the dense agroforests of oil palm will continue to help to clean up air from pollution by absorbing CO_2 and emitting O_2 thereby creating also an oxygen-enriched and healthier environment.

In a scenario of shrinking resources such as land and water, the challenge is to combine conventional system of planting to increase biological yield of oil palm per hectare to feed the growing world population yet produce fibre and fuel with the dense agroforest systems to improve the ecological foundation where such marginal and degraded soils can be devoted for production of biomass for fibre and renewable fuel energy and for creating areas of enriched biodiversity and oxygen.

ACTUALIZING THE CHALLENGES OF THE 3FS OBJECTIVE

From the outline of the two prior considerations above, the Malaysian oil palm industry has to explore whether it has the potential to actualize the challenges of the 3Fs objective of food security, fibre material production and fuel conversion from palm oil.

This potential can be actualized through a combination of policy change and infrastructure support from the government on one hand and the strengthening of the synergies on the other hand among the various players throughout the whole value supply chain. Each player must fulfill their roles over the whole field of agriculture, rural development and mill processing so as to result in the export of quality end-use products from food, fibre and fuel agro-businesses to customers. Basically the policy change is to strengthen rural infrastructure support by the government for a faster agricultural development, promote value addition from accelerated agro-business development, create employment in rural areas thereby securing a fair standard of living, and discourage migration to urban areas because the jobs created that allow the rural populace to face the new global challenges arising from economic liberation and globalization better. The 3Fs objective is discussed separately for each food, fibre and fuel production though they are closely interlinked.

Food security

This will be discussed under three separate headings of how the oil palm industry can contribute to food security: (1) to understand food security, (2) to exceed food security requirement, and (3) to meet the requirement of the three major food types of oils and fats, protein and carbohydrate.

Understanding what food security means to the oil palm industry

Food security is a complex issue. First it involves food scarcity that affects the number of undernourished people. In 1996, the World Food Summit reported that there were 854 million undernourished people [10] and over 25,000 people died every day from hunger. In the 2004 FAO Report [11], the number of undernourished improved slightly reducing the number to 815 million people coming from 35 countries of which 777 million were from the developing countries comprising mainly of 24 countries in Africa. The causes of food scarcity may be from natural disasters (flood, drought) or man-

made (famine, war). Food scarcity is generally more a developing country problem as they often lack mechanisms for food production, storage and distribution.

Second, food security is defined as the availability of enough food in order to sustain life and good health of all the world population at all times, across all countries and regions, across all income groups and across all members of individual households [12]. Such a food security definition requires policies to take on both economic and political dimensions and involves three categories of factors – getting prices right, optimal storage and supply enhancement.

Third, food security is a physical, environmental, economic and social issue. It involves not just production but access, not output but process, not just technology but policy, not just global balance but national condition, not just national figures but household realities, not just rural but urban consumption and not just quantity but quality.

Finally, the concept of food security covers every individual who has the means to have physical, economic, and environmental access to a balanced diet with macro and micro nutrients, drinking water, sanitation, hygiene, health care and education to lead a healthy and productive life. Thus the steady production of quality palm oil at relatively low cost and effective promotion is ready to feed the world [13].

How to meet food security requirements by the Malaysian oil palm industry?

There are several considerations to reflect Malaysia's superiority in meeting the food security requirements through the oil palm system.

1. Requirement of cheap supply of nutritious food. For a nation that depends on food import annually to feed her population, Malaysia today is more than self sufficient in oils and fats thanks to the oil palm industry that exported palm oil to over 150 countries. The supply of palm oil from Malaysia as a cheap, reliable and nutritious food fits nicely as a candidate for use to meet the requirements in food security development for the importing countries that face food scarcity.
2. Food requirement for part of the daily diet. Oils and fats are an important food item and are a regular part of the human diet and act as the calorie dense components. Each gram of oil and fats provides 9 kilocalories (kcal) of energy as compared with 4kcal/g from carbohydrates and proteins. Oils and fats are an essential component of a balanced human diet, and the World Health Organization (WHO) recommends that 30% of the energy (calorie) requirements of an individual should be obtained from oils and fats. This works out to a per capita consumption of about 20-24 kg oils and fats per year. But for most of the world population these figures are not realized, mainly due to unavailability and affordability. Thus food security in oils and fats should be a crucial issue [14].
3. Requirement for a steady supply of palm oil. The progress made by the Malaysian oil palm industry in the agricultural production of oils and fats during the past five decades has been one of the biggest success stories of independent Malaysia. From a mere 54,000 ha in the early 1960, it reached 3.87 million ha in 2004. Malaysian palm oil production and exports in the 1960s were in the region of 90,000t and by the mid 1970s palm oil export was in the region of 1.5 million t. By the decades of 1980, 1990 and 2000 and in 2004 (Table 1), palm oil export reached 2.3, 5.7, 9.1 and 12.6 million t respectively. Thus palm oil constitutes one of the single largest contributors to Gross Domestic Products (GDP), earning RM 30.41 billion in 2004 [15] up from RM 26.23 billion in 2003.

Table 1. Malaysian palm oil production and export from 1980-2004 (in tonnes).

Year	Production	Export
1980	2,573,173	2,271,222
1990	6,094,622	5,727,451
2000	10,842,095	9,081,553
2004	13,976,182	12,575,401

(Source: MPOB)

4. Requirement for food types of protein and carbohydrate besides oils and fats. Despite the impressive gains, Malaysia at present finds itself in the midst of the paradoxical situation. On one hand there is surplus in oils and fats where the total oil palm products exported (vide Table 2) comprising of palm oil, palm kernel oil, palm kernel cake, oleo-chemical and finished products to the tune of 17.35 million t in 2004 up from 16.82 million t in 2003. On the other hand it had to import protein and carbohydrate types of foods.

Journal of Science and Technology in the Tropics (2005) 1: 19-33

Table 2. Malaysian exports in 2003 and 2004 (in tonnes).

Export	2003	2004
Palm oil	12,266,064	12,575,401
Palm kernel oil	868,658	778,857
Palm Kernel cake	1,809,957	1,795,918
Oleochemical products	1,568,239	1,776,441
Finished products	259,472	374,345
Others	48,945	57,277
Total	16,821,334	17,348,239

Source [15]

Table 3. Export of palm oil to four major destinations in 2004 (in tonnes).

Country	Export (t)
China P.R	2,799,702
EU-25	1,967,111
Pakistan	953,772
India	941,863
Rest of the World	5,912,953
Total	12,575,401

Source [15]

5. Requirement of 'non-religious' and versatility of oils and fats in food products. As palm oil is non-religious food that can be used by Muslim and non-Muslin countries and is very versatile due to its unique properties that encourage its use in a wide range of end products and cost effectiveness, it is exported to over 150 countries. The four major importing countries in 2004 are China P.R, European Union-25, Pakistan and India (Table 3) where together the offtake amounted to 53% of Malaysian export.

From the aforementioned requirements, though Malaysia has a surplus in export in oils and fats, she has to tackle and reduce the import of two types of food viz., protein and carbohydrate. What are some plans the oil palm industry can do to reduce or overcome the level of imports?

What the oil palm industry can assist in reducing the imports of the two food types of protein and carbohydrate?

The challenge is met by four strategies.

1. Requirement to strengthen livestock and crop integration. The existing plantations at 3.87 million ha of oil palm or 60% of the 6.02 million ha of land designated for agriculture under the Third Agricultural Plan (1998-2010) [16] are to be used to raise the production of protein and carbohydrate types of food through livestock and crop integration. In a scenario of limited land availability in Peninsular Malaysia and lack of human resources like labour over the whole country, the challenge is even more daunting to maintain the oil palm productivity and continue to export palm oil without damaging the ecological foundation when livestock and food crops are integrated. It is important that packaging this challenge for which the growers, who have to bear the cost, will be able to benefit not only from this investment but also that the methodology developed will sustain the welfare and incomes of the workers.
2. To be in line with the government aspiration for agriculture. The approach is to look further into the agricultural productivity of the oil palm industry. Since the Abdullah Administration's return to power in the 2004 General Election with a bigger majority in the House of Parliament it has decided to revitalize agriculture as the third engine of growth by focusing on its productivity as a whole with an emphasis on raising that of the small holders. To respond the industry must examine the issuen of agricultural structure in the country that requires long-term solutions. A strategic approach to modernize plantation agriculture is to use the agroforestry and value-added enhancement concepts.
3. Use of the agroforestry concept. Under the agroforestry approach, the increasingly depleting resources such as land availability and water would require adoption of optimization of resource use of the same land for agriculture and forestry development simultaneously. There are obvious sub-benefits.
   a. The aim is to integrate agriculture with forestry development as mutuall compatible and complementary industries. The integrated approach allows sharing of land resources for production of both agricultural and forestry products on the same land thereby mitigating the demand pressure for new arable land. The symbiotic relationship such as planting of forestry species with industrial crops is to optimize land utilization and maximize returns. During the long gestation period of agroforestry investment, it is also

the time, as the agroforestry crops are maturing, to have opportunities for mixed enterprise for intercropping for which the private sector are encouraged to participate.

b. For this to happen in the oil palm industry, there must be an adoption of the double planting avenues with more space between planting rows for intercropping for cattle and food crop integration. It is anticipated that about 120,000 ha of oil palm will be replanted annually over the next 5 years from 2006-2010. As reported previously [3], the country had attempted to produce protein through cattle rearing by clearing large tract of land and planting grasses with cattle as the main monoculture, but this was found not profitable as compared with oil palm.Likewise production of carbohydrate such as rice through large tract of lands was found also not profitable as oil palm. For the local needs, rice is partly imported and its production subsidized. Even using the agricultural land to produce rubber as an industrial commodity was also found to be less profitable compared to oil palm cultivation, and therefore over the years, substantial areas of rubber had been replaced with oil palm. Though cocoa may be considered as a food item by being a beverage, its cultivation was found to be not as profitable as oil palm and its land had been replanted with oil palm. With such large planting of oil palm there is little choice but to look deeper into livestock/crop integration.
c. The fibre from the oil palm itself which is largely untapped should now be purposefully exploited as a source of material fibre production from both the field e.g. harvest of petioles from fronds or from trunks at replanting, and from mills through shell, fibre and empty fruit bunches. The fibre when converted to value added medium density fibre-board products will indirectly reduce the over exploitation of the forests.
d. When the sums are added up, even tough for example in 2002 the country imported RM12 billion of food products, it still exported more food products in the form of palm and kernel oil and products and cocoa products with a net RM8 billion surplus from export earnings. By being a net exporter of food products, the country is able to import at cheaper prices other food items that the country cannot grow efficiently. This is attributed to the superior agricultural productivity and profitability of the oil palm plantations agriculture where agricultural outputs are levied with export taxes rather than be given subsidies. By specializing in plantation agriculture the country has better technological andeconomic advantages and deliberately importing other food item the country is able to optimize its resources.
e. Thus food security is adequately assured if oil palm continues to be developed under integrated agricultural industry with oil palm land to be jointly developed to produce protein and carbohydrate types of food. Optimizing of land use through livestock-crop integration (LCI) is gaining ground where today about 78 estates have embarked into cattle integration. Likewise crops like hill paddy, sweet corn, maize, watermelon are being integrated. Thus with greater persistence into the livestock-crop integration the import bills for protein and carbohydrate are expected to drop further.

4. Fourthly, a requirement for value-added activities over the whole supply chain. With larger quantity of protein and carbohydrate being produced, there will be more opportunities for downstream manufacturing and such facilities may have to be expanded to process besides oils and fats from oil palm but also carbohy-drates from paddy and food crops and protein from livestock and fisheries. In this way value-added downstream products with the spawning of small food agribusiness units may be expanded. With the implementation of the value chain management, the sub benefits areas follow:
   a. To be competitive the oil palm industry must continually add value to its core products of palm oil, fibre and fuel i.e. the 3Fs and services in order to create future security [8]. To do so there must be a broad framework of variables that would significantly influence the future development of themfactors that would enhance competitiveness of the oil palm industry.
   b. Under this enhancing of product-based

value-added approach, the aim is to meet the demands of customers worldwide for products that are specific to their needs and preferences. Such value-added products are made accessible through information communication technology (ICT) that supports the customers' ability to seek, identify and procure these products, processes and services. This is a definite shift from the commodity-based strategy that limits the effectiveness to serve the markets that are now be coming to be of higher value and more segmented.

c. By relating the end products directly to the primary production, the value-added product–based approach will strengthen the strategic role of up stream agricultural and forestry production with value adding activities over the whole value supply chain.
d. The product-based approach allows identification of opportunities for market expansion for agro-based manufacturing and other economic activities.
e. This will include opportunities for R &D and technology generation, improve primary production, processing, manufacturing of intermediate and final products as well as distributing and marketing of the end products and services to the consumers.

Fibre material production

The oil palm is a prolific producer of biomass particularly the fibre products. These materials are available daily throughout the year from the plantation in the form of empty fruit bunches, fibre and shell in the mill and its related methane production in the effluent ponds to be harvested as biogas. In the field, during replanting, large quantities of trunk and fronds are also available. The dry weight of biomass fibre available each year is at least twice that of palm oil. When manufactured into medium density fibreboard (MDF) or pulp, a tonne of whose fibre is usually worth more than a tonne of palm oil. The quantity of trunks and fronds at replanting is shown in Table 4.

The strategy is as follows:

1. On a national scale, there are about 14.483 million t of frond petioles available for fibre production (Table 4). However, in order not to over exploit or mine the land for excessive removal of food, fibre and fuel from the same land, the petioles, though available will be selectively exploited so as to leave some organic matter in the field to retain soil fertility.
2. The other potential sources of material for fibre production is from the trunk and fronds at time of replanting estimated at 9.155 and 1.755 million t respectively but these materials are spread over 120,000 ha of replant through the country.
3. Fibre material from the mills. Normally palm and kernel products constitute only 10% of the total harvested biomass, there are great opportunities for the industry to exploit the fibre from the biomass of the fruit bunches after the oil and kernel have been extracted. Based on the quantity of FFB processed in 2004 amounting to 69 million t there are potentially close to 28.290 million t fibre material for extraction coming from 15.180, 9.315 and 3.795 million of EFB, fibre and shell respectively (Table 5).
4. Bioenergy in the form of biogas [17]. In the processing of FFB, there are large quantities of palm oil mill effluent produced. Though there is no fibre material to be extracted, the effluent remains a source of potential energy coming

Table 4. Amount of dry weight of trunks and fronds at replanting in 2003.

Parameter	2003
Total area (10^6 ha)	3.802
Immature (10^6 ha)	0.499
Mature (10^6 ha)	3.303
Rate of replanting (4%)	0. 04
Dry wt of trunk (t/ha)	75.46
Dry wt of frond (t/ha)	14.47
Dry wt of trunk at replanting (10^6 t/ha)	9.155
Dry wt of frond at replanting (10^6 t/ha)	1.755
Dry wt of Annual frond pruning (10^6 t/ha)	43.887
Dry wt of Annual frond petiole (10^6t/ha)	14.483

Table 5. Excess of biomass surplus to mills' requirement in 2004.

Parameter	2004
FFB processed (106 t)	69
EFB @ 22% FFB (106t)	15.180
Fibre @ 13.5% FFB (106t)	9.315
Shell @ 5.5% FFB (106)	3.795
Effluent	
Steriliser condensate @ 12% FFB	8.280
Clarification sludge @ 50% FFB	34.500
Hydrocyclone washing @ 5% FFB	3.450
Total	46.230

from the methane gas. There are technologies being developed to efficient capture the biogas for heat and energy production. This aspect will be discussed further in below.

With these potential benefits in mind, the overall material management from fibre, shell and empty bunches from the mill, methane as biogas from effluent ponds, and trunk wood chips and pruned frond from the field have to be reexamined from the point of how they, as outlined in the 3Fs objective, can be used efficiently. To actualize the 3Fs objective the competing use of fibre material in the field as mulching, as value-added products such as ecomats, medium density fiberboards, etc and contribution to overall energy management and efficiency for combustion is the more efficient boilers and even through pyrolysis, without affecting the overall productivity of the plantations. This forms the efforts made to realize the second challenge.

Fuel production

With increase in awareness and importance attached to global warming, the fibre resources from the field and the mill should be developed through combustion in efficient boilers as alternative to fossil fuels. There are two strategies.

Biodiesel production

1. Requirement to deal with the high year-end palm oil stock. For biodiesel production from palm oil, the following actions are to be taken:
   a. There is a need to deal with the annual increases in production of palm oil from Malaysia that frequently lead to higher year-end stocks and this invariably results in declining prices even though there have been continuous upsurge in the palm oil export. The year-end stocks in 2003 and 2004 are shown in Table 6.

Table 6. Closing stocks at December 2003 and 2004 (in tonnes).

Closing Stock	2003	2004
Palm oil	1,166,541	1,487,387
Palm kernel	112,398	167,476
Palm kernel oil	169,743	194,934
Palm Kernel cake	238,417	211,979

Source [15]

   b. From Table 6 it can be seen that among the closing stocks of the four major palm and kernel products in December 2004, what had affected the CPO price is only the palm oil stock of which at 1.487 million t, up 320, 846t or 27.5% over 2003. The temporary increases often require that the excess palm oil stocks be reduced by conversion to biofuel through the palm biodiesel process leading to improved price situation for palm oil subsequently due to the market perception of low stock. For price stabilization of palm oil, collaboration with the Indonesian palm oil producers may be considered if the programme is to be made more effective.
   c. The biodiesel available could be considered for the blended fuel programme.
2. Requirement of biodiesel to assist in prolonging the petroleum energy reserves. By the use of palm biodiesel pathway initially for price stabilization mechanism, it has in fact opened a new avenue for palm oil as a regular component of biofuel energy resources. MPOB has been the pioneer in researching into palm diesel project since the 1980s. An initiative has started with the National Oil Giant PETRONAS work has begun to develop a patented technology to transform palm oil into a viable biodiesel to substitute diesel from petroleum. Being renewable, the biodiesel has been recognized as an answer to the diminishing petroleum energy reserves.
3. Requirement for biodiesel to be used for running vehicles. The palm biodiesel was exhaustively evaluated by MPOB as diesel fuel substitute for over a decade from 1983-1994. The tests included a large number of vehicles ranging from taxis, trucks, passenger cars and buses with many vehicles having completed the 300,000 km run. The biodiesel technology is now available for commercialization as diesel engine application is so widespread all over the world. The tests of various percentages of palm olein in the petroleum diesel allowed branding of biodiesel into B2, B5 and B10 to denote 2, 5, and 10% palm olein in petroleum diesel and tested since 2002.
4. Requirement for safety net for palm oil prices. Another benefit of the biodiesel production is that it offers a safety net for the Malaysian palm oil industry at time of glut of palm oil in the market.

Editorial

The Journal of Science and Technology in the Tropics (JOSTT) is born, created by COSTAM (Confederation of Scientific and Technological Associations in Malaysia). COSTAM embraces a wide spectrum of basic and applied sciences embodied in 35 associations which are constituent members of COSTAM. It is always challenging for COSTAM to organize scientific events including publications which do not overlap the activities of its members. The concept of JOSTT does not only meet this criterion but turns out to be useful and relevant to this region.

Science is indeed universal in its fundamental laws and applications. However, the tropical belt of the earth is distinctly unique and presents an interesting area for the laws of nature to operate. The fauna and flora offer an immense source of information yet to be fully documented. The potential for future drugs for AIDS and other diseases has been realized but insufficient initiatives are being undertaken. The challenges for researchers in the biological and health sciences are unimaginable.

The climatic conditions in the tropics with abundant sunshine and conventional rain provide conducive environments for growth and life. What if biotechnology could genetically modify important economic crops of the temperate region to thrive in the tropics? This will increase the productivity of these crops by many folds. The possibility of renewable energy via the biomass and solar energy is real and could be realized with more intense scientific and technological research. The tropical conditions also present many challenges to architects for ideal living habitat and to engineers for sustainable development. The science of lightning and thunderstorms is yet another opportunity.

Tropical medicine and tropical agriculture are established areas of scientific research. In fact, the first premier research institute in the country is the Institute of Medical Research which has distinguished itself with many outstanding research outputs. The Serdang Agriculture College, predecessor to Universiti Putra Malaysia spearheaded the development of tropical agriculture in Malaysia. These formed the foundation for excellence in research in these areas and exemplified by the research outputs of RRIM (now LGM) and PORIM (now MPOB). The challenges for sustainable development are expected to result in further developments of high standard, not only in biological sciences but also physical sciences.

We hope that JOSTT will be the catalyst for scientific renaissance with regard to research on problems of the Tropical Region.

Academician Tan Sri Dr Augustine S.H. Ong
Chairman, Editorial Board

With the removal of excess stock the price can be stimulated to rise. A small removal of half a million t at year-end stock would stabilize price of palm oil.

5. Requirement to obtain valuable co-products. The palm oil biodiesel project is unique in that it can be used to produce carotenes (pro-vitamin A) and vitamin E as co-products.

Bioenergy from oil palm products

1. Requirement to move into bioenergy. The oil palm industry is in for an exciting time as far as the biomass bioenergy production is concerned [17]. Modern bioenergy technologies that can produce electricity, heat and solid, liquid and gas fuels are now available. The strategy is to use bioenergy resources that are renewable from the oil palm plantation to replace the fossil fuels. The biomass of the oil palm consists of the solid fractions of fibre, shell empty fruit bunches in the mill, trunk wood chip and fronds from the field, liquid biofuel from biodiesel and gas from the biogas generated from the methane from the effluent ponds.
2. Requirement to have large quantity of biomass for production of bioenergy. For the biomass to be used to meet the 3Fs objective, there must be a better scientific understanding of the process, the potential impact on society and the economic values attached to these impacts.

The total energy potential available from mills in the country is shown in Table 7. Based on the surplus biomass available the total energy potential is about 144.76 10^9 MJ, with the largest contribution coming from EFB and the least from fibre as most had been used to fire the boilers for energy production needed for the mill operations. The total energy potential could be considered for use in the various programmes such as Small Renewable Energy Project (SREP).

THE 10 RECOMMENDATIONS FOR POLICY REFINEMENT TO ACTUALIZE THE 3FS OBJECTIVE

The oil palm industry is at a crossroad again. With the global demand for food, fibre and fuel on the rise, there is an imposition on the oil palm planters who then have to consider what necessary actions would be implemented to sustain their welfare and income without degrading the environmental sustainability. It must be borne in mind that among the 3Fs only food has advanced well into the supply chain management compared with the fibre and fuel. Now besides food, the fibre and fuels would be optimally taken out from the same land. Agricultural development centers on the integrated use of natural resources such as soil, water, climate and biological diversity [19] that may be used for the production of the 3Fs. The integration of agricultural practices with management and the protection of ecosystem are to promote agricultural productivity and environmental sustainability.

In actualizing the vision of the 3Fs objective there are 10 recommendations for refinement of policy that need to be addressed.

1. Ensure equal participation at all four levels company, industry, nation and global

For a start, at the four levels of participation, viz. local company, industry, nation and global, the players are increasingly being confronted with policies, legal and institutional issues, intellectual property rights, exchange, transfer and trade in agriculture for actualizing the 3Fs objective [20,21]. The participatory processes and involvement of various stakeholders can help, particularly for the latter 2Fs of fibre and fuel production, to find answers to such concerns particularly those of developmental and environmental sustainability.

Table 7. Total energy potential available from mills.

Biomass resources	Quantity (10^{6t})	Calorific Value (MJ/Kg)	Moisture Level (%)	Total Energy Potential (10^9MJ)
EFB	15.180	6.0	65	91.08
Shell	3.795	18.8	10	26.30
Fibre (0.7% EFB)	10.626	10.0	45	4.78
Biogas (14.4 M^3/t FFB)	993.6 M^3	22.8	Methane 67% CO_2 33%	22.60

Source [18]

Towards this, it is crucial to develop a framework for a unified programme to enhance the diverse efforts within the four levels to tackle such developmental and environmental issues and made them well understood. Yusof [20] had indeed provided a firm strategy for global competitiveness for the Malaysian palm oil industry where the national programmes must collectively focus at the increasing competitions from future challenges in the international oils and fats market. There are a lot of mutual learning and sharing of information from the developmental and environmental issues from the food by the fibre and fuel producers. It is hoped that the fibre and fuel producers will catch up with the current knowledge attained by the food producers in terms of supply chain management. For the programmes of the 3Fs objective for food, fibre and fuel they should involve Government and their policies, public and private institutions, all plantation companies, the whole industry, NGOs, communities and individuals especially from the environmental and developmental sectors, and finally from the end users in the overseas countries.

2. Relook at agriculture and related policies

Once the necessary government bodies and institutions are aware of the vision of the 3Fs objective of the oil palm industry, it is crucial to develop and strengthen appropriate monitoring of policies and legislative measures to create an enabling environment for sustainable agriculture and rural development, and environmental sustainability of the oil palm industry along this 3Fs objective. Such an enabling environment would promote access by the smallholders to use their land to start their various agro-businesses involving the 3Fs. It would include activities such as collecting and producing fibre for supply to larger companies that collect it, better use of water resources and agricultural inputs. The enhanced land tenure and taxation incentives for companies to move quickly into these new agro-businesses would be accompanied with better protection for the indigenous knowledge and common intellectual property used in the agro-businesses. There is encouragement for adoption of the resource management systems to ensure that there is no over-exploitation of the land now that the 3Fs products are taken out by building local capacities for better management of such natural resources.

The government should consider and introduce new policies and necessary infrastructure development to expand the activities towards the 3Fs objective. Policies should stress on land reform like rehabilitating the steep and degraded land with the dense oil palm agroforests for biomass production rather than FFB yield per se. There must be well-defined enforceable land rights with security of tenure to move into oil palm agroforests purely to harvest biomass for fibre production. There should also be development of agro-ecological relevant technologies based on understanding of local conditions and resource management. R&D into oil palms should be balanced to meet the 3Fs objective.

3. Promote sustainable agriculture and rural development

Despite the new demand on the land, agriculture as practised is directly linked to the many facets of sustainable development including poverty eradication, sustainable consumption and production, management of natural resources, energy, fresh water, health, education, trade and market access as well as technology transfer and capacity building. Sustainability should be seen in the context of different agro-climatic zones and the indicators for sustainable development should be identified for actualization of the 3Fs objective.

The R&D effort should be directed to the integration of livestock and crop under oil palm so that food security is assured yet have capability to produce fibre and fuel. At the same time, it is critical that the industry continues to develop new technologies and implement them with the business approach aimed at high productivity through the 3Fs objective, environmental sustainability and social development.

4. Promote equitable distribution and access to supplies

The challenge to the oil palm industry is to ensure the physical supply of food, fibre and fuel to all importing countries. It is important that production is increased to ensure that food, fibre and eventually fuel in the longer term are available for export to other developing countries through a steady supply with reduced transport cost. At the national level, there should be an emphasis on economic access on the supply for all three food, fibre and fuel that meet the needs for sustainable livelihood and improvement of income of the growers through the multiple income-earning opportunities offered by the 3Fs objective.

5. Secure food security

The issue of food security is related to the whole 3Fs objective. The elimination of hunger and malnutrition

is not just a food problem but is related to poverty reduction and the opportunities offered by the 3Fs objective. This would need to look at the increase of the productivity throughout the value chain from production, processing, manufacturing, distribution and marketing of new products. Food security also involves population growth. Raising food output is essential but so is the slowing down of population growth and maintaining ecological balance to be considered equally important.

The major challenge to produce additional food, fibre and fuel must be accompanied by the conservation of the depleting natural resources. The attempts here by the oil palm industry to actualize the 3Fs objective by using the same oil palm land for the production of protein and carbohydrate through the livestock and crop integration should be supported as food security initiatives so as to strengthen the focus on a diversified food basket and not just oils and fats. Food security must not be based on market demand alone but rather on supply on self-reliance and sufficiency, and efforts by the oil palm industry as a whole.

6. Ensure appropriate application of research, science and technology

The impact of R&D on the 3Fs objective is decisive in that there should be monitoring, evaluation and improvement of field and mill operations when actualizing the 3Fs objective. An area-specific database of the natural resources should be developed and made available for planning, implementation, research and extension. Existing data information should be assembled, verified and put into a useful and easily accessible form. Such well-designed information technology package once developed should help serve as market information network together with other weather, pest and disease monitoring systems that could also be used as a storehouse of current technologies and practices for the realization of the 3Fs objective.

The farming system should be refined to achieve the 3Fs objective. It is best to harness the eco-technologies resulting from a blend of indigenous knowledge with frontier technologies. Such tools should include biotechnology, information and communication technology, GIS mapping, renewable energy technologies, management and marketing technologies. In the case of biotechnology, the bio-safety and bio-surveillance are considered as important factors. The 3Fs production should originate from the efficient and environmentally sound production technologies that conserve natural resources.

7. Recognising the value of biodiversity

The value of plantation or planted trees in relation to agricultural biodiversity would depend on what was previously present on the site and also on the type of landscape in which it occurred. The reforestation of degraded logged-over land and abandoned land with dense oil palm planting would produce the greatest benefit from such tree crop management. It is vital to recognize the intrinsic value of agricultural biological diversity lies in its ecological, social, economic, scientific education, cultural and aesthetic importance. In the oil palm plantations this agricultural biodiversity is being rediscovered to enhance the actualization of the 3Fs objective..

The high priority given to safeguarding as much of the existing unique and valuable agricultural biodiversity [19], both in the ex-situ collection of plant genetic resources such as the various oil palm germplasm collection, and through the in-situ conservation in their oil palm habitat such as the various soil types and locality, has led the oil palm plantations using the natural predators in the implementation of integrated pest management. Cooperation with the national programmes and international institutions to sustain *in-situ* and *ex-situ* conservation efforts need to be strengthened further. Efforts to catalogue and classify the vast agricultural biodiversity within the oil palm system with special emphasis of preserving species involved in IPM and other natural control is highly commendable.

8. Strengthen extension and capacity building mechanisms

Agricultural extension must focus on increasing production and productivity of the 3Fs in an economically and environmentally sustainable way. It must be done to strengthen rural livelihoods and rural communities. Extension services must result in positive changes in rural areas. This means helping the smallholders towards sustainability and increasing productivity. It also demands measuring the success in terms of their contribution to the achievement of the 3Fs objective. The extension services should also support a system that could meet the needs of information especially for the educated women and youth so that they are empowered with the new skill and techniques from the new agro-businesses that foster sustainable agriculture.

9. Promote awareness and education activities

National policies and planning should recognize that public awareness do play an important role in establishing a firm basis for the 3Fs objective to be fulfilled in a sustainable manner. Public awareness should be extended to all four levels of the local company, industry, nation and global arena. National strategies should strengthen the 3Fs objective for the target audiences, partners and tools for public outreach. Government and industry should encourage NGOs in raising public awareness with the 3Fs objective. It is important to organize public information programmes and public discussions that would help to share relevant work to publicize the 3Fs objective.

10. Create favourable economic climate

Agriculture has over time become a relatively unrewarding profession due mainly to the fluctuating price regimes, low level of value addition, abandoning of farming and increasing migration from the rural areas. With the 3Fs objective in place and the integration of livestock and crops, there will be corrective measures taking place to stem the tide of rural-urban migration and bring back a better image for agriculture. There are better opportunities available with the agro-businesses being started by the 3Fs objective. It will bring back the shine to agriculture. A favorable economic and supportive environment and management from the food, fibre and fuel agro-businesses will become the key pillars for promotion of sustainable agriculture and food security.

With increasing income and companies own investment in the production of the 3Fs products, these are new avenues provided to combat the current uneven playing field faced by palm oil as a commodity which had to face the distortions from the heavily subsidized agricultural productions of oilseed crops in developed countries. The 3Fs will open external and internal market reforms, backed by the government domestic market structure for the 3Fs products. This will create a favourable economic environment for agriculture so the rural populace involved in the 3Fs objective can better withstand the impact brought about by the globalisation and trade liberalization. The flexibility in determining the domestic agricultural policies and pricing arising from the 3Fs products will improve the productivity, enhance income levels, and reduce market fluctuations by ensuring stability prices. All these efforts are made to create a level playing field in the global marketplace

In the context of globalisation of the food market, growers can improve their own market with the downstream value added products arising from the 3Fs objective where the agriculture sector can now address its own production, pricing, distribution and access. With the agricultural food processing agro-business industries in place and with international health standards being promoted locally, this will facilitate international agreements for our food products that should allow the livelihood of the large agricultural dependent sector to start their own economic ventures overseas. Likewise the biomass-based entrepreneurship and the fuel sector agro-business should be promoted to generate wealth in the rural sector. In fact all the players along the whole value chain should be evaluated based on the indicators to monitor their performance as food, fibre and fuel processors, retailers service providers and distributors all the way to the end users.

DISCUSSION

In the effort to adopt sustainable development, the oil palm industry has moved the whole concept of sustainability forward by paying special attention to the development of the 3Fs objective based on better land use, land-use change and forest (LULUCF) activities. The replanting cycle of the oil palm fields up to 25 years offers biological mitigation of GHG through LULUCF and they are tackled by three strategies. They are: (1) conservation of existing carbon pools i.e. avoid deforestation in terms of production of palm oil due to its higher yield per ha over the annual oil seed crops; (2) sequestration by increasing size of carbon pools e.g. through afforestation and reforestation where the land is under semi-permanent tree canopy cover offered by the oil palm plantations; and (3) due to its fibre and fuel production they can be renewable substitution of fossil fuel energy by use of such biomass.

This approach is now taken seriously at all four levels at local company, industry, national and global where the agricultural policy is being reviewed to protect the emerging agricultural food, fibre, and fuel industries to ensure high quality food, fibre, and fuel products are available at modest prices.

During the past decade we have made inroads in agriculture. We brought on the fusion of space age technologies with other scientific facts and skillfully managed crop production system. Yields have started to be improved again and environmental protection enhanced. Most activities have benefited suppliers,

producers and consumers along the value supply chain. The contributions of the leaders and the followers are gratifying. The testimony will encourage the followers to step up the challenge of bringing agriculture to even greater height. This is to be spearhead by R&D along the following broad areas:

1. Improvement of crop yield. We need to evaluate the priority for the next decade how the 3Fs objective is to be fulfilled. Areas like biotechnology, site-specific precision agriculture, nutrient management planning, and influence of management would receive higher priority. They all lead to improvement of crop yield. We believe that this single overarching objective is critical to reducing unit costs for growers, meet global food needs and enhance environmental quality.
2. Crop quality and specific end use such as nutraceutical and functional foods to be incorporated into food use. Through the biodiesel fuel production pathway these phytonutrients are efficiently extracted.
3. Use of internet for effective dissemination of information more rapidly and in a more site-specific fashion so as to optimize the efficient use of the depleting natural resources.
4. Improvement of crop yield by narrowing the gap between attainable yield and realizable yield and what key practices, such as nutrient management planning to apply to narrow the gap.
5. To employ sound science to deal with issues on soil, water, air and environment.

Can oil palm agriculture system provide sufficient food, fibre and fuel for the world's growing population with the shrinking per capita land base? The answer is yes. The oil palm industry can do it, provided if science continues to develop new technologies that allow us to grow more per unit area of land and we remain committed to stewardship of the 3Fs.

Taken together the 3Fs objective provides the working perspective for us to contribute to the improvement of agricultural productivity, the economics and the environmental protection. Among the 3Fs, once the first F 'food security' is provided, people and their societies will develop in significant and meaningful ways to go beyond science, research, and education to use the second and third Fs of fibre and fuel to boost the real income of the society.

Finally we ask ourselves the question "Am I making a difference?" How well we do and in bettering the lives of people then we can start to address the issue of the 3Fs. We have good and dedicated researchers in oil palm. We have to replace the outdated policies and convince those people who are against change. Luckily there are enough positive people to harness together so that each positive individual contribution added together had resulted in an industry positive action. We need to replicate these positive people to reach out to others in science and education, in industry, in policy making and in plantation. That together we will make the difference.

CONCLUSION

Commitment to excellence characterizes the planting community. They all deserve a tip of the hat for their contributions they made to the industry, local community and the global economy. Agronomists and soil scientists are literally people with their feet on the ground and their hands on the soil. What they do brings progress to the society. We must not be slowed down by the limitation of the minds. Together we can challenge the limitation of the minds. Let us bring together teams of skilled, committed and experienced people from different disciplines and diverse background and as a team they are fundamentally important in moving agriculture forward, have sufficient food produced for nations and provide environmental security for our global village. What is critical to us is to challenge to actualize and fulfill the 3Fs objective by optimally exploiting the oil palm land.

REFERENCES

1. Chan K.W., Bek-Nielsen C. and Tek J. (2004) Sustainability of oil palm plantations – Present and future issues and solutions. Paper presented at the MOSTA 2004 Agronomy and Crop Management Workshop 6 on "Effective Oil Palm Agronomy" at MPOB, Bangi, 14 August 2004. 25pp.
2. *Yusof Basiron and Chan K.W. (2002) Going back to basic: Producing high palm oil yields sustainably.* Proc. ISP National Seminar on Going Back to Basic*: 3-17. Kuala Lumpur, Incorporated Society of Planters.*
3. *Yusof Basiron and Chan K.W. (2003). Enhancing competitiveness in the oil palm industry. In: E Pushparajah and Chee K H (Eds)* Globalisation and its Impact on the Oil Palm Industry, *Vol I (ed. E. Pushparajah and K.H. Chee) pp 271-299. Kuala Lumpur, Incorporated Society of Planters.*
4. *Bek-Neilsen, C. (2004). Replant or Perish.* Proc. 4th National Seminar on Replant or Perish*: 33-35. Kuala Lumpur, The Incorporated Society of Planters, Kuala Lumpur.*
5. *Rao V. (2004) Sustainable palm oil agriculture – between theory and practice. Paper presented at the* 4th National Seminar on Replant or Perish, *14-15 June 2004, Ipoh, Perak. Kuala Lumpur, The Incorporated Society of Planters. 25pp.*
6. *Yusof Basiron (2001) The role of palm oil in the global supply and demand equation. Paper presented at the 72nd World Congress of the International Association of Seed Crushers,* Industry Challenges for the 21st Century, *17-20 September 2001 Regent Hotel Sydney Australia. 20pp.*
7. *Yusof Basiron (2002) Use of biomass.* The Planter *78(916): 347-349.*
8. *Yusof Basiron (2002) Value additions to the oil palm industry.* The Planter *78(918): 479-482.*
9. *Yusof Basiron (2002) Future challenges of the palm oil industry: Global perspective. Paper presented at the* Malaysian Science and Technology Convention 2002 (MASTEC 2002)*, 9-10 September 2002. Kuala Lumpur, Academy of Sciences Malaysia. 19pp.*
10. *Stryker J.D. and Metzel J.C. (1998)* Meeting the food summit target: The United States contribution. *Agricultural Policy Project, Phase III. Research Report 1039. USAID Contract No. LAG-C-00-93-00052-00.*
11. FAO (2004) Food shortage in 35 nations. Associated Press as reported in New Straits Times 16 December 2004.
12. *Berck P. and Bigman D. (1993) The multiple dimension of the world food problem. In:* Food Security and Food Inventories in Developing countries *(ed. P. Berck and D. Bigman). Wallingford, CAB International.*
13. Yusof Basiron and Chan K.W. (2004) The role of R&D strategies in food safety, GAP, DMP and GDP in the Malaysian palm oil industry. Paper presented at the EUREPGAP ASIA 2004 Conference, Kuala Lumpur. 17pp.
14. Yusof Basiron, Nagendran B. and Noraini Sudin (2001) Food security in oils and fats for the Muslim world. Institute of Islamic Understanding Malaysia (IKIM) Seminar Food Security from the Islamic Perspective. Kuala Lumpur, IKIM. 15pp.
15. Palmoil Update (2005) January 2005 Vol.25 No 01/05. Malaysian Palm Oil Board, Ministry of Plantation Industries and Commodities, Malaysia. 64pp.
16. Third Agricultural Plan (1998-2010) Policy. Kuala Lumpur, Percetakan Watan Sdn Bhd. 265pp.
17. *Yusof Basiron (2005) Bioenery comes of age.* The Planter *(submitted).*
18. Ravi Menon (2005) Personal Communication. MPOB.
19. *Chan K.W. (2004) Agricultural biodiversity in oil palm plantations. Paper delivered at the* Forum on Oil Palm Industry and the Environment *held in Hotel Sandakan, 9-10 July 2004. 17pp.*
20. *Yusof Basiron (2003) Firm strategy for global competitiveness: A case study of the Malaysian palm oil industry. Paper presented at the Seminar on* Public-Private Collaboration in Science and Technology: Policy Development, Training and Awareness-ASEAN, *4-6 September 2003 Hanoi, Vietnam. 14pp.*
21. *Yusof Basiron and Chan K.W. (2004) Technology transfer in agro-industry. Paper presented at the* Agricultural Congress' Innovation Towards Modernised Agriculture, *4-7 October 2004 at Hotel Palace of the Golden Horses, Serdang. 16pp.*

Journal of Science and Technology in the Tropics (2005) **1**: 35-41

A brain-computer interface for control of a prosthetic hand

S. Y. Goh, S. C. Ng, Y. M. Phang, X. Y. Yong, E. Lim, A. M. Yazed and Y. Shuhaida
Department of Biomedical Engineering, Faculty of Engineering, University of Malaya,
50603 Kuala Lumpur, Malaysia

Received 25 April 2005; accepted 21 May 2005

Abstract Changes in EEG activity measured using electrodes placed at the scalp as a result of imagined motor action is used in a brain-computer interface (BCI) system to control a prosthetic hand. The BCI system is designed so that the bio-signal amplifier, filters and the analog to digital converter are grouped together in a data acquisition unit that communicates with the computer using standard communication protocols commonly found in palmtops, laptops and desktop computers. The two communication options provided are either a USB communication port or a wireless Bluetooth RS232 module. The BCI system was used to control 4 main actions of a prosthetic hand. Preliminary results show that the BCI system can be used successfully to select and control a prosthetic hand.

Keywords brain-computer interface – rehabilitation – prosthesis – hand

INTRODUCTION

People who have lost a hand through accident or amputation would need a prosthetic hand to restore some manipulative hand functions. It would be preferable that the prosthetic hand possesses a certain degree of intelligence, for example, one that can be controlled by intent. This has become possible because of recent advances in the development of Brain-Computer Interface (BCI) systems [1]. BCI systems provide communication and control capabilities to people with severe motor disabilities such as those that are completely paralyzed or "locked-in".

Changes in electrical potential as a result of brain activity can be recorded using electrodes that can be placed on the scalp, on the brain or in the brain. The first method is noninvasive and the latter two require invasive surgery to implant the electrodes on or in the brain. Brain signals obtained from electrodes placed on the scalp are in the form of electroencephalogram (EEG) signals. Electrocorticogram (ECoG) signals are obtained from electrodes place on the brain. Electrodes implanted in the brain provide cortical Neuronal Action Potentials. Because EEG electrodes are noninvasive, these electrodes are the most commonly used in BCI systems that are developed for communication or for controlling devices.

The types of brain signals that have been used in BCI systems are (a) Slow Cortical Potentials (SCP) [2-4] (b) Oscillations (ERD/ERS, μ and ^{2}) [1,5-8], (c) Evoked Potentials [9-12] and (d) Neuronal Action Potentials [13]. The brain can voluntarily produce spontaneous brain potentials such as the SCP, Oscillations and Neuronal Action Potentials. Evoked potentials are event related and are produced as a result of an external stimulus. Examples of evoked potentials are visual evoked potentials (VEP) or P300 evoked potentials (P300) that occur about 300 milliseconds after a stimulus.

It has been shown that there is an Event Related Cortical Desynchronization (ERD) and Event Related cortical Synchronization (ERS) of EEG signals obtained from electrodes placed at specific locations on the scalp as a result of actual and imagined hand movements [1].

Journal of Science and Technology in the Tropics (2005) 1: 35-41

MATERIALS AND METHODS

A BCI system for a prosthetic hand

The present BCI system consists of the following elements:

(a) Electrodes placed on the scalp
(b) A BCI box containing -An EEG amplifier and filter, An ADC , USB port/Bluetooth RS232 unit, A Fuzzy Logic Controller
(c) A computer containing -A main program Signal processing software
(d) A prosthetic hand

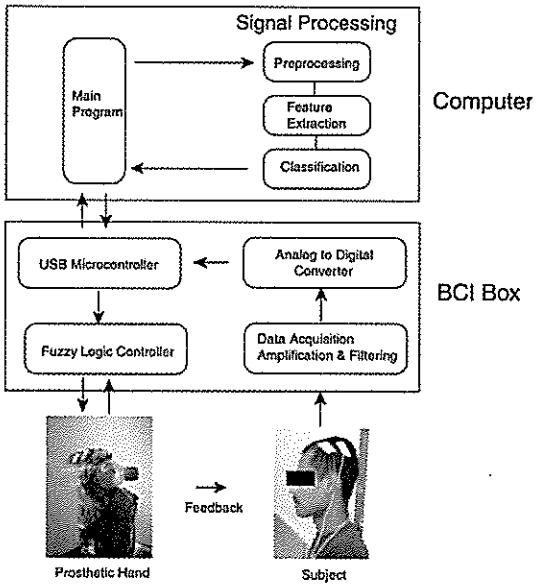

Figure 1. BCI with USB wire communication option.

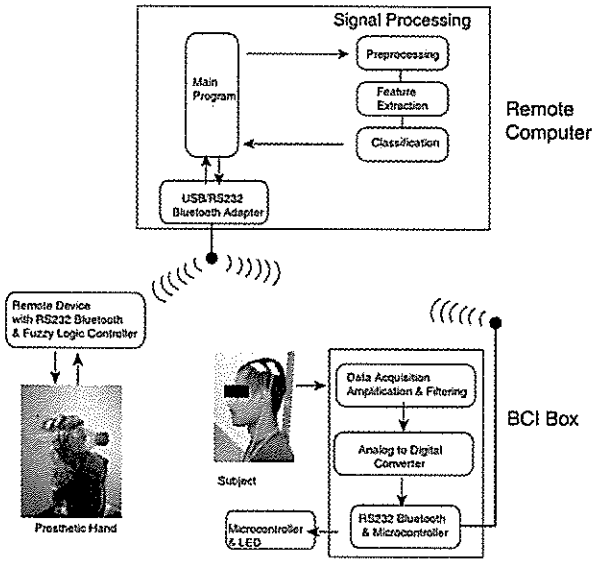

Figure 2. BCI with Bluetooth RS232 communication option.

Brain EEG signals are acquired through electrodes placed on the scalp of a subject.

In the BCI box, the EEG signals are amplified and filtered to remove the unwanted bands of frequencies. The filtered signals are fed into separate analog-to-digital converters to be digitized. The digitized data are communicated to a computer through either a universal serial bus (USB) wire or a wireless Bluetooth RS232 unit.

Signal processing, feature extraction and classification of the signals are carried out in the computer. The classification results are sent out either through the USB port or the wireless Bluetooth RS232 unit to the Fuzzy Logic control to drive the prosthetic hand or other remote devices.

The present BCI system is designed so that the BCI box communicates with the computer through standard communication protocols commonly found in palmtops, laptops and desktop computers. The two communication options provided are either a USB communication port (Fig.1) or a wireless Bluetooth RS232 capability (Fig.2). This is selected so that the BCI can be designed to be independent of the processing unit - the computer. As and when more compact and more powerful portable computers become available, they can be used as the processing unit of the BCI as long as they possess a USB port. Alternatively, a desktop computer may be used and placed within the wireless Bluetooth RS232 communication range which is about 20 metres in an enclosed environment.

Data acquisition, amplification and filtering

EEG signal properties

The intensity of brain signals recorded using scalp electrodes range from 0.5 to 100μV. The frequencies of these brain waves range from 0.5 to 100 Hz. Electrode skin impedance is usually between 1 kΩ to 10 kΩ. EEG amplifiers must have very high input impedances, typically above 10 MΩ, so as not to degrade the signal [14].

The EEG amplifier

The bio-signal amplifier board that is developed has 4 channels - 2 channels for EEG signals (¼V range input) and 2 channels for EOG or EMG artifacts (mV range input). Should there be a need for more channels, additional boards may be added.

The bio-signal amplifier is a bipolar amplifier with a sufficiently high differential DC input range even when high amplifier gain is used [15]. DC suppression is implemented by feeding back the integrated output to its negative input. A driven-right-leg (DRL) circuit is used to provide a return path for bias currents of the input stage op amps and to reduce common mode interference in signal [16].

Analog to digital converter and USB port/bluetooth RS232 communication

The analog signals are digitized in a 16 bit analog to digital converter (ADC) at a sampling rate of 256 Hz for each channel. A microcontroller on the ADC board is programmed to read the data from the ADC and to transmit the data to the computer via a USB wire or a Bluetooth RS232 communication unit.

For wireless operation on computers that do not have built in Bluetooth capability, a Bluetooth USB Dongle is connected to the USB port of the computer to enable communication with other Bluetooth devices. Data sent from the Bluetooth module at the BCI box are received through a designated virtual COM port in the computer.

After the data has been processed and classified in the computer the results of the classification are communicated via the USB wire or the Bluetooth Dongle to the fuzzy logic controller to control the prosthetic hand.

EEG processing system

The signals acquired by the computer are digitally filtered from 5-40 Hz by an elliptic bandpass filter to reduce noise. Then, the autoregressive, AR model order 8 are found for every 1 second (256 data) with no overlap. The mathematical equation of an AR process is shown in Equation **(1)**.

$$y[n]=\sum_{k=1}^{p} a_k\, y[n-k]+w[n] \qquad \textbf{(1)}$$

where $y[n]$: current output; $w[n]$: white noise with mean zero; variance σ^2; a_k : AR coefficients; p : AR model order.

Linear Discriminant Analysis (LDA) is used as the classifier in the present study because it is simple and robust. Furthermore, it requires smaller training samples to estimate its coefficients [17] and it does not assume that the populations are from multivariate normal distribution [18]. However, the LDA does assume the populations have a common covariance matrix. Therefore, the sample pooled covariance matrix, S^{-1}_{pooled} is used.

The LDA coefficients can be obtained by maximizing the variance between populations. The mathematical formula is shown in Equation **(2)**.

$$\max_b \frac{(b'(\bar{x}_1-\bar{x}_2))^2}{b'S_{pooled}b} = (\bar{x}_1-\bar{x}_2)'S^{-1}_{pooled}(\bar{x}_1-\bar{x}_2) \quad \textbf{(2)}$$

where $\bar{x}_i$ = sample mean of group i, i=1,2;

b = LDA coefficients = $(\bar{x}_1 - \bar{x}_2)' S^{-1}_{pooled}$;

$b_0 = \log(\frac{n_1}{n_2}) - \frac{1}{2}(\bar{x}_1 - \bar{x}_2)' S^{-1}_{pooled} (\bar{x}_1 + \bar{x}_2)$

For a new observation x, the allocation rule of Fisher's LDA is as follow:

Allocate x to group 1 if $b_0 + bx > 0$ OR
Allocate x to group 2 if $b_0 + bx < 0$

The prosthetic hand and fuzzy logic controller

The prosthetic hand is designed to replicate the appearance and performance of a natural hand as closely as possible. Figure 3 shows the 4 main desired actions of a prosthetic hand are *the Grab, the Pulp to Pulp Pinch, the Tripod Pinch and the Key Pinch.*

A parallel 6-plate design was used for the finger to represents distal, proximal and middle segments accordingly. The sizes of the plates are fabricated based on the Fibonacci sequence except for the little

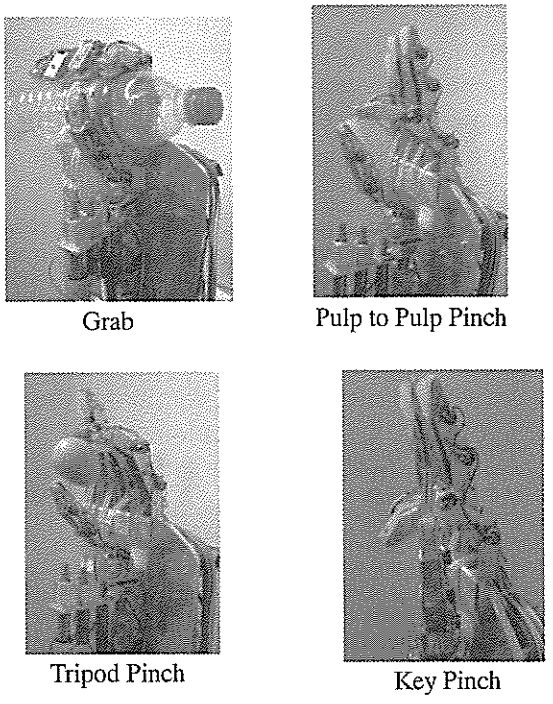

Figure 3. The 4 desired actions of the prosthetic hand.

finger [19]. The two adjacent segments are interconnected by a hinge joint. This arrangement provides 3 degrees of freedom (DOF) for flexion–extension of each finger. Three DC motors are used to actuate the finger flexion–extension movement, each segment requiring one motor. A flexible cable is used to pull the segment for flexion. Extension of the finger to its original extended position is accomplished by the use of a return helical spring. The thumb has 4 DOF and uses six parallel plates, representing the distal, proximal and metacarpal segments. The metacarpal segment gives the thumb the ability to perform abduction–adduction movement. The thumb requires the use of 4 motors including one for rotation.

The prosthetic hand is controlled by Fuzzy logic controllers with a distributed control monitoring system. A H-bridge switch provides speed and bi-directional control to each motor. The control is accomplished by adjusting the PWM duty cycle and a directional signal to the H-bridge. Sugeno Defuzzification technique is used to provide the *PWM duty cycle* value and the direction of the DC motor [20]. The membership functions are tuned until a good response is achieved. Each finger is monitored and controlled by a separate microcontroller. Positioning control feedback is accomplished by mounting potentiometers at the finger hinge joints between the finger segments. The potentiometers provide the relative angular displacement of adjacent segments of the finger. Each finger is also equipped with a tactile sensor placed on the fingertip for pressure feedback.

EEG recording

Two 24 years old right-handed female subjects participated in this study. The experiments were conducted in an air-conditioned room without any electric or magnetic shielding or soundproof system. The subject was seated comfortably on a chair with armrest. Each subject looks at a computer monitor about 100 cm in front of her.

Online experiment

The online experiments are conducted using the present BCI system. There are 2 channels on the ADC board that are used to collect artifacts that can be used to verify that the artifacts are not inadvertently being used to control the BCI system. Earlier offline analysis results showed that, for both subjects, one bipolar electrode derived from aCz and Cz in Figure 4 is sufficient to obtain EEG data that can be used to classify Left Hand and Foot Movement.

Generally, there are two phases in the experiments conducted using online system. They are the classifier set-up, the subject-training and application phases (Table 1).

In the classifier set-up phase, the experimental paradigm is similar to the one used in the offline experiments except that only two types of imagined movement (leg and left hand) are used. There are 3 sessions in the classifier set-up and the resting interval between two sessions is 2-10 minutes. Each

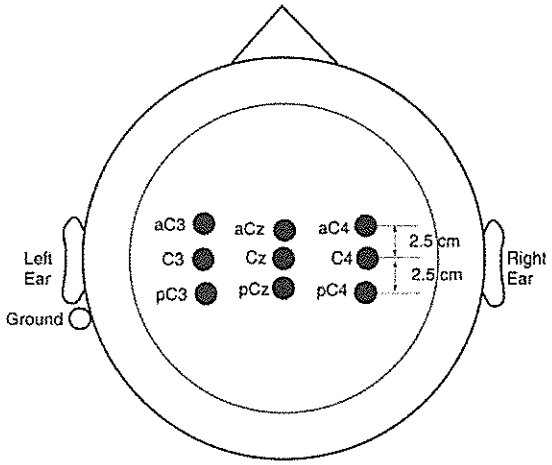

Figure 4. aCz & Cz montage.

Table 1. Description of the classifier set-up, subject-training and application phases in the online experiments.

Phase	Description
Classifier set-up	EEG trials were collected to set up the classifier. No feedback was provided.
Subject training	The LDA set up in the classifier set-up phase was used to classify the EEG trials. The EEG signals were classified only during the time window when the user was given command by the computer.
Application	Application phase was conducted on subject who could achieve at least 80% accuracy in the subject training phase. The ongoing EEG signals were classified and the subject would decide when to activate the desired control device.

session consists of 40 trials (20 trials for each imaginary task). After collecting the data for 120 EEG trials, the data are filtered before finding its AR coefficients. The LDA classifier template is then set up based on the AR coefficients. The computational time for each classification is less than 1 second for a Pentium 4 (2.4GHz) computer.

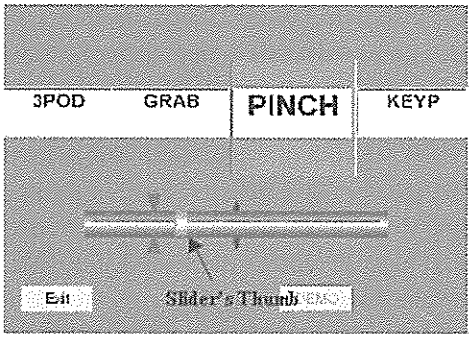

Figure 5: GUI used to select the 4 desired hand movements.

The subject-training phase allows the subject to practice thinking in the "proper" manner to achieve a better control of this system. The experimental paradigm is similar to the one used in classifier set-up phase. The EEG signals are processed and classified by the LDA set up once every second. The result of each classification is fed back to the subject in the form of a slider's thumb movement. The thumb would move one step to the right/left if the output of the LDA were FOOT/LEFT. After each trial, the thumb would move back to its original position (center position of the slider bar).

After the subject is able to consistently achieve success rate more than 80% in the subject-training phase, she will proceed to the application phase that will enable the user to activate the LED's on the ADC board or to select any of the 4 movements for the prosthetic hand. An example of the GUI designed for the application phase is as shown in Figure 5.

Table 2. Results of success rates (%) from the synchronous subject-training using USB wire communication.

	Subject 1 Experiment									
Session	1		2		3		4		5	
	F	L	F	L	F	L	F	L	F	L
1	70	100	90	100	90	90	100	100	100	100
2	60	80	90	90	100	80	100	80	67	80
3	90	90	70	100	100	100	100	90	100	97
4	70	90	70	80	90	100	100	100	100	100
5	70	100	80	100	70	100	100	80		
6	90	100	100	90	90	100	100	70		
7	70	100	90	90	90	100				
8	30	90	100	100	100	100				
9	40	100								
Average	80.0		90.0		93.8		93.3		94.0	

Table 3. Results of success rates (%) from the subject-training using wireless Bluetooth RS232 communiction.

Session	Subject 1 Experiment				Subject 2 Experiment	
	1		2			
	F	L	F	L	F	L
1	58	100	100	58	62	92
2	30	100	100	64	58	94
3	80	91	100	83	70	100
4	75	90	73	92	86	100
5	80	91			60	100
6	90	91			60	100
Average	82.4		83.8		83.3	

F: Imagined foot movement; L: Imagined left hand movement

Journal of Science and Technology in the Tropics (2005) 1: 35-41

RESULTS AND DISCUSSION

The BCI system performance in the subject-training phase

Table 2 shows the success rates of the present BCI system (using USB wire communication) to identify the intent of subject 1 during 5 experiments conducted on different days. Table 3 shows the success rates of the BCI system (using wireless Bluetooth RS232 communication) to identify the intent of both subjects during the subject-training phase.

The BCI system in the application phase

In the application phase, the subject is *talked through* to select a desired action of the prosthetic hand. This is repeated until the subject has successfully selected all the 4 desired prosthetic hand actions. The above experiments were conducted initially using the USB wire and later the Bluetooth RS232 communication systems. Video recordings of these experiments were made.

To confirm bi-directional Bluetooth RS232 capability during asynchronous mode, the subject was asked to select one of four LED's on the ADC board. This was achieved successfully. As a test of operating a remote device, the prosthetic hand fitted with a Bluetooth RS232 communication module was placed 6 metres away from the computer controlling the BCI system and in an adjacent room. The subject was able to select the desired hand action and activate the remote prosthetic hand. For future studies, a randomly generated sequence of selections of all the 4 desired hand actions will be displayed on the GUI and the time taken to complete the selection of the sequence will be recorded. It is to be expected that the time taken to complete the selection of all the desired hand actions will become shorter as proficiency in using the BCI system improves.

Work is also currently being carried out to build a small LCD display that will mimic the computer monitor displaying the selection GUI. This LCD display will provide the selection options as well as feedback for the BCI system. In this manner, the computer fitted with Bluetooth RS232 capability may be kept at a remote place and plugged into a mains power supply. The LCD display together with the Bluetooth enabled BCI box will form the mobile BCI that will accompany the subject. This arrangement will reduce the battery power requirements for a mobile BCI system.

These preliminary studies on the present asynchronous BCI system to control a prosthetic hand show good promise. Further improvements to the system are now necessary to improve the speed and success rate of the system. Another element that needs to be looked into is what type of mental training will improve the capability of the subject to control his/her brain signals in a way that can be used in a BCI system.

REFERENCES

1. Wolpaw J.R., Birbaumer N., Mcfarland D.J., Pfurtscheller G. and Vaughan T.M. (2002) *Clinical Neurophysiology* **113**: 767-791.
2. Birbaumer N., Hinterberger T., Karim A.A., Kubler A., Neumann N. and Veit R. (2004) *Proceedings of the 2nd International BCI Workshop and Training Course 2004,* 17-18 September 2004, Graz, Austria, 1-4.
3. Hinterberger T., Mellinger J. and Birbaumer N. (2003) *Proceedings of the 1st International IEEE EMBS Conference on Neural Engineering*, Capri Island, Italy, 2003. 603-606
4. Birbaumer N., Hinterberger T., Kubler A. and Neumann N. (2003) *IEEE Transactions on Neural Systems and Rehabilitation Engineering* **11**(2): 120-123.
5. Guger C., Edlinger G., Harkam W., Niedermayer I. and Pfurtscheller G. (2003) *IEEE Transactions on Neural Systems and Rehabilitation Engineering* **11** (2): 143-147.
6. Wolpaw J.R., McFarland D.J. and Vaughan T.M. (2000) *IEEE Transactions on Rehabilitation Engineering* **8** (2): 222-226.
7. Pfurtscheller G., Neuper C., Guger C., Harkam W., Ramoser H., Schlogl A., Obermaier B. and Pregenzer M. (2000) *IEEE Transactions on Rehabilitation Engineering* **8**(2): 216-219.
8. Pfurtscheller G., Neuper C., Muller G.R., Obermaier B., Krausz G., Schlogl A., Scherer R., Graimann B., Keinrath C., Skliris D., Wortz M., Supp G. and Schrank C. (2003) *IEEE Transactions on Neural Systems and Rehabilitation Engineering* **11**(2):177-180.

9. Krepki R., Blankertz B., Curio G. and Muller K.R. (2003). *9th International Conference on Distribute Multimedia Systems* (DMS'03).
10. Birch G.E., Mason S.G. and Borisoff J.F. (2003) *IEEE Transactions on Neural Systems and Rehabilitation Engineering* **11**(2): 123-126.
11. Farwell L.A. and Donchin E. (1988) *Electroencephalography and Clinical Neurophysiology*. **70**(6): 510-523.
12. Donchin E., Spencer K.M. and Wijesinghe R. (2000) *IEEE Transactions on Rehabilitation Engineering* **8**(2): 174-179.
13. Kennedy P.R., Bakay R.A., Moore M.M., Adams K. and Goldwaithe J. (2000) *IEEE Transactions on Rehabilitation Engineering* **8**: 203-205.
14. Webster J.G. (Ed.): *'Medical instrumentation: Application and design'*, John Wiley & Sons, New York, pp 156-175,183.
15. MettingVanRijn A.C., Peper A., Grimbergen C.A. (1994) *Med. Biol. Eng. Comput.* **32**: 305-310.
16. Winter B.B. and Webster J.G (1983) *IEEE transactions on BioMedical Engineering* **30**(1): 62-65.
17. Pfurtscheller G., Neuper C., Schlogl A. and Lugger K. (1998) *IEEE Transactions on Rehabilitation Engineering* **6**(3): 316-325.
18. Kong X. (1997) *Proceedings-19th International Conference-IEEE/EMBS*, 1997, pp. 1215-1217.
19. Park A.E., Fernandez J.J., Schmedders K. and Cohen M.S. (2003) *The Journal of Hand Surgery* **28**(1): 157-160.
20. Reza L. and Dongyoon H. (2001) *Intelligent Control: International Proceedings of the 2001 IEEE*, pp. 337-342.

Journal of Science and Technology in the Tropics (2005) **1**: 43-49

Experiment with single surface atoms by use of atomic resolution microscopy

Tien T. Tsong
Institute of Physics, Academia Sinica, Taipei, Taiwan 11529

Received 16 March 2005; accepted 1 April 2005

Abstract The field ion microscope (FIM), and the atom-probe FIM are the two most instruments of atomic resolution microscopy, namely the atomic resolution imaging of the sample and the chemical analysis of pre-selected sample atoms, for the first time in scientific history. For the atom-probe, unfortunately the analysis is destructive to the sample. As Müller was focused on inventions, I thought I should devote my scientific career on the use of atomic resolution microscopy for the true atomic scale study of surface phenomena. As microscopy progresses, now both electron microscope and scanning probe microscope have also achieved atomic image resolution. STM may one day be able to do non-destructive chemical analysis of surface atoms using thermally stable and chemically inert single atom sharp tip through electronic density of states mapping of the surface or selected atoms. Here, I will discuss how FIM studies have instigated some later studies of scanning tunneling microscopy in surface and nano science applications.

Keywords atomic resolution microscopy – single surface atoms

INTRODUCTION

Two important aspects of atomic resolution microscopy are the imaging and chemical analysis aspects [1,2]. Historically the field ion microscope and the Atom-Probe FIM, both invented by Erwin W. Müller, are the first microscopy to achieve atomic resolution in both aspects. By 1955, FIM succeeded in revealing the atomic arrangement of a tungsten tip surface. As to the chemical identification, it was first attempted from the image contrast of surface atoms in ordered alloys, but finally succeeded with the invention of a new instrument know as the Atom-Probe FIM. The major application of these instruments is now in the study of metallurgical problems. I will present here with a few examples in surface and nano science applications that field ion microscopy has also stimulated the progress of many studies by other atomic resolution microscopy, especially scanning probe microscopy. In addition, I will discuss a principle of nondestructive STM chemical mapping of the sample surface or selected surface atoms.

SOME APPLICATIONS IN SURFACE ATOM DYNAMICS

Random walk of single atoms and clusters

An important application of the FIM to surface and nano science is the study of surface diffusion of single atoms and small atomic clusters by direct observation of particle displacements [3]. The possibility of observing single atom diffusion was recognized by Müller quite early [4]. In 1966, Ehrlich and Hudda started such studies by direct observations of single atom movements using random walk analysis [5]. Bassett followed by extending the study to adatoms of different metals using the same method [6]. In 1968, he observed clustering of adatoms [7], to isolated effects of atomic interactions. Later Tsong started to control the number of adatoms deposited on a facet [8]. As an atomic jump last ~10^{-12} sec, tracking with a time constant of ms [9] or s should not make a significant difference. I also found the cooperative walk of adatoms in the neighbor surface channels of the W(112) surface. In random walk (RW) studies of single atoms and small atom clusters,

information sought includes diffusion parameters such as activation barrier heights and frequency factors, and jump length and displacement distributions [3]. Additional information of great interest is the diffusion mechanism, or how an adatom or a cluster moves, etc. While extremely detailed information can be derived, FIM experiments are always limited by the kind of material systems and the size of the sample surface available for experiments.

A TEM image represents the cross sectional view of a sample. Whereas direct observation of an atom at a knife-edge of a sample or on a suspended nano-wire or nano-tube can be done, it is not easy to perform a quantitative study of surface diffusion of an atom on such a sample. STM, on the other hand, can be used to directly observe the motion of single atoms or clusters or molecules on the surface [10]. The material limitation is much less stringent, and the surface area can also be much larger. In its early development, diffusion data were mostly derived from observation of the temperature dependence of the island size distribution from which diffusion parameters are derived based on complicated theoretical analyses or numerical simulations [11]. However, as the time goes on, it is now well developed that direct observations of single particle random walks can be done on diversified systems, including single atoms, molecules and atomic clusters, of a wide range of sizes on surfaces of many materials [12]. Methods of data analyses are also much more diversified. It is possible to use theoretical models of epitaxial growth to derive not only parameters for growth, but also diffusion parameters. One would have to be aware though such methods are not direct, but may in fact sensitively dependent on the validity of the model used. The validity of the model is not easy to ascertain when too many parameters are involved in the model.

There are many advantages of the STM in surface diffusion studies as compared with the FIM. Not only most surface atomic sites are revealed in the image, but the materials applicability is much wider. With an STM, direct observations of random walk diffusion of individual atoms and molecules can be done on diversified systems, including gaseous and biological molecules on metal and semiconductor surfaces. I would just mention our own study of O_2 on the Si(111)-7x7 surface where site and path specific diffusion parameters have been obtained [13]. Based on both STM image analyses of intermediate states and a theoretical study [14], a tumbling mechanism of molecular diffusion of O_2 on the Si(111)-7x7 surface has been proposed.

Random walk under a driving force

When there is a driving force, or there is a gradient in the chemical potential, an adatom will perform random walks with its movement biased toward the direction of the force, or the direction of lower chemical potential. The driving force can be produced by a field gradient or by atomic interactions. On the facet of a field ion emitter surface under the imaging field, the applied field is higher by ~15 % near the edge of the (110) step of a W field ion emitter than at the center of the facet. This field gradient will induce a directional motion of an adatom from the central area of the facet toward the step edge area, as first observed and interpreted by Tsong and Walko [15], and later used for deriving the surface polarizability and dipole moment of 5d transition metal adatoms on the W(110) surface [16].

A field gradient induced directional motion of adatoms is the cause for a field forming effect of a field emitter tip, or the sharpening of a tip while it is heated by the field emission current [17,18]. A similar effect produced by both a field gradient and an intrinsic atomic interaction can be used to move an adatom at a surface to a desired location using the STM tip [19], a technique known as atomic and molecular manipulation [20]. In fact, field evaporation can be used to transfer atoms between the tip of an STM and the sample surface [19]. A similar effect was observed in a study of a sample heating current polarity biased diffusion of Si magic clusters [21]. It is found that when a Si(111)-7x7 surface is heated to ~450 ÚC, clusters of a definite size, having 9 to 15 atoms, can detach from and re-attach to the edge of a lattice step. They move preferentially in the direction of the heating current. This dynamic behavior can be directly observed with an STM. This observation immediately identifies the effect of electromigration of Si magic clusters at that temperature. Whether or not the magic cluster accumulates a sufficient net charge to produce such a large chemical potential gradient needed of this biased migration is still a mystery. Nevertheless the importance of a chemical potential gradient driven motion of adatoms and clusters in electromigration as well as in atomic manipulation is now being well recognized.

Adatom-adatom interactions

Inside a metal, an impurity atom can scatter electrons, thus perturbing the electronic charge density distribution in an oscillatory manner around the impurity atom, known as Friedel oscillation. A similar effect should occur at the surface of a metal. In 1972, based on combination of a random walk analysis and the dissociation energy of a diatomic cluster, it was concluded that the interaction potential between two Re adatoms on the W(110) exhibited at least a repulsive region and an attracted region, or the pair potential is non-monotonic in distance [8]. This was first assumed to arise from Friedel oscillation, but later learned of the indirect adatom-adatom interaction discussed by many eminent theorists [22,23]. Further measurements of pair distributions reveal the very weak and long range oscillatory nature of adatom-adatom interactions [24,25], but reliable quantitative data were very difficult to derive without the modern convenience of a PC image digitizer. When this became available, Watanabe and Ehrlich could derive data of greater precision, revealing the directional nature of the pair interactions [26]. Despite great efforts, the long-range nature of indirect electronic interactions could be observed, but their quantitative distance dependences could not be established.

The adsorbed atoms usually do not aggregate into a closely packed layer, but rather form a superstructure, is because of the existence of a repulsive region in the adatom pair interaction. In principle, an adsorption layer superstructure should be correlated to the pair interaction. However, the accuracy of the pair interaction obtained was not good enough to predict the adlayer superstructure. A different method was used by Tsong and Casanova to find this correlation [27]. They observed the relative abundance of different pair configurations, same as the atomic configuration distribution coined later by Österlund et al. [31] of Si on the W(110) from which the pair potential at small distances was obtained. From such data it was possible to predict that an adsorption layer superstructure should be formed which was later confirmed by a direct observation.

Several groups of investigators have succeeded in deriving the potential of mean force for adatom-adatom interactions using STM [28-30]. In the low adatom density limit, this potential approximates the pair potential well. As STM samples have a much larger surface area with many adatoms, statistically reliable sets of data are much easier to collect. In addition, long range interactions can be probed with a much greater precision, thus even the asymptotic form of the functional dependence could be derived over a larger distance. The pair interactions derived could be directly correlated to the adlayer superstructures also. This latter correlation could also be found by measuring the atomic configuration distributions [31]. Whether or not many body effects have to be taken into account depends of course on the material system and the size of the super lattice formed.

CHEMICAL ANALYSIS OF SINGLE SURFACE ATOMS

Image contrast

An attempt to distinguish atoms of different chemical species was successfully done for ordered binary alloys PtCo and Pt_3Co [32,33]. It was found that in these alloys, Co atoms were not imaged. Therefore many defects and domain structures of the ordered alloys such as anti-phase and orientation domains, could be clearly identified. In partially ordered alloys, Pt atoms tend to form one-dimensional chains in a certain crystallographic direction [34]. In other words, clustering of a chemical species can be studied also. Later, it was found by various investigators that in other ordered alloys, one of the species could either be invisible, or could give rise to a much dimmer image [35]. Such image characteristics can therefore be used to distinguish the chemical species.

What is most interesting is that in STM, different chemical species in ordered alloys can also give rise to different image contrast [36,37]. Thus it is possible to determine the composition of the top surface layer by counting the number of atoms of the alloy species. It is also possible to detect clustering of an atomic species as that found in the FIM. Again, the advantage of STM is the much larger scanned area. Not only statistically reliable amount of data can be more easily collected, the material applicability is also much wider for the STM.

Chemical analysis

In field ion microscopy, chemical analysis of sample atoms can be done by the ToF atom-probe FIM though unfortunately destructive. This capability of FIM is still unique to atomic resolution microscopy. With the development of 3D Atom-Probes, this power can only improve with time [38-40]. A good application of the

atom-probe for studying surface and nano science problems is the composition depth profiling of binary alloys in alloy segregations. As field evaporation of metallic samples usually proceeds from the edges of a surface layer, I realized that a procedure of composition depth profiling was to aim the probe-hole at the edge of a surface layer, and then slowly field evaporated the layer. When the size of the layer gradually decreased, the probe-hole was adjusted accordingly. Once the top layer was gone, the probe-hole was then aimed at the edges of the second layer. In so doing, both the step edge effect in surface segregation and the true composition depth profile could be obtained [41,42].

The first ToF atom-probe absolute composition depth profile measurement with true atomic layer depth resolution was reported by Ng et al. in a study of surface segregation of a Ni-Cu alloy [41,42]. Since then a number of other studies have been reported. Some of the interesting results are the composition can oscillate with the depth of the surface layers, and co-segregation with sulfur atoms can reverse the segregation species [43]. Atom-probe studies were able to correct results of some of the earlier studies using other techniques such as AES where not only depth resolution was limited, depth profiling by ion bombardment produces additional atomic mixing effect that further deteriorates the depth resolution. In LEED and photoemission spectroscopy, with the advancement in computational techniques, it is claimed that composition depth profiles can now be derived with sufficient accuracy and Gauthier et al. has reported an oscillatory composition depth profile of Pt-Ni alloys [44].

The question is whether atom-by-atom chemical analysis can be done with other atomic resolution microscopy. In transmission electron microscopy, with the improved special resolution and the sensitivity, it is now possible to observe single atoms in an atomic wire or a nano-crystal suspended by a carbon nanotube. As the electron beam becomes better and better focused, it is likely that single atom chemical analysis of such atoms can be achieved fairly soon. On the other hand, for a single atom chemical analysis of a more natural surface, this author cannot see how to solve the electron scattering problem where signals can come from a region having the size of the electron mean free path.

In scanning tunneling microscopy, in principle, chemical analysis of single atoms can be done by measuring the electronic density of states of each atom. As can be seen form Fig. 1, the tunneling current density J should be proportional to [45,46],

$$J \propto \int_0^{eV} \rho_t(E_F - \varepsilon)\rho_S(E_F - eV + \varepsilon)T(d, eV)d\varepsilon.$$

In this equation, ρ_t is the electronic density of states of the tip, ρ_s is that of the surface, and $T(d, eV)$ is the electron tunneling probability. If ρ_t is a delta function, or if ρ_t and $T(d,eDV)$ are nearly constant, then

$$\frac{dJ}{dV} \propto \rho_S(E_F - eV).$$

In other words by measuring dJ/dV vs. bias voltage V, the density of states of a sample atom can be derived provided, of course, that the STM tip is really atomically sharp. On the other hand, even if these conditions are not met, as long as ρ_t is either a smooth function or d-function like, the detailed structure of ρ_s may still help identify the chemical species of the surface atom provided again that the probe tip aims at the specified surface atom. In other words, in principle atomic resolution chemical mapping of the sample surface can be done provided we have a stable single atom sharp tip of known apex atom.

It is possible to create a thermally and chemically unstable single atom sharp tip with a rather complicated procedure, i.e. by combination of applied field and high temperature heating [17,18]. What is most important is really creating a thermally stable and chemically inert single atom sharp tip. We have recently succeeded in using a surface and nano science technique [47,48] to create an atomically sharp tungsten pyramidal tip which is covered with a physical monolayer of chemically inert Pd or Pt or Rh atoms. We are planning to use an ultra high vacuum FIM-STM-TEM system to first characterize the tip by FIM and TEM. Then the tip is used for an STM scanning and spectroscopy. During the density of states mapping of the surface or a selected atom, the tip is continuously monitored with the TEM, or checked again afterward. This procedure is illustrated in Figure 2. In this way, the chemical analysis of a specified surface atom could be achieved without destroying the surface by field evaporation. Whether we can succeed or not will depend on the skill of the operator, but the principle is quite clear. The advantage of the atom-probe is that inside atoms can be analyzed, but of course the analysis is destructive to the tip shape sample.

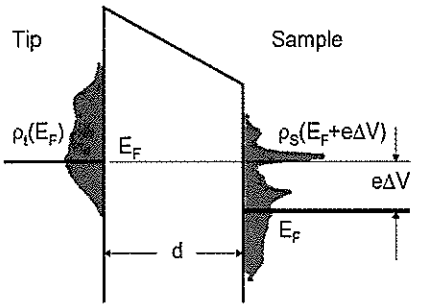

Figure 1. Principle of atomic resolution chemical analysis of the sample surface by a density of states mapping of the surface with a single atom tip of known apex atom.

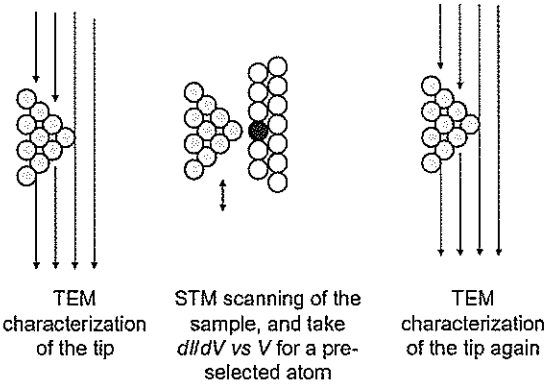

Figure 2. A procedure for chemical mapping of the surface, or a selected surface atom, through electronic density of states measurement. A combination of STM and TEM is a viable method.

OTHER APPLICATIONS TO SURFACE AND NANO SCIENCE

Stability of cluster ions

After magic clusters were found for xenon and alkali atoms [49,50], I used high power laser pulses to stimulate field evaporation for studying the relative abundance of cluster ions of covalent bond materials silicon and carbon [51,52]. It was found that for Si, even number cluster ions are more stable than odd number cluster ions. For C, the reverse is true. Similar studies were later done with a laser ablation method [53]. Theoretical studies confirmed our results [54,55]. Another interesting problem is the smallest size of a stable doubly charged ion. For inert gas cluster ions, if the size is too small, Coulomb explosion of the cluster ion can occur [56]. On the other hand, I was able to establish the stability of Mo_2^{2+} ions [57], the smallest of doubly charged cluster ions.

Field dissociation of compound ions

Field dissociation by atomic tunneling was originally predicted to occur by a theoretical calculation for light compound ions such as H_2^+ or HD^+ where one of the atoms could tunnel out of the ion in an applied electric field [58]. The applied field can distort the binding potential curve similar to that in field electron emission. This effect was used later to explain a long tail observed in the ion energy distribution of hydrogen ions in field ionization mass spectral lines [59]. Unfortunately a tail can be produced by many effects. One unavoidable effect is the poor resolution of the spectrometer and the other is the further ionization of H_2^+ ions followed by Coulomb explosion. In that early experiment, everything was speculative and nothing new was learned.

A truly remarkable discovery which could be explained in terms of field dissociation came from a study of the formation of $HeRh^{2+}$ ions when a Rh tip is field evaporated in ~10^{-8} Torr of helium [60,61]. In the mass spectrum were three mass lines, $HeRh^{2+}$, He^+, and Rh^{2+} with a very well defined low energy secondary peak. Rh^{2+} ions in the low energy peak came from the fact that a small part of the energy was carried away by those He atoms tunneling out of the compound ions. As atomic tunneling should exhibit a strong isotopic mass effect, the same experiment was carried out by replacing ^4He with ^3He. To my amazement, field dissociation no longer occurred even though one would expect ^3He with its smaller mass to tunnel more easily. The beauty is that from the theory, one can expect $^3HeRh^{2+}$ to be more difficult to dissociate than $^4HeRh^{2+}$ because of a center of mass transformation in the relative motion of He atom and Rh^{2+} ion. This is the most dramatic demonstration of the complicated nature of the concept of particle tunneling as well as the dissociation reaction by atomic tunneling of a compound ion. The dissociation reaction is affected by both the particle tunneling probability and a center of mass transformation. More importantly, particle tunneling is not really tunneling of the lighter mass particle through a potential barrier as envisioned from WKB Approximation and made popular by FN theory and solid state phenomena, but more accurately the mutual separation of the two atoms or particles or two systems, prohibited by classical mechanics because of insufficient energy but allowed by quantum mechanics. What started out to be a simple observation of helide ions of Rh develops into a study of a scientific subject

Journal of Science and Technology in the Tropics (2005) **1**: 3-18

Diamondtrypanum new genus (Protozoa: Trypanosomatidae) with seven new species in the blood of Malaysian amphibians

Akira Miyata[1], H. S. Yong[2] and Hideo Hasegawa[1]
[1]Department of Biology, Oita Medical University, Hasama, Oita 879-5593, Japan
[2]Institute of Biological Sciences, University of Malaya, 50603 Kuala Lumpur, Malaysia

Received 27 December 2004; accepted 21 January 2005

Abstract A new genus *Diamondtrypanum* is proposed with seven new species and two named species from Malaysian amphibians – 1. *D. chattoni* (Mathis and Léger, 1911), new combination (=*Trypanosoma chattoni*) (genotype), in *Bufo melanostictus*; 2. *D. kodok*, new species, in *Bufo asper*; 3. *D. bungateratai*, new species, in *Rana blythi*; 4. *D. katak*, new species, in *Rana hosii*, *Rana erythraea*, *Rana chalconota* and *Rana nicobariensis*; 5. *D. tsunezomiyatai* (Miyata, 1978), new combination (=*Trypanosoma tsunezomiyatai*), in *Rana limnocharis*; 6. *D. katakpadi*, new species, in *Rana cancrivora*; 7. *D. amolops*, new species, in *Amolops larutensis*; 8. *D. sarawakense*, new species, in *Staurois natator*; 9. *D. gemuk*, new species, in *Occidozyga laevis*. *Diamondtrypanum* is characterized in having a round or spherical body, and in the absence of a trypomastigote stage in the vertebrate host.

Keywords Protozoa – Trypanosomatidae – *Diamondtrypanum* new genus – *Trypanosoma* – taxonomy – amphibian host

INTRODUCTION

Mathis and Léger [1] described *Trypanosoma chattoni* in the blood of *Bufo melanostictus* from Vietnam. This trypanosome is very different from other known species in the absence of a trypomastigote stage in the blood of the vertebrate host; the genus *Trypanosoma* is defined to possess the trypomastigote stage. During our study of 53 species of amphibians from various localities of Peninsular Malaysia and Sarawak, we encountered the trypanosomes of *T. chattoni*-type in the blood of 12 anuran species. In all cases, we did not observe the trypomastigote form. We conclude that this type is clearly different morphologically from other known trypanosomes, and propose herein a new genus with seven new species from Malaysian anurans.

MATERIALS AND METHODS

Collection of anurans

Frogs and toads were captured by hand mostly at night in various localities of Malaysia from 1988 to 1991. They were anesthetized to death with chloroform. After collection of blood samples, they were fixed in 10% formalin. Identification was made based on Berry [2], Inger [3], Inger and Stuebing [4], and Inger, Voris and Walker [5].

Preparation of blood smears

The blood smears prepared from cardiac blood of frogs or toads were fixed in absolute methanol and stained with 3% Giemsa solution for about 30 minutes. The smears were examined under x200 for screening, and if a trypanosome was detected, it was examined and photographed under oil immersion (x1000) for measurement and study of morphological detail.

Morphological features and measurement

The trypanosomes of *T. chattoni* type were larger than the host amphibian blood cells and in the fresh smear, usually seen as a round organism with many granules in its cytoplasm as shown in Figure 11. The locomotion of body or flagellum was not clearly evident except as slight movement with fluid flow. Diamond [6] reported

of more fundamental nature difficult to be investigated by any other technique.

Binding energy of kink site atoms

The concept of kink site atoms was introduced by Stranski in the 1930s [62]. A kink site atom has exactly one half the atomic coordination number of a bulk atom. A kink site is therefore also called the half crystal site. What is most interesting is that the binding energy of a kink site atom should be identical to the cohesive energy per atom of the solid. While this elegant concept and its consequences are really very simple to understand, there has been no experimental measurement to substantiate this theoretical result.

Field evaporation of atoms from a metal surface starts from kink sites. Thus in principle it is possible to measure the binding energy of kink site atoms from the ion energy distribution of field evaporated ions. In reality, however, one will have to improve the resolution of the instrument to at least 1 part in 50,000. The other requirement is that an absolute energy scale has to be established.

This is one of the most difficult experimental challenges I had ever taken. I solved it by extending the length of our pulsed-laser ToF atom-probe to nearly 8 meters, by using electronic timer of 156 ps time resolution, by using a dc power supply of extreme stability, by measuring the voltage with a digital voltmeter having 8 reliable digits, and by developing a method of absolute ion energy determination using the very accurate isotope masses available from years of nuclear physics research [63]. We are able eventually to measure the binding energy of kink site atoms of several metals which all agree with their cohesive energy to within the accuracy of our experiments which is about ±0.2 eV.

CONCLUSION

In this short review, I have presented a personal view of contributions of field ion microscopy to the study of surface and nano science related problems on the atomic scale, and how some of these experiments have instigated studies by other atomic resolution microscopy. In fact not all the good and difficult FIM experiments have been recognized, nor being understood already. As scientists are now more than ever interested in atomistic knowledge of nanostructures, I believe atomic resolution microscopy studies are going to become more and more important in our understanding of the properties of these material structures. I am therefore very optimistic of the further contribution of atomic resolution microscopy, be it field ion microscopy, scanning probe microscopy or electron microscopy to surface and nano science.

REFERENCES

1. Müller E.W. and Tsong T.T. (1979) *Field Ion Microscopy, Principles and Applications*. Elsevier, New York.
2. Tsong T.T. (1990) *Atom-Probe Field Ion Microscopy.* Cambridge Univ. Press, Cambridge.
3. Tsong T.T. (1988) *Rpt. Prog. Phys.* **8**: 127.
4. Müller E.W. (1957) *Z. Electrochem.* **61**: 43.
5. Ehrlich G. and Hudda F.G. (1966) *J. Chem. Phys.* **44**: 1039.
6. Bassett D.W. and Parsely M.J. (1969) *J. Phys. D: Apply. Phys.* **2**: 13.
7. Bassett D.W. and Parsely M.J. (1969) *Nature* **221**:1046.
8. Tsong T.T. (1972) *Phys. Rev. B.* **6**: 417.
9. Swartzentruber B.S. (1996) *Phys. Rev. Lett.* **76**: 459.
10. Barth J.V. (2000) *Surf. Sci. Rpt.* **40**: 75.
11. Mo Y.W., Kleiner J., Webb M.B. and Lagally M.G. (1991) *Phys. Rev. Lett.* **66**: 1998.
12. Tsong T.T. (2001) *J. Phys. Chem. Solids* **62**: 1689.
13. Hwang I.S., Lo J.L. and Tsong T.T. (1997) *Phys. Rev. Lett.* **78**: 4797.
14. Tsai M.H., Tang Y.H., Hwang I.S. and Tsong T.T. (2002) *Phys. Rev. B.* **66**: 241304.
15. Walko R.J. and Tsong T.T. (1972) *Physica Status Solidi (a)* **12**: 111.
16. Tsong T.T. and Kellogg G.L. (1975) *Phys. Rev. B.* **12**: 1343.
17. Fink H.W. (1986) *IBM J. Res. Dev.* **30**: 460.
18. Binh V.T. and Garcia N. (1992) *Ultramicroscopy* **42**: 80.
19. Tsong T.T. (1991) *Phys. Rev. B.* **44**: 13703.
20. Stroscio J.A. and Eigler D.M. (1991) *Science* **254**:1319.
21. Ho M.S., Hwang I.S. and Tsong T.T. (2000) *Phys. Rev. Lett.* **84**: 5792.
22. Einstein T.L. and Schrieffer J.R. (1973) *Phys. Rev. B.* **7** : 3629.
23. Lau K.H. and Kohn W. (1977) *Surf. Sci.* **65**: 607.
24. Tsong T.T. (1973) *Phys. Rev. Lett.* **31**: 1207.

25. Tsong T.T. and Casanova R. (1981) *Phys. Rev. B.* **24**: 3063.
25. Tsong T.T and Casanova R. (1981) *Phys. Rev. B.* **24:** 3063.
26. Watanabe F. and Ehrlich G. (1992) *J. Chem. Phys.* **96**: 3191.
27. Tsong T.T. and Casanova R. (1981) *Phys. Rev. Lett.* **47**: 113.
28. Repp J. et al. (2000) *Phys. Rev. Lett.* **85**: 2981.
29. Knorr N. et al. (2002) *Phys. Rev. B.* **65**: 115420.
30. Silly F. et al. (2004) *Phys. Rev. Lett.* **92**: 016101.
31. Österlund L. et al. (1999) *Phys. Rev. Lett.* **83**: 4812.
32. Tsong T.T. and Müller E.W. (1967) *Appl. Phys. Lett.* **9**: 7.
33. Tsong T.T. and Müller E.W. (1967) *J. Appl. Phys.* **38**: 3531.
34. Berg H., Cohen J.B. and Tsong T.T. (1973) *Act. Met.* **21**: 1589.
35. Newman R.W. and Hren J.J. (1967) *Phil. Mag.* **16**: 211.
36. Schmid M., Stadler H. and Varga P. (1993) *Phys. Rev. Lett.* **70**:1441.
37. Wouda P.T. et al. (1996) *Surf. Sci.* **359**:17.
38. Panitz J.A. (1973) *Rev. Sci. Intrum.* **44**: 1034.
39. Cerezo A., Godfrey T.J. and Smith G.D.W. (1988) *Rev. Sci. Instrum.* **59**: 862.
40. Blavette D., Bostel A., Sarrau J.M., Deconihout B. and Menand A. (1993) *Nature* **363**: 432.
41. Ng Y.S., Tsong T.T. and McLane S.B. (1979) *Phys. Rev. Lett.* **42**: 588.
42. Tsong T.T., Ng Y.S. and McLane S.B. (1980) *J. Chem. Phys.* **73**: 1464.
43. Ahmad M. and Tsong T.T. (1985) *J. Chem. Phys.* **83**: 388.
44. Gauthier Y., Joly Y., Baudoing R. and Rundgren J. (1985) *Phys. Rev. B.* **31**: 6216.
45. Bardeen J. (1960) *Phys. Rev. Lett.* **6**: 57.
46. Tersoff J. and Hamann D.R. (1983) *Phys. Rev. Lett.* **50**: 1998.
47. Fu T.Y., Cheng L.C., Nien C.H. and Tsong T.T. (2001) *Phys. Rev. B.* **64**: 113401.
48. Kuo H.S. et al. (2004) *Nano Letters* **4**: 2379.
47. Echt O., Sattler K. and Recknagel E. (1981) *Phys. Rev. Lett.* **47**: 1121.
49. Knight W.D. et al. (1984) *Phys. Rev. Lett.* **52**: 2141.
50. Tsong T.T. (1984) *Appl. Phys. Lett.* **45**: 1149.
51. Tsong T.T. (1984) *Phys. Rev. B.* **30**: 4946.
52. Bloomfield L.A., Freeman R.R. and Brown W.L. (1985) *Phys. Rev. Lett.* **54**: 2246.
53. Raghavachari K. (1986) *J. Chem. Phys.* **84**: 5672.
54. Raghavachari K. (1987) *J. Chem. Phys.* **87**: 2191.
55. Sattler K. et al. (1981) *Phys. Rev. Lett.* **47**: 160.
56. Tsong T.T. (1986) *J. Chem. Phys.* **85**: 639.
57. Hiskes R. (1961) *Phys. Rev.* **122**: 1207.
58. Beckey H.D. and Knoppel H. (1966) *Z. Naturforschg. A.* **21**: 1920.
59. Tsong T.T. and Liou Y. (1985) *Phys. Rev. Lett.* **55**: 2180.
60. Tsong T.T. (1985) *Phys. Rev. Lett.* **55**: 2826.
61. Stranski N. and Krastanov L. (1938) *Sitzungsber. Akad. Wissenschft Wien.* **146**: 796.
62. Liu J., Wu C.W. and Tsong T.T. (1992) *Phys. Rev. B.* **45**: 3659.

Journal of Science and Technology in the Tropics (2005) 1: 51-54

Correlation between the current sheath dynamics in the axial acceleration phase of the plasma focus and its ion beam generation

C. H. Lee[1], D. Ngamrungroj[2], C. S. Wong[1], R. Mongkolnavin[2], Y. K. Low[1], J. Singh[1] and S. L. Yap[1]

[1]Plasma Research Laboratory, Physics Department, Faculty of Science, University of Malaya, 50603 Kuala Lumpur, Malaysia

[2]Plasma Research Laboratory, Department of Physics, Faculty of Science, Chulalongkorn University, Bangkok, Thailand

Received 26 April 2005; accepted 3 May 2005

Abstract The current sheath dynamics at the axial acceleration phase of a plasma focus discharge is believed to have a significant effect on its ion beam generation. To illustrate this, the correlation between the axial acceleration phase dynamics of the United Nations University/International Centre for Theoretical Physics (UNU/ICTP) plasma focus device [1] filled with argon gas and its ion beam generation is obtained from two series of experiments. In one series of experiments, the magnetic pickup coil is used to study the dynamics of the current sheath by measuring the arrival time of the current sheath at various axial positions. The average current sheath velocities at varying argon operating pressures are thus estimated. In another series of experiments, the energies and intensities of the ion beams generated from discharges with similar conditions as the first series are obtained. Results show that for discharges performed at relatively low pressure, the current sheath velocity is higher. Correspondingly, the ion beam generated from discharges with similar condition has higher energy as well as intensity.

Keywords current sheath dynamics – axial acceleration phase – plasma focus – ion beam generation

INTRODUCTION

A plasma focus device is a high power pulsed discharge which is able to produce a compressed dense plasma at the end of its coaxial electrodes. This system has also been found to be an intense source of neutrons, x-ray, ion and electron beams. The dense focussed plasma formation is affected by the current sheath formation and dynamics. It is believed that the ion beam production and its characteristics may be related to the focusing action of the plasma, which is strongly dependent on the condition of the plasma preheated by the axial acceleration phase. Thus, in order to make use of the ion beam produced, a better understanding of the correlation between the dynamics of the various phases of the plasma focus operation is needed.

The dynamics of the plasma focus is commonly divided into four main phases [2]: the initial breakdown and lift-off phase, the axial run-down phase, the radial compression phase, and the final focusing phase. The gas breakdown occurs initially across a glass insulator which separates the outer and inner electrodes. The resultant current sheath is first pushed radially outwards from the insulator surface, and then accelerated axially towards the truncated end of the electrodes by the **J** x **B** force, where **J** is the radial component of current density and **B** is that self-induced magnetic field in the azimuthal direction. The current sheath collapses radially inward when it reaches the end of the central electrode producing the final focusing phase. This is where the hot and dense focused plasma is formed. The ions are believed to be ejected out along the axis to form a beam after the m=0 instability causes the dense plasma to break up. Thus abrupt change in the plasma impedance gives rise to the high transient electric field which in turn drives the ions out in the axial direction.

The experiments reported here are conducted in two parts. The first part is the measurement of the plasma dynamics in terms of its speed in relation to the operating pressure during the axial acceleration phase.

The second part of the experiments is the measurement of the energy of the ion beam generated from the focussing phase of the plasma operated at varying pressures by the time-of-flight technique. The measurement of the plasma dynamics cannot be carried out simultaneously with the ion beam measurement as the insertion of the magnetic probe will inevitably affect the plasma dynamics and hence the ion beam generation. It is assumed that the dynamics of the current sheath is reproducible between discharges of similar conditions.

THE EXPERIMENTAL SETUP

Figure 1 shows the schematics of the plasma focus device and the diagnostic setup. This Mather-type UNU/ICTP PFF plasma focus device is powered by a single 15 kV, 30 μF capacitor. In the experiments performed, the capacitor is charged up to 13.5 kV, which corresponds to an input energy of 2.7 kJ. From a series of experiments using argon gas, an optimum focussing discharge is obtained at the pressure of 1.5 mbar.

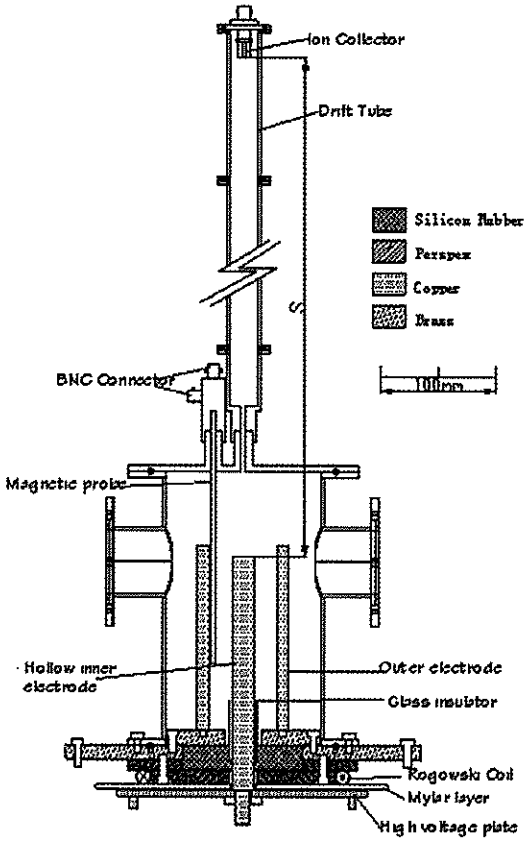

Figure 1. Schematics of the plasma focus device and the diagnostic setup.

For the measurement of the plasma dynamics, a magnetic pickup coil is placed into the plasma chamber to detect the arrival of the current sheath. The coil is placed inside a glass tube and inserted into the space between the electrodes as illustrated in Figure 1. In this particular experiment, it is placed near to the outer electrode to minimize the disturbance of the probe to the current sheath motion. Figure 2 shows the typical signals of the magnetic probes. Since the detected signal corresponds to the rate of change of the magnetic field, the point where it crosses the zero level line is the peak of the magnetic field profile and it is taken to be the arrival time of the current sheath.

For the measurement of the energy of the ion beam, an ion collector is placed at 30 cm away from the tip of the inner electrode in the axial direction as shown in Figure 1. The detection area of this ion collector is 4.4×10^{-4} m^2 and it is biased at -100 V. A pinhole with a diameter of 2 mm is placed at 185 mm from the tip of the inner electrode to act as a collimator. Only those ion beams which pass through the collimator can be detected by the ion collector.

The Time-of-Flight (TOF) method is used to deduce the energy of the ion beam. By evaluating the time difference between the focus voltage spike and the ion beam signal, we may calculate the average ion beam velocity and its average kinetic energy from the simple expression below:

$$v = \frac{S}{\Delta t}$$

$$K.E. = \frac{1}{2} m v^2$$

where v is the speed of the ion, S is the distance from the focussing point to the ion collector and Δt is the time taken for the ion to travel the distance of S. The kinetic energy formula is used to convert the speed of the ion to kinetic energy by introducing m which is the mass of the ion. It is assumed that the production of the ion beam occurs just above the inner electrode where the focussing action takes place. Thus the distance S is taken to be 30 cm.

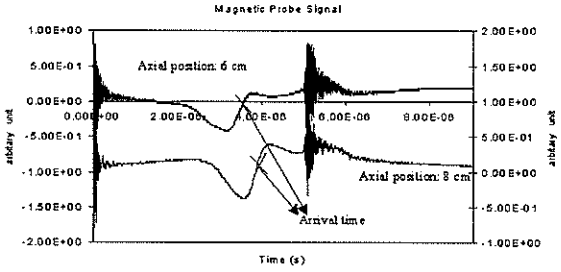

Figure 2. The magnetic probe signals at axial positions of 6 cm and 8 cm at 1.5 mbar operating pressure.

RESULTS AND DISCUSSION

From the magnetic probe signals, the arrival times of the current sheath at different positions are determined. Figure 3 presents the current sheath trajectory for six different operating pressures. The average speed of the current sheath during its axial acceleration phase is estimated from the gradient of the linear graph. Figure 4 shows the average current sheath speed as a function of the operating pressures. The result is comparable with the reported axial speeds of between 3-10 cm/μs [3]. It is obvious that at higher pressure, the average velocity is lower. In addition, from this series of experiments, it is hard to obtain a good focussing discharge when the operating pressure is above 2 mbar, as can be concluded based on the current and voltage signals.

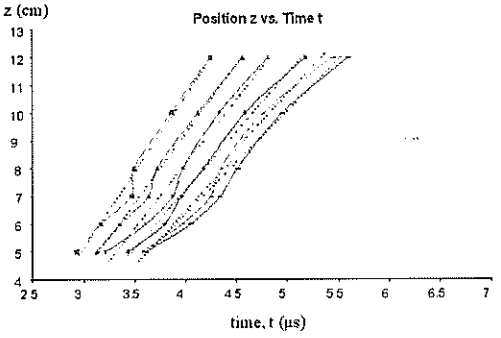

Figure 3. The current sheath trajectory for six different operating pressures.

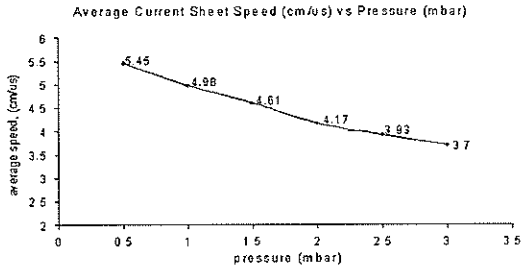

Figure 4. The average current sheath speed at various pressures.

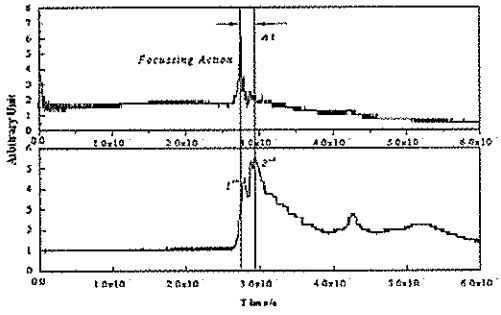

Figure 5. Typical waveforms obtained from argon discharge at the pressure of 0.5 mbar. (a) Voltage signal, (b) Ion beam signal from -100 V biased ion collector.

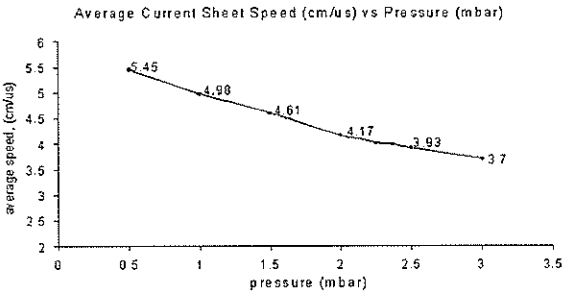

Figure 6. The average ion beam energy at various operating pressures.

Figure 5 shows a typical focus voltage spike and ion beam signal detected at the pressure of 0.5 mbar. The occurrence of the strong voltage spike is considered as the reference point of the ion beam source since it corresponds to the beginning of the dense plasma focussing phase. Two peaks can be observed in a typical ion collector's signal. The first peak is believed to be the emission of UV light and X-ray from the focussing plasma, as it synchronizes with the occurrence of the voltage spike. The second peak is therefore caused by the ion beam.

Using the TOF method, the estimated energy of the ion beam at the four optimum operating pressures is shown in Table 1 and Figure 6. For each operating pressure, five shots are fired and these results are the averaged values.

Table 1. The average ion beam velocity and its corresponding energy.

Pressure (mbar)	Ar	
	Average ion beam velocity, v (cm/μs)	Average ion beam energy, E (keV)
0.5	144.4	500±200
1.0	101	220±40
1.5	85	150±20
2.0	71.6	110±10

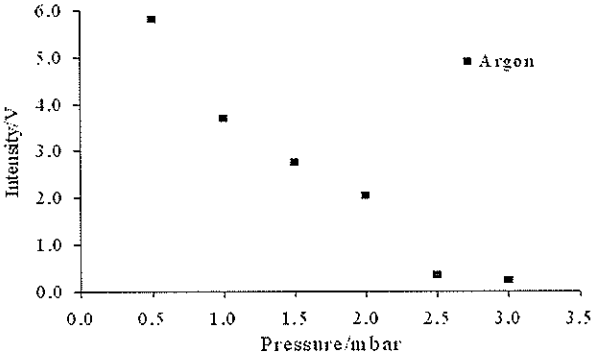

Figure 7. The intensity of the ion collector's signal at various pressures.

The intensity of the ion collector signal is also studied as a function of filling gas pressure, which ranges from 0.5 mbar to 3.0 mbar. The result is shown in Figure 7. It is evident that the intensity decreases while the gas pressure increases. There may be two possible reasons of this ion beam property. As the ion beam traverses through the ambient gas, attenuation of the ion beam energy and divergence of the beam may be caused by collisions of the ions with the ambient particles. Higher pressure will give rise to a larger number of collisions, hence greater attenuation. For instance, at relatively high operating pressures such as 2.5 mbar and 3.0 mbar, the noise-to-signal ratio of the ion beam signal is too large and it is difficult to extract any meaningful information from the ion beam signal. The other reason for the decreasing intensity of the ion beam at higher operating pressure is related to the dynamics of the plasma focus discharge. A faster current sheath velocity during the axial acceleration phase may give rise to a stronger focussing action and hence a more intense ion beam.

CONCLUSION

For the UNU/ICTP PFF plasma focus device operated with argon gas, stronger focussing action takes place at the operating pressure of 0.5 mbar to 1.5 mbar. However, the higher current sheath velocity at lower pressure may produce strong and intense but unstable focussing action, which results in multiple focussing effects. Discharges with good single focus are most likely to be obtained at operating pressure range of 1.0 mbar to 1.5 mbar.

From the experiments carried out, the average energies of the argon ion beams produced by the plasma focus are in the range of 100 keV to 500 keV at the operating pressure of 0.5 mbar to 2.0 mbar. It is found that the device may produce ion beams with higher energy and greater intensity at lower pressure conditions.

The characteristics of the ion beam produced from a plasma focus device are dependent on the intrinsic ambient gas condition and the current sheath dynamics. In order to produce high energy and intense ion beams, the plasma focus of this configuration should be operated at the pressure range of not more than 1.5 mbar where in this case the pressure of 0.5 mbar to 1.5 mbar have been demonstrated.

Acknowledgements - The authors would like to acknowledge the Ministry of Science, Technology and the Environment, Malaysia for funding this research project under IRPA Grant 09-02-03-EA0027

REFERENCES

1. Lee S. (1984). Technology of the Plasma Focus. First Tropical College on Applied Physics, World Scientific, Singapore, pg 387.
2. Wong C.S. (1984). Basic Plasma Diagnostic Techniques. First Tropical College on Applied Physics, World Scientific, Singapore, pg 361.
3. Lee S. (1984). Technology of the Plasma Focus. First Tropical College on Applied Physics, World Scientific, Singapore, pg 410.
4. Mather J.W. (1965). *Phys. Fluids.* **8**: 366.
5. Mather J.W. and Bottom P.J. (1968). *Phys. Fluids.* **11**(3): 611.

Journal of Science and Technology in the Tropics (2005) **1**: 55-65

Real-time team oriented production scheduling of presses for manufacturing molds

Sam R. Thangiah[1], Anthony Webber[1] and Justin Liebler[2]
[1]Artificial Intelligence and Robotics Laboratory, Computer Science Department,
Slippery Rock University, Pennsylvania, U.S.A.
[2]Armstrong Cable Corporation, Butler, Pennsylvania, U.S.A.

Received 23 March 2005; accepted 28 April 2005

Abstract In this paper we describe an algorithm and a graphical user interface system used for solving a real-time job shop scheduling problem. The problem involves scheduling presses for manufacturing molds using a predefined set of teams, assigned to scheduling tasks or jobs, based on skill levels. It consists of a set of presses, machines used for creating molds, into which only compatible cavities or tools, for making molds, can be inserted for scheduling a set of jobs to be completed. Each tool consists of a defined number of cavities and can produce one or more different types of products depending on the design of the tool. The implemented system obtained improved solutions to a real world problem in a few seconds on an 800 MHz computer system compared to the manual solution. It required a few hours to obtain a manual solution to the same problem. The solution obtained by the algorithm reduced the time to produce the required molds by six hours in comparison to the manual solution. In addition, the design of the system allows it to be used for dynamic or real-time scheduling.

Keywords Scheduling Problem – Real-Time – Production

INTRODUCTION

In this paper we introduce a real-time algorithm and a graphical user interface system for scheduling presses for manufacturing molds using a predefined set of teams, assigned to scheduling tasks, based on skill levels. The molds are created by placing granular materials into the cavity of the press and applying extreme pressure that causes the material to fill the mold cavity. In some cases, heat is applied to the process until the desired shape is obtained. The problem consists of scheduling a set of presses, machines used for creating molds, into which only compatible cavities or tools, for making molds, can be inserted to complete a set of jobs. Each tool consists of a certain number of cavities and may produce one or more different products depending on the design of the tool. This problem is not limited to a parts manufacturer, but rather for any situation in which multiple devices request or requires a single resources' time. A set of teams, determined by skill levels of the workers, are assigned to work on the different presses. The objective of the problem is to minimize the total number of tool changes and produce all the required molds in the least amount of time. The problem has hard time limits on the molds to be produced. That is, all productions have to be done before the required deadline as industries that require the molds have just-In-time inventory and would levy penalties on any late orders.

The real-time aspect of the problem was introduced to consider realistic events that take place such as the change in an order, change in inventory level of materials, breakdown and/or maintenance of presses to name a few. The CPU time it takes to obtain a good solution after the occurrence of a real-time event was of critical importance. This has led to researchers developing algorithms for scheduling in real-time [1-3]. Problems in various industrial environments are combinatorial. This is the case for numerous scheduling and planning problems. Scheduling can be defined as a problem of finding an optimal sequence to execute a finite set of operations satisfying most of the constraints.

The problem formulated in this paper is extremely difficult to solve as it comprises several concurrent goals and with different resources which must be allocated to obtain the required goal. The main goal of the process is to maximize the utilization of individuals and/or machines and to minimize the required time to complete the entire job scheduling process.

The next section details the production scheduling problem. Section 3 lists the mathematical expressions and the static version of the scheduling problem. Section 4 describes the ordering and scheduling process for the company. Section 5 explains the production algorithm used to solve the static and dynamic or real-time version of the problem. Computational results on a real-world problem are detailed in Section 6 with summary and conclusions in Section 7.

PRODUCTION SCHEDULING PROBLEM

The use of automated manufacturing systems for optimizing the problem of assigning operations to a set of machines has been an area of intense research [4]. From the combinatorial optimization perspective finding an optimal production schedule is known to be NP-complete [5-6]. That is, the time to solve the problem increases exponentially with respect to the increase in the number of jobs. As such heuristic solutions that give good solutions within a reasonable amount of time are preferred over optimal algorithms. Heuristics have played an important role in finding solutions for such problems [7-9]. A great deal of previous research on job-shop scheduling has concentrated on static job shop problems. However in reality the problem is dynamic with changes taking place in real-time.

The advent of flexible manufacturing systems operating "just-in-time" (JIT) has placed increasing demands on the production scheduling problem. The importance of meeting traditional performance criteria such as makespan and flow time need to be weighted to reflect other important operating requirements. Specifically, lateness is unacceptable in situations where an assembly line running under JIT relies on timely production of components.

In a manufacturing system all jobs have release times that define their date of arrival at the shop floor. Job releases can be affected by unforeseen events, and consequently, neither the release times of jobs nor the specific processing requirements are known in advance. Therefore, scheduling is a non-deterministic problem dealing with an open-horizon. The control of the jobs in manufacturing systems is referred to as rescheduling because unforeseen events frequently require schedule revisions. In practice, predominantly priority-rule based control has been used for rescheduling [10]. The temporal decomposition of the non-deterministic problem into a series of dynamic, but deterministic problems also opens this domain for optimization methods [11]. The next section defines the mathematical expressions and heuristic model used in solving the real-time job shop scheduling problem.

JOB SHOP SCHEDULING

In this section we will provide the mathematical notations, the necessary mathematical expressions and the complexities involved in solving the scheduling problem.

Mathematical Expressions

I = $\{1,...I_{max}\}$ set of available presses
K = $\{1,...,P_{max}\}$ set of products to be manufactured
T = $\{1,...,T_{max}\}$ set of tools for presses
L = $\{1...,L_{max}\}$ set of teams for presses
O = $\{1...,O_{max}\}$ set of orders for products
J = $\{1...,J_{max}\}$ set of jobs for scheduling
D = current date
U_o = unscheduled order o ($o \in O$) for product k ($k \in K$)
C_{jk} = current job j($j \in J$) for product k ($k \in K$)
P_{ij}^{kl} = time taken by press i ($i \in I$) to make product k ($k \in K$) using tool j ($j \in J$) in team l ($l \in L$)
ORD_k = current order level for product k ($k \in K$)
REO_k = reorder level for product k ($k \in K$)
CUR_k = current inventory level for product k ($k \in K$)
MAX_k = maximum inventory level for product k ($k \in K$)
MIN_k = minimum inventory level for product k ($k \in K$)
d_j = due date of job j ($j \in J$)
c_j = completion date of job j ($j \in J$)
w_j = priority value of job j ($j \in J$)
s_t = setup time for tool j ($t \in T$)
r_t = removal time for tool t ($t \in T$)

A_{ij}^{kl} = assignment of product k ($k \in K$), tool j ($j \in J$), team l ($l \in L$) to press i ($i \in I$).

$Q(P_{ij}^{kl})$ = total number of jobs in press i ($i \in I$).

$T(P_{ij}^{kl})$ = total number of tool changes in press i ($i \in I$).

L = number of days for look ahead.

α = penalty weight for scheduled tardy order

β = penalty weight for number of tool changes

γ = penalty weight for unscheduled late orders

THE PRODUCTION SCHEDULING MODEL

The static model of the problem solved consists of a manufacturing system with I presses $M_1,\ldots,M_i$, K products $P_1,\ldots,P_k$, J tools $T_1,\ldots,T_j$ and L teams $G_1,\ldots,G_l$. A press is a machine into which a tool, consisting of cavities for the mold, is installed to make a product. All tools are not compatible with all machines, as only certain tools can be loaded into specific machines. The products that need to be manufactured are not compatible with all tools. Associated with each machine, tool and product is a team of workers. Teams based on skill levels, with respect to the presses and tools, are associated in the making of a product. As such compatibility has to exist with respect to P_{ij}^{kl} which is the time taken by press i used to make product k using tool j by team l. In addition, it is assumed there is at least one press with one tool and one team compatible to make the product. Each product has a minimum, maximum and current inventory level. The primary objective of the problem is to ensure that the current inventory of a product is as close to the maximum inventory to be maintained for that product. The current inventory level for product k, CUR_k, is the amount of inventory that is available on a product that can be used to ship out when a request for that product is requested. Each product k has a maximum inventory level, MAX_k, and a minimum inventory level MIN_k. If CUR_k drops below the reorder level for product k, REO_k, then an automatic reorder takes place. The CUR_k of a product is kept below MAX_k in order to minimize inventory costs. The due date d_j of the job j represents the committed shipping or completion date (the date the job is promised to the customer). The weight w_j of the job is the priority factor, denoting the importance of the job j relative to the other jobs that need to be processed or being processed in the system.

The objective of the company is to ensure that $MIN_k <= CUR_k <= MAX_k$ in order to service the customer requests without delay. Each tool t has a tool setup time, s_t, and a tool removal time, r_t. During production scheduling the primary objective is:

$$\text{Min} \sum s_j + r_j + \alpha (max(0, c_j - d_j) + \beta \sum T(P_{ij}^{kl}) + \gamma \sum \max(0, d_{U_o} - D) \quad (1)$$

Equation (1) computes the cost of scheduling with the total time taken for setup and removal of tools, tardy time for a scheduled job, total number of tools in a press and tardy value, in days, of unscheduled orders. The penalty weights for a, b and g was set to 60%, 30% and 10% of the total cost. The constraints are manufacturing the products by the required deadline and the use of compatible teams on a press with compatible tools.

The goal of this research was to develop a scheduling software tool for a manufacturer. The company has a group of presses in which molds (tools) are installed onto press types. There are five different press types available at this particular plant, and only certain tools will fit into certain press types. Each tool consists of a certain number of cavities and may produce one or more different products depending on the design of the tool. This is not limited to a parts manufacturer, but rather can work for any situation in which multiple devices request or require a single resources' time.

The products to be manufactured are energy absorbers for automotive assembly lines. There are 70+ products produced, however, not all are high volume products. Each order has the type of part to be produced, the number of parts to be produced, the priority of the order and the due date and time. There are several different press types: Erlenbach, Teubert closed-back, Teubert open-back, Teubert stretch open-back, and

Table 1. Compatibilities between Press types for manufacturing molds.

Tool Type	Press Type				
	Erlenbach	Teubert			
		TVZ	Closed	Open	Stretch Open
Erlenbach	X				
TVZ		X			
Closed			X	X	X
Open				X	X
Stretch Open					X

the movement as follows: "The movement can best be described as a discontinuous jerky rotation which proceeds in one direction for a time and than completely reverses itself".

In stained smears, the organism appeared very thin and flat. The peripheral part of the body was sometimes turned upward as shown in Figure 3, folded as in Figure 9, doubled over on itself like a 'Chinese fried dumpling stuffed with minced pork' as shown in Figure 4, or rolled like an egg roll as in Figure 5.

We adopted the following body measurements for species descriptions (Figs. 1 and 2): longest and shortest diameters of body through nucleus; longest and shortest diameters of nucleus; length of flagellum; distance from kinetoplast to nuclear membrane.

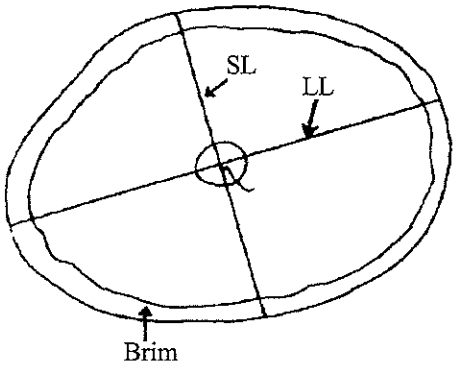

Figure 1. Body measurement. LL: longest length (diameter); SL: shortest length (diameter).

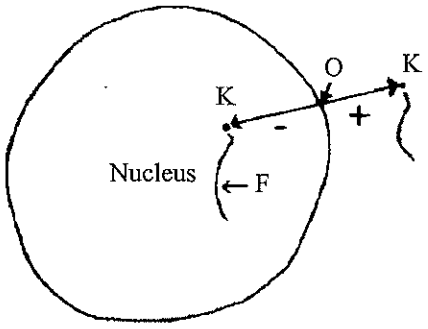

Figure 2. Measurements of nucleus and length of flagellum. F: flagellum; K: kinetoplast.

The kinetoplast was often very close to the nucleus, seen to overlap with the nucleus in the stained specimen. Therefore, the distance between the kinetoplast and the nuclear membrane was expressed as follows: if the kinetoplast was seen inside or outside the nuclear outline, the distance was expressed with - or + symbol in front of each measurement. All measurements, in micrometers, expressed as the range, followed in parentheses by mean ± SD.

The flagellum also usually overlaid on the cytoplasm or the nucleus, and it was sometimes very difficult to distinguish. However, a white trace or a white line could be seen from the kinetoplast, and the length of the line corresponded with the real length of the flagellum. Actually if the flagellum was seen, it just passed through the middle of the line from the kinetoplast to the end of the line.

All type smears used for the description were deposited in the Department of Biology, Oita Medical University, Hasama, Oita 879-5593, Japan.

In the present report, the old names for the amphibian hosts are used so as to facilitate easy recognition and retrieval of information. The species *Rana cancrivora*, *Rana limnocharis* and *Rana nicobariensis* are now placed under the genus *Fejervarya*, while the species *Rana blythi* is under the genus *Limnonectes*.

DESCRIPTION

Diamondtrypanum new genus

Diagnosis – Protozoa: Kinetoplastida: Trypanosomatidae. Body circular, or elliptical, or somewhat extended elliptical; edge of body very thin, often forming pleats or brim; nucleus rounded and located near centre of body; kinetoplast present on or near nucleus; short free flagellum originated from near kinetoplast; undulating membrane absent. Parasite in blood of anurans.

Type species – *Diamondtrypanum chattoni* (Mathis & Léger, 1911), new combination (=*Trypanosoma chattoni* Mathis & Léger, 1911).

Included species – *D. amolops* new species; *D. bungateratai* new species; *D. celastinai* (Brumpt, 1936), new combination (=*Trypanosoma celastinai* Brumpt, 1936); *D. gemuk* new species; *D. katak* new species; *D. katakpadi* new species; *D. kodok* new species; *D. sarawakense* new species; *D. tsunezomiyatai* (Miyata, 1978), new combination (=*Trypanosoma tsunezomiyata* Miyata, 1978).

Etymology – The genus name is dedicated to Dr L. S. Diamond for his great contribution to protozoology. Gender neuter.

Teubert TVZ. A tool designed to fit into an Erlenbach will only fit into an Erlenbach press. A tool designed to fit into a Teubert TVZ will only fit into a Teubert TVZ press. A tool designed to fit into a Teubert closed-back press, will fit into a closed-back press, an open-back press, or a stretch open-back press. A tool designed for an open-back press will fit an open-back, or a stretch open-back. A tool designed for a stretch open-back will fit into only a stretch open-back. Table 1 illustrates the compatibilities between the teams and presses.

The assignment of tools to presses is listed in Table 3. The teams have the ability to work anywhere from 0 to 168 hours per week in order to complete production requirements.

At this plant, there are 15 presses. 3 are Erlenbach, 2 are Teubert closed-back, 2 are Teubert open-back, 1 is Teubert TVZ, and 7 are Teubert stretch open-back presses. The presses on the shop floor have been divided and assigned into four separate teams. The teams are independent of one another, and have the ability to work different schedules depending on the demand for production from the tools in their team. In the initial solution, the tools have been assigned to the teams based on press capacity and similarity of customers, and for likeness of the parts being produced. The initial assignments are feasible, but are very unlikely to be optimal. The algorithm transfers tools between the teams if a better solution can be obtained. The team breakdown for the presses is listed in Table 2.

Table 3 lists a sample of the tool information used in the production schedule. A tool to be used for producing a part has an associated product, the description of the part, three preferences of the press types to be used, number of cavities in the tool, cycle

Table 2. Team assignment for press types.

Team 1	Team 2	Team 3	Team 4
Erlenbach (E-1)	Teubert Stretch Open-back (T-4)	Teubert Open-Back (T-8)	Teubert TVZ (T-12)
Erlenbach (E-2)	Teubert Closed-Back (T-5)	Teubert Stretch Open-Back (T-9)	Teubert Stretch Open-back (T-13)
Erlenbach (E-3)	Teubert Closed-Back (T-6)	Teubert Stretch Open-back (T-10)	Teubert Stretch Open-back (T-14)
	Teubert Open-back (T-7)	Teubert Stretch Open-back (T-11)	Teubert Stretch Open-back (T-15)

Table 3. Press types with available work hours, up time and repair time.

Team Press	Press No.	Sun Type	Mon	Tue	Wed	Thu	Fri	Sat	Up	Repair Time	Time
1	1	ERL	0	24	24	24	24	24	0	0.85	3
1	2	ERL	0	24	24	24	24	24	0	0.86	3
1	3	ERL	0	24	24	24	24	24	0	0.89	3
2	4	TOS	0	24	24	24	24	24	0	0.96	2
2	5	TCB	0	24	24	24	24	24	0	0.98	1
2	6	TCB	0	24	24	24	24	24	0	0.97	1
2	7	TOB	0	24	24	24	24	24	0	0.95	2
3	8	TOB	24	24	24	24	24	24	24	0.96	2
3	9	TOS	24	24	24	24	24	24	24	0.97	1
3	10	TOS	24	24	24	24	24	24	24	0.94	2
3	11	TOS	24	24	24	24	24	24	24	0.97	1
4	12	TVZ	0	24	24	24	24	24	0	0.95	2
4	13	TOS	24	24	24	24	24	24	24	0.94	2
4	14	TOS	24	24	24	24	24	24	24	0.96	1
4	15	TOS	24	24	24	24	24	24	24	0.95	2

ERL – Erlenbach; TOS – Teubert stretch open-back; TCB – Teubert closed-back; TOB – Teubert open-back; TVZ – Teubert TVZ;

time in seconds, yield value, tool installation and removal time in hours, minimum, maximum, reorder and current inventory levels.

Tool changes in a press leads to delay or downtimes in the processing time of a job. Downtimes for tool changes are the attributes of the individual tools. The time it takes to install a tool, and the time it takes to remove a tool from a press will be the two tool downtime attributes. For a change from tool #1 to tool #2, there will be downtime incurred in removal of tool #1 and then downtime incurred in installing tool #2. The sum of the two times will be the total tool change downtime for the changeover. Reducing tool change downtime is another desirable metric for determining a better solution. In order to reduce tool changes, though, it may require building a higher amount of inventory. This can lead to an undesirable situation when inventory levels get too high leading to an increase in inventory costs.

The amount of inventory produced must be enough to cover shipments without the need to backorder any requirements. In fact, there are no tool set ups in which we will be permitted to backorder for lack of inventory. The solution must provide parts for 100% on-time delivery. Each tool has different production characteristics or attributes. A tool may have one or more cavities of the same part. Each tool will require different cycle times. A cycle time is the minimal amount of time required in order to produce an acceptable part. If a tool has 3 cavities, and runs at a 180 second cycle time, the tool will produce 60 parts per hour. This hourly rate is a perfect world number. In reality, some portion of the parts may be scrapped because of breakage or other non-conformity. The actual parts produced may be only 50 of the 60 originally produced. The yield percentage is different for different tools depending upon their complexity. Therefore each tool will carry along a yield attribute that will be used to determine how many net parts can be counted from a typical run. The gross number will also be considered for raw materials ordering. Though not part of the solution to the scheduling problem, it will be helpful for drawing conclusions from the solution. If the manufacturer drives the yields up, it will have direct impact on the total time required for obtaining a solution.

Each part has different attributes as well. The product can be up to 16 alphanumeric characters. The shipment frequency can be daily, weekly, or monthly. There is also an order amount for each item, and a carton quantity. The order amount will be determined statistically from sales history and shipment forecasts for the shipment amount. Since some orders may be erratic, the amount used in the data file will be at least one standard deviation above the mean. The carton quantity will be used to determine how much space the inventory will require in the warehouse. If the total square footage is too high based on carton quantity,

Table 4. Sample of the part types, preference of machines, cavities, yield, installation and removal time and minimum, maximum, current and reorder inventory levels.

Team	Product	ERL	TCB	TOB	TOS	TVZ	No. of Cavities	Cycle Time (sec)	Yield	Intsall	Remove	Min	Reorder	Max	Current
1	1044	1	0	0	0	0	3	179	0.9393	4	4	532	1612	8060	4072
1	2260	1	0	0	0	0	4	220	0.9809	4	4	424	1284	6420	5287
1	2261	1	0	0	0	0	4	223	0.8964	4	4	561	1700	8500	4296
2	2264	0	0	0	1	0	3	186	0.9574	4	4	364	1104	5520	3947
2	2564	0	1	2	3	0	4	160	1.00	3	3	114	344	1376	2188
2	2565	0	1	2	3	0	4	143	0.9412	3	3	209	634	1268	297
2	2565	0	0	0	1	0	2	217	0.9529	4	4	105	318	636	315
2	2571	0	1	2	3	0	3	172	0.9412	3	3	236	716	1432	3150
2	2571	0	0	0	1	0	3	192	0.9617	4	4	283	859	1718	3083
2	2572	0	1	2	3	0	3	185	0.8875	3	3	57	173	346	841
2	1638	0	1	2	3	0	14	149	0.9354	3	3	1429	4331	8662	20618
2	5116	0	1	2	3	0	8	157	0.9636	3	3	1208	3661	7322	3978
2	5261	0	1	2	3	0	4	123	0.9281	3	3	193	584	2920	2216
2	5261	0	1	2	3	0	5	154	0.9424	3	3	89	270	1350	1616
2	5261	0	1	2	3	0	3	166	1.00	3	3	30	90	1000	458

Journal of Science and Technology in the Tropics (2005) 1: 55-65

storage space will not be available for the product. For daily shippers, that is not such an issue, but for monthly shipments, one does not want to go above one or two months of inventory since storage costs become unreasonable.

The main problem to solve is to determine a rotation for the tools in the presses in order to cover shipments, minimize inventory, reduce tool change downtime, and reduce total production time required. A team of presses has an initial group of tools assigned to them. The solution should, based upon the attributes of the tools, presses, and parts, give the team a sequence of tools to run and how many parts to make per run. The resulting sequence would then be released to the floor to be used as a production schedule. As results come in, as far as production is concerned, the schedule should be re-calculated to see if any shortages or overages have adversely affected it.

THE ORDERING AND SCHEDULING PROCESS

The ordering process determines the scheduling process used in the manufacturing of the parts. Figure 1 displays the ordering process and the processing that takes place once an order is made. When an order arrives for a specific product, the order is checked against the inventory. If sufficient quantity of the required material is available in the inventory, then the order is fulfilled and the required parts are moved to the shipping stage area where it will be loaded into a truck and shipped to the customer. If the product falls below the reorder level, then a tool run will be scheduled to produce the required products to be maintained in inventory.

On the other hand if the required order cannot be fulfilled from inventory then a tool run will have to be scheduled for the required number of parts to be met by the deadline.

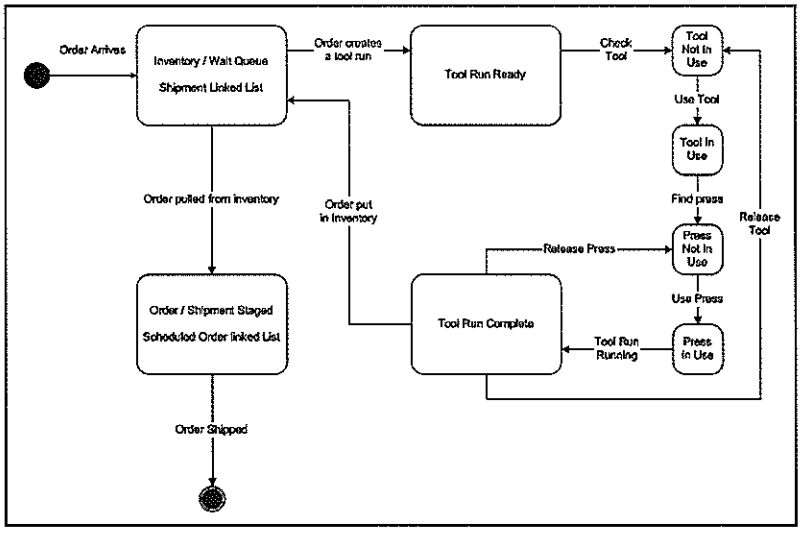

Figure 1. The ordering and tool run process for a product.

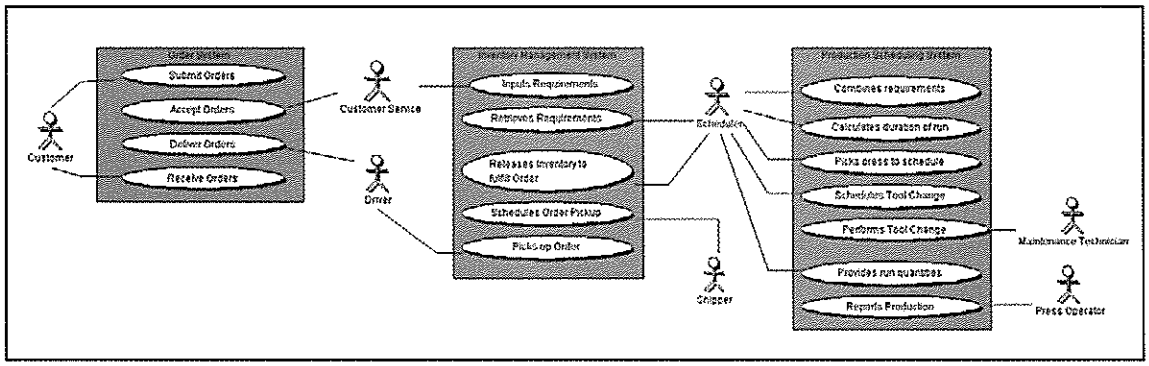

Figure 2. People involved in the part order and production process.

Figure 2 is a case diagram of the ordering and tool run process for a product. The figure models the people participating in the part order and production process. In this model the scheduler is responsible for executing the implemented program. The scheduler would have to interact with a number of people in the ordering and production process in order to complete a schedule of orders. The figure shows all the people involved starting from the customer who makes the order to the shipper who delivers the required parts. The order system is represented by in the system by the orders table, which holds all of the orders that need to be processed. The tools for use are located in the tools table and directly relates to the Inventory Management System (IMS).

THE PRODUCTION SCHEDULING ALGORITHM

The production algorithm uses the cycle time, cavities, and yield percentage, to determine the amount of time required to build inventory up to the maximum, while considering the orders for the next L days.

The Algorithm

Step 1: $Q(P_{ij}^{kl}) = 0, \forall i, (i \in I)$;
Step 2: Set L = 5;
Step 3: Sort all orders in ascending order of priority w_j
Step 4: While (unscheduled orders exist and $j < J_{max}$ where $(j \in J)$)
Obtain the next unscheduled job j for product k, C_{jk}
Accumulate all orders for product k over the next L days and place it at the top of orders to fulfilled.
If $((ORD_k - CUR_k) > REO_k)$
$ORD_k = ORD_k - CUR_k$
Complete the order and ship it out
else
For (all available presses)
Find A_{ij}^{kl}
If (press is found)
Insert the order using equation (1)
Else
If $((ORD_k - CUR_k) > MIN_k)$
Find A_{ij}^{ol} such that REO_o is maximum in comparison to all other scheduled jobs.
A_{ij}^{ol} is scheduled out using one of the following combinations:
Remove A_{ij}^{ol} and insert A_{ij}^{kl}
Remove A_{ij}^{ol} and insert A_{ij}^{kl} and insert A_{ij}^{ol}
Remove A_{ij}^{ol}, insert new press m and insert A_{mj}^{kl} and then insert A_{mj}^{ol}
Else
Add a penalty cost for being below re-order point, and get next order.

Step 5: Use a modified 1-Opt and 2-Opt to realign the execution of the scheduled jobs for all presses.
Step 6: Exchange one job from one press with a different press for all presses.
Step 7: Exchange one job from one press with another job in a different press for all presses.
Step 8: If there are more jobs to be scheduled, go to Step 4.

The algorithm initially places all the orders to be fulfilled into a list. The first order is selected and the product type for the order is used to collect all orders for the same product type and place it at the top of the list. This allows orders for the same product type to be scheduled sequentially. If the quantity for the current order is greater than the quantity for the reorder level, then the order is fulfilled from the available inventory and the next order is obtained. If the quantity requested results in the inventory for the product falling below the reorder level, then it is scheduled for production. The algorithm initially locates a free press or a press that has been set up to produce the requested part for adding the current order. If a press cannot be found, then it locates a job that needs to be swapped out of the orders that have been scheduled using the presses. The order that has the highest reorder level in comparison to all the scheduled processes is selected to be swapped out. Different combinations of swapping orders are tried and the one that results in the least cost with respect to equation (1) is selected. If the order cannot be scheduled then a penalty cost is added for all orders that cannot be fulfilled and the next order is obtained for scheduling. Once all the orders are scheduled modified 1-opt and 2-opt [12-13] and modified exchanges [14-15]are

executed to improve the solutions. If any improvements took place, then the orders that were not fulfilled were attempted to be placed into the presses. This process continues until no improvements are obtained an no more orders can be scheduled.

COMPUTATIONAL RESULTS

The implemented algorithm was tested on a real-world problem from the manufacturing environment. The manufacturing environment had 15 presses of 5 different types, 4 teams and tools for producing more than 70 different types of molds. There were a total of 785 orders with each order consisting of the part number, customer, priority, due date and time and total quantity of the required product. The part number in each order is used to obtain the part number information from the tools table. The tool table consists of a collection unique part numbers. Associated with each part number is the description of the part, the preferred presses, number of cavities, cycle time, yield, installation and removal time, and maximum, minimum, recorder and current inventory levels for the part. The collective information of the orders, presses, teams and part numbers are used to schedule the production of molds. The parameter values were set to L=5, α=0.60, =0.30 and γ=0.10. The day on which the production is to start was set to different values of starting the production a few days before the requested order, same day as the requested order and a few days after the requested order. Starting the schedule before the requested order were set to three days before (-3), two days before (-2) and one day before (-1) before the requested date of the order. Starting the schedule after the date of the requested order was set to one day after the requested order (+1), two days after the requested date (+2) and three days after the requested date (+3). Production schedule was also tested on orders that were started on the same day as requested (0). The results of the analysis are listed in Table 5. The analysis was used to measure the total number of tool changes required to complete the orders, the number of orders that were late and the total time, in minutes, of all late orders.

The solutions obtained were compared with an available manual solution. The manual solution took approximately six hours to compute, required a total of 58 tool changes and did not have any tardy orders. The best solution obtained by the implemented algorithm required 55 tool changes and no tardy solutions. The drop in 3 tool changes is a savings of six hours of work and the solution was obtained in a few seconds for a five day schedule.

In addition to obtaining better solutions in a fraction of the time, in comparison to a manual solution, the graphical user interface (GUI) for the system (see Appendix A) allows the users to try out "what-if" scenarios and obtain solutions to the scenarios in a few seconds.

The GUI supports a number of different functionalities that allows for real-time scheduling. Initially the parametric weights need to be set before implementing the algorithm. The algorithm can be implemented to obtain a solution with and without local and global optimizations. Once the solutions are obtained, the schedules can be viewed with respect to

Table 5. Computational results on solving a real-time problem.

Type	Days before request													
	-3		-2		-1		0		1		2		3	
	TC	LO	TC	LO	TC	LO	TC	LO	TC	LO	TC	LO	TC	LO
Init	59	0	59	0	59	0	59	2	62	9	62	25	62	28
Ex1	57	0	59	0	56	0	59	1	62	7	62	14	60	20
Ex2	57	0	55	0	56	0	59	2	62	9	62	25	60	28
Ex3	57	0	55	0	56	0	59	1	62	7	62	14	60	20
Ex4	57	0	55	0	56	0	59	1	62	7	62	14	60	20
Ex5	57	0	57	0	56	0	60	1	63	8	61	14	60	21
Ex6	57	0	55	0	56	0	56	2	64	8	64	14	61	20
Ex7	57	0	57	0	56	0	59	1	62	8	62	13	62	20
Ex8	57	0	55	0	56	0	55	2	63	8	64	14	63	20

Init – Initial solutions; TYPE – Types of experiments executed on data: Ex1: 1-Opt; Ex2: 2-Opt; Ex3: 1opt-2opt; Ex4: 2-opt, 1-opt; Ex5: Ex 1-0, 1-Opt, 2-Opt; Ex6:Ex 1-1, 1-Opt, 2-Opt; Ex7:Ex 1-0, 1-Opt, 2-Opt, Ex 1-1, 1-Opt, 2-Opt; Ex8: Ex 1-1, 1-Opt, 2-Opt, Ex 1-0, 1-Opt, 2-Opt; TC – Tool changes; LO – Number of late orders.

the individual presses, types of presses and teams. In each of these views the user can manipulate the data to the real-time conditions and obtain new solutions. In addition, the individual orders can also be changed based on real-time data. For example, an order can be added, deleted or changed in real-time during the production and execution of the orders.

Table 5 lists the solutions obtained using the implemented algorithm with different local and global heuristic methods. As expected, the scheduling of the process obtains good solutions for those orders that are known well in advance (DBR=-3, -2, and -1). As the advance knowledge on orders are reduced (DBR=0, 1, 2, 3) the number of tool changes and total number of tardy orders increase. When orders are known in advance an algorithm that uses the exchange 1-1 with local one- and two-opts obtains good solutions. For orders that are not known in advance, an algorithm that incorporates exchange 1-1 and exchange 0-1 with local one- and two-opts opts obtains good solutions. Though this might not apply in all situations, it gives a generic idea on what type of algorithms to apply for real-time events. That implemented system has the added advantage of being able to apply more than one type of algorithm to obtain a solution in real-time as it takes only a few seconds to obtain a solution to a given problem on 800 MHz Pentium machine with 512MB of memory running on a Windows 2000 operating system.

The implemented system is only one-part of the whole process and is affected by all the other factors that scheduler has to deal with in order to produce a good schedule. The implemented system is an invaluable tool that takes away the complexity of scheduling the orders once all of the required information is available. In addition the tool allows the scheduler obtain multiple solutions and also execute "what-if" scenarios which were not an option when trying to solve the scheduling problem manually.

CONCLUSION

We described a job shop scheduling algorithm and a graphical user system used for solving a real-time scheduling problem. The problem involves scheduling presses for manufacturing molds using a predefined set of teams, assigned to scheduling tasks, based on skill levels. The problem consists of a set of presses, machines used for creating molds, onto which only certain cavities or tools, for making molds, can be inserted that need to be scheduled to complete a set of jobs. Each tool consists of a certain number of cavities and may produce one or more different products depending on the design of the tool. The implemented system obtains improved solutions to a real world problem in a few seconds on an 800 MHz system in comparison to the manual solution. It required a few hours to obtain a manual solution to the same problem. The solution obtained by the system to the real world problem reduced the total time required for completing all the jobs by six hours over a five day period.

In addition, the system allows for the manipulation of the scheduling problem in real-time. The graphical user interface (GUI) gives the user the capabilities to visually inspect the scheduling process and manipulate any attributes of the system in real-time.

REFERENCES

1. Bierwirth C., Kopfer H., Mattfeld D.C. and Rixen I. (1995) Genetic Algorithm Based Scheduling in a Dynamic Manufacturing Environment. In (pp. 439-443). IEEE Press.
2. Lin S., Goodman E. and Punch E. (1997) A Genetic Algorithm Approach to Dynamic Job Shop Scheduling Problems. In T. Bick (Ed.), (pp. 481-489). San Mateo, California: Morgan Kaufmann.
3. Nof S.Y. and Grant F.H. (1991) Adaptive/Predictive Scheduling: Review and a General Framework. *Production and Planning Control.* **2**:298-312.
4. Parunak H.V.D. (1992) Characterizing the Manufacturing Scheduling Problem. *Journal of Manufacturing System.* **10:** 241-259.
5. Garey, M. R. & Johnson, D. S. (1979). *Computers and Intractability: A Guide to Theory*
6. Blazewicz J., Domschke W. and Pesch E. (1996) The Job Shop Scheduling Problem. *European Journal of Operational Research.* **93**: 1-3.
7. Anderson E.J., Glass C.A. and Potts C.N. (1997) Machine Scheduling. In E.H.L.Aarts & J. K. Lenstra (Eds.), *Local Search Algorithms in Combinatorial Optimization* (pp. 361-141). New York: John Wiley.
8. Graves S.C. (1981) A Review of Production Scheduling. *Operations Research.* **29**:646-675.
9. Pinedo, M. (2002). *Scheduling: Theory, Algorithms and Systems.* (2nd ed.) Prentice Hall.

10. Baker K.R. (1974) *Introduction to Sequencing and Scheduling*. New York: John Wiley.
11. Raman N. and Talbot E. (1993) The Job Shop tardiness Problem: A Decomposition Approach. *European Journal of Operational Research.* **69:** 187-199.
12. Lin S. (1965) Computer Solutions of the Traveling Salesman Problem. *Bell Systems Technical Journal.* **44***:* 2245-2269.
13. Lin S. and Klingman D. (1973) An Effective Solution to the Traveling Salesman Problem. *Operations Research* **20***:* 498-516.
14. Thangiah S.R. (1999) A Hybrid Genetic Algorithm, Simulated Annealing Tabu Search Heuristic for Vehicle Routing Problems with Time Windows. In L.Chambers (Ed.), *Practical Handbook of Genetic Algorithms: Complex Coding Systems, Volume III* (3 ed., pp. 347-383). CRC Press.
15. Thangiah S.R. and Petrovic P. (1998) Introduction to Genetic Heuristics and Vehicle Routing Problems with Complex Constraints. In D.Woodruff (Ed.), *Advances in Computational and Stochastic Optimization, Logic Programming, and Heuristic Search* (pp. 253-286). Kluwer Academic.

APPENDIX

The Graphical User Interface for Scheduling Teams and Presses

The main window, Figure A1, for the graphical user interface for scheduling the teams and processes allows the user to select a number of different options: starting date of the schedule, number of days in the scheduling process, penalty weights for lateness, tool runs and late orders, creating the initial schedule and the type of local optimization m ethods to be used for improving the initial solution.

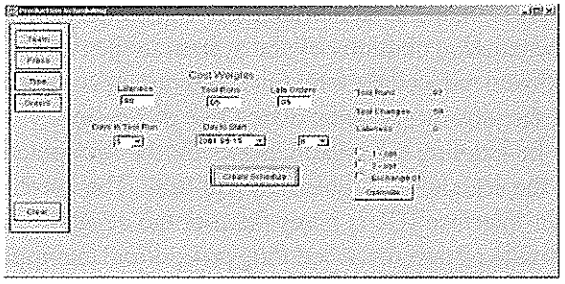

Figure A1. Main window to the graphical user interface for scheduling teams and presses.

The initial schedule for the problem is obtained by clicking on the Create Schedule button. Once the initial solution is obtained, the user has the option to select different combinations of local optimization methods that can be used to improve the initial solution. Selecting the different combinations of optimization methods followed by clicking of the Optimize button will result in local optimization being applied to the initial solution.

Once the initial solution and local optimization have been implemented on the problem at hand, the panel on the left hand corner of the main widows can be used to view result details of the results. The results can be viewed from the aspect of the teams, individual presses, press types or orders. This gives a panoramic view of the whole process.

Pressing the Team button on the panel will display the teams and their job assignments (see Figure A2).

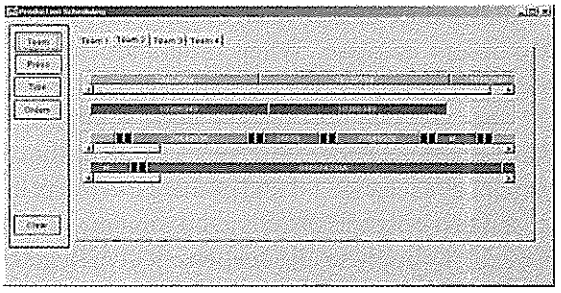

Figure A2. Display of the teams and assigned jobs.

In Figure A2, the information on different teams can be accessed using the tab panel. Each tab panel displays the job assignment to the presses for a particular team. Each of the jobs in the different presses is color coded. If two different jobs, that are scheduled one after another, are displayed by the same color, it indicates that no tool changes are required between the two jobs. Two consecutive jobs that require tool change between then are represented in two different colors with two black color coded squares between them. The two black color coded squares indicate the time for removal of the tool and installation of a different tool that is compatible with the next job.

Figure A3 displays the individual presses and the assigned jobs. Figure A4 gives a different perspective of the presses where one can display the jobs that have been assigned to the different press type.

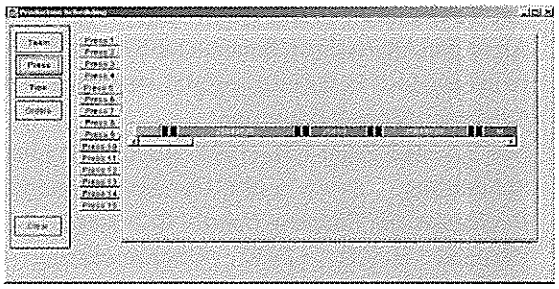

Figure A3. Display of the presses and the assigned jobs.

Selecting any of the panels that is used to display the jobs that have been assigned to the team, individual presses, or press types and clicking on a job will give all the details of that job. This allows the user to have both a global view of the job assignments and also local view of the job details (Figure A5).

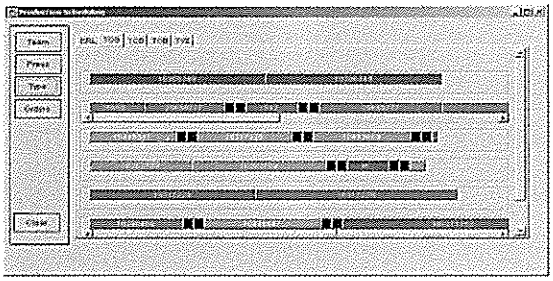

Figure A4. Display of the different press types and the assigned jobs.

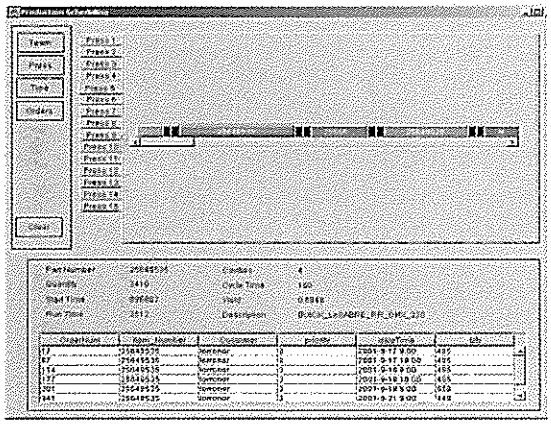

Figure A5. Display of the different press types and the assigned jobs.

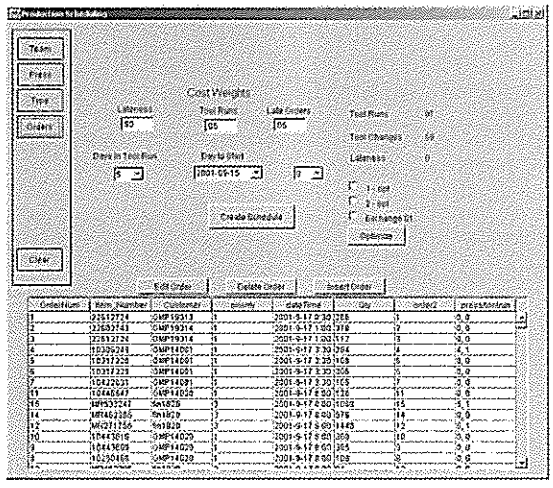

Figure A6. Display of the different press types and the assigned jobs.

In Figure A6 clicking on the Orders button displays all the orders that are in the database at the current time. The user has the option to edit an order, Figure A7, insert a new order, Figure A8, or delete an order, Figure A9. The edit, insertion and deletion of the orders allow the system to handle real time issues in which information on orders can change in real-time. An insertion, edit or deletion of an order will result in the algorithm being re-executed to consider the changes. As the algorithm is able to obtain good solutions in a few seconds, the re-execution of the entire algorithm is applicable for real-time scheduling.

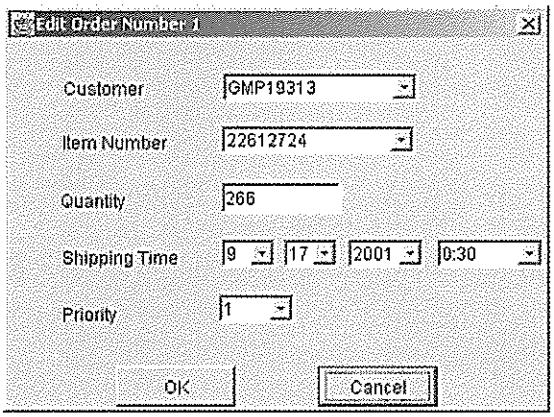

Figure A7. Display of the edit frame for editing information on a job.

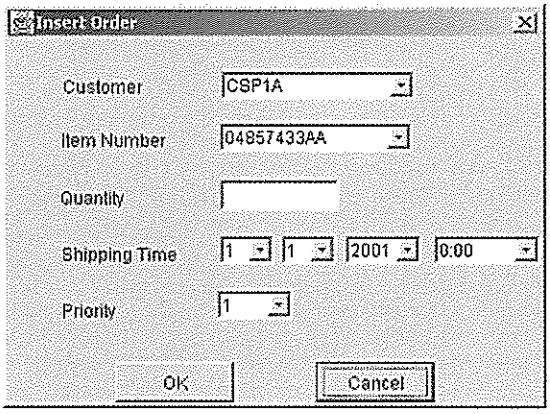

Figure A8. Display of the frame for inserting a new job into the system.

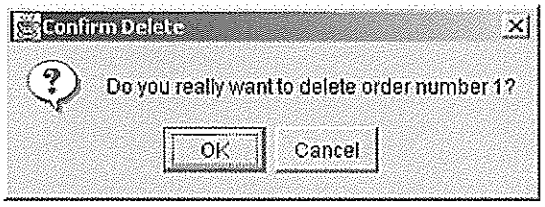

Figure A9. Display of dialog box when deleting a job.

Journal of Science and Technology in the Tropics (2005) **1**: 67-77

The fiber-fluid model of the human heart

N. Selvanathan, S. Y. Tan, S. Nagappan and M. Sankupellay
Faculty of Computer Science and Information Technology, University of Malaya,
50603 Kuala Lumpur, Malaysia

Received 7 April 2005; accepted 18 May 2005

Abstract The virtual heart model is based on moving fluid as streamline flow based on the Navier-Stoke equation. The fluid is the blood moving within the walls of the heart, which is represented by fibers. The boundaries of the heart are not fixed. It is moving based on the elasticity of the fibers (heart wall mechanics). The study of fluid motion within a moving boundary has been a difficult and challenging research problem and the fiber-fluid model proposed by Peskin and McQueen can serve to partially address this issue of the moving boundary. This paper serves to address this issue of linear fluid flow within a moving boundary in the context of the left ventricle of the human heart. A simulation study of the heart structure reconstruction and cardiac fiber reconstruction was carried out. The fiber-fluid model (Immersed Boundary Method) was implemented and the cardiac dynamic and blood flow results were studied.

Key words virtual heart – heart modeling – immersed boundary method – fiber fluid-cell model

INTRODUCTION

The study of the heart encompasses many varied disciplines. The mechanical activity of the heart is closely linked with the electrical activity and this again is related to the transmembrane calcium fluxes, which affect the cardiac contractual state. The myocardial stress and strain field is related to cardiac wall motion and to the ventricular pressure within the chamber. There is also a complex relationship between mechanical activity, myocardial metabolism and stress field affecting coronary blood supply and also the influence of local metabolic production which regulate blood flow through a variety of mechanisms. It is still not possible to understand the relationship between mechanics, electrical activity, metabolic production and oxygen transport.

Simple models of the heart have been used to study the structure and material properties. A cylindrical finite model was used to analyze passive Left Ventricle (LV) inflation by Guccionne *et al.* [1]. They demonstrated the material anisotropy associated with fiber orientation, and the twisting that occurs during passive filling.

Similar findings [2-3] in axially symmetrical constructed model of the canine LV have been reported. The strain distribution predicted for different levels of passive LV inflation were compared with experimental results [4]. Active contractions were compared with predicted strains [5]. Usyk *et al.* [6] tested the hypothesis that the difference between predicted and measured transverse shear strain might be due to material orthotropic.

Vetter and McCulloch [7] described a model using anatomically deflated representation of the right ventricle (RV) and LV geometry. There is excellent agreement between measured and predicted epicardial strains from the demonstrated fiber orientation in the rabbit heart. Accurate representations of ventricular anatomy have been used with a "pole-zero" material law to model passive filling in the dog's heart [8] and predict active and passive deformation in the pig's heart [9]. The correlation between predicted and observed strain is good.

Hunter *et al.* [4,5] provides detailed reviews of FEM for the heart, which is another popular approach to represent the heart anatomy where a reference mesh is

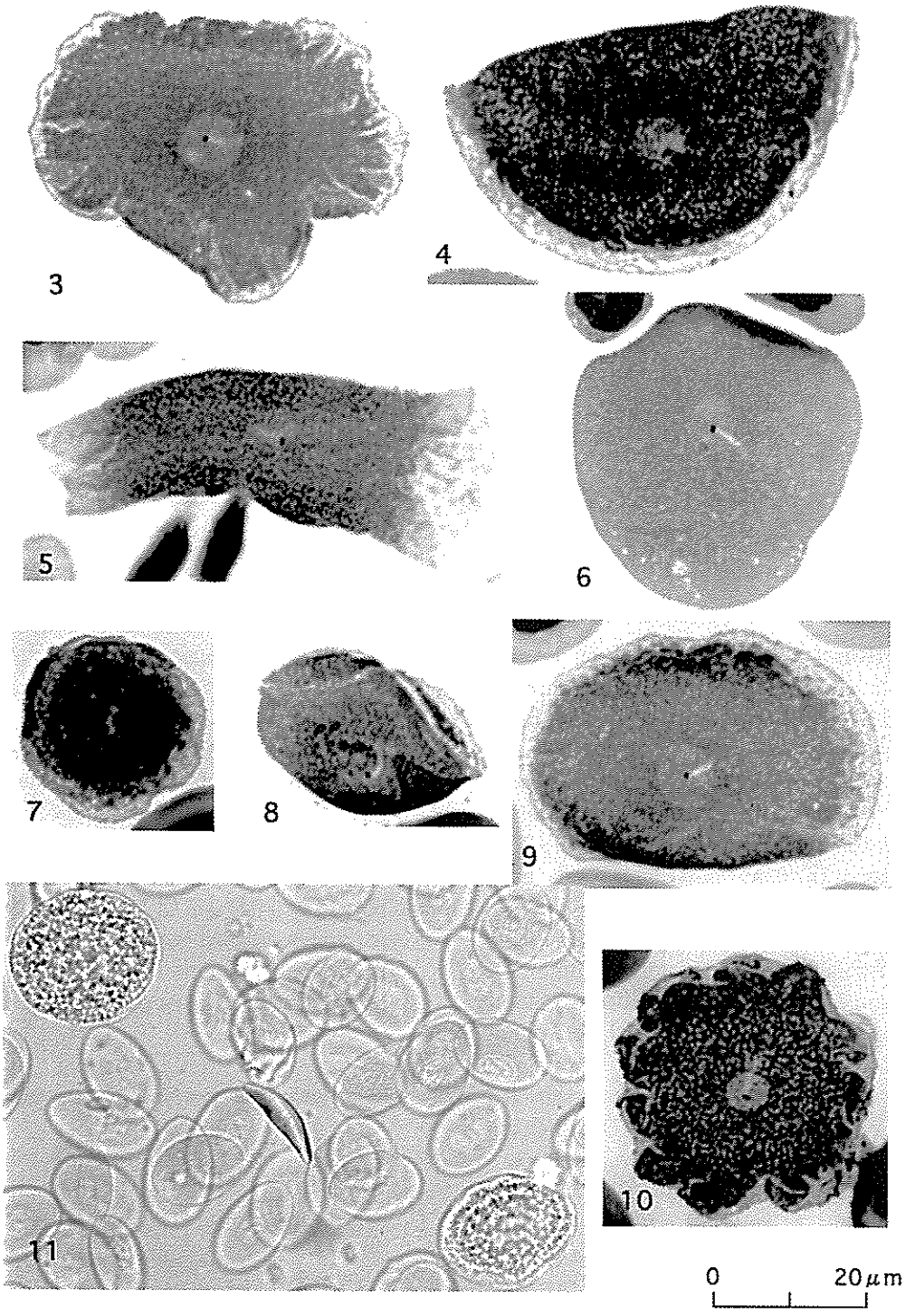

Figures 3-11. **3:** *Diamondtrypanum chattoni* (Mathis & Léger, 1911), new combination, in *Bufo melanostictus*. **4**: *Diamondtrypanum katak* new species, in *Rana chalconota*. **5**: *Diamondtrypanum katak* new species, in *Rana erythraea*. **6**: *Diamondtrypanum chattoni* (Mathis & Léger, 1911), new combination, in *Bufo melanostictus*. **7-8**: *Diamondtrypanum tsunezomiyatai* (Miyata, 1978), new combination, in a Malaysian frog, *Rana limnocharis*. **9**: *Diamondtrypanum chattoni* (Mathis & Léger, 1911), new combination, in *Bufo melanostictus*. **10**: *Diamondtrypanum bungateratai* new species, in *Rana blythi*. **11**: *Diamondtrypanum katak* new species, in fresh material of *Rana hosii*.

defined so as to match the geometry of the cardiac chambers. A field variable is defined for each element, interpolated with values associated with the element nodes. Linear Lagrange basis functions provide the linear interpolation that maintains continuity at element boundaries. Large number of linear elements is required to produce complex spatial variation faithfully.

Besides the geometry information, the material properties of cardiac tissues are required to be considered in deep in order to capture the dynamic of the human heart model. The properties of the material require detailed information about the relationship between force and length. For the purpose of modeling, the material properties of passive myocardium soft tissue modeled as incompressible elastic solids for which the components of the second Piola-Kirchhoff stress tensor T_{ij} is given as [26]:

$$T_{ij} = \frac{1}{2}\left(\frac{\partial W}{\partial E_{ij}} + \frac{\partial W}{\partial E_{ji}}\right) - PC_{ij}^{-1}$$

where E_{ij} is Green strain components
P is Hydrostatic pressure
C_{ij} is Cauchy-Green strain tensor

The indices refer to the material axes aligned with the fibrous-sheet structures at every grid point. Strain energy function of the form

$$W = \frac{1}{2}C\left(e^{Q} - 1\right)$$

has been used to model the material property [6,28-31] where Q is the function in which the strain component E_{ij} refers to the local structure based coordinates. Robust material laws that accurately represent the mechanical properties of passive and active myocardium in different regions of the heart are essential for 3D modeling. There is still a lot of research work that needs to be done in this area.

The study of myocardial mechanic, which is an important research field to explore, requires researchers to construct a human heart model. The mechanical behaviors of cardiac structures have been studied extensively [10]. There is fairly a good understanding of the mechanics of the heart at gene/cellular level but this information is not sufficient to understand the 3D mechanical behaviors of the heart. Heart wall motion and myocardial deformation and strain can be estimated quite accurately. Complete heart modeling based on continuum mechanics principle enable us to bridge the gap in the understanding of the normal heart functions.

In a nut shell, the continuum models of the cardiac mechanical function have two requirements:

(a) Appropriate representation of the 3D geometry.

(b) Information about time-varying mechanical behaviors of contracting and non-contracting tissue in different regions of the heart.

It is then possible to solve equations that obey physical laws of conservation of mass, momentum and energy, subjected to pressure and displacement boundary conditions [11]. At present, the accuracy of continuum modeling is constrained by incomplete knowledge of the constitutive relations between the 3D mechanical behaviors of myocardium and the anatomic description of the heart. The use of a model to minimize the difference between predicted and observed results provide a means of addressing this issue. Information about 3D wall motion deformation and strain in normal and abnormal hearts are available from X-rays with radio-opaque markers or Cardiac Magnetic Resonance tissue tagging.

METHODOLOGY

The virtual heart model implemented in this paper is the Immersed Boundary Method of McQueen and Peskin [12]. The formation of the model can be summarized as follows:

(a) The geometry of the heart is represented as fibers.
(b) The tissue material is represented as a 1D fiber extension relation.
(c) The tissue structure is immersed in blood.
(d) Momentum is exchanged between the fluid and tissue fibers by means of a special interpolation scheme.

Detailed description of (a), (b), (c) and (d) is given below. The computing architecture of the immersed boundary method is also described. The model neglects tissue inertia and the shear properties of the myocardium.

The fluid mechanics of the blood flow in the heart (the Navier-Stokes equations) are well understood [13-14, 20]. In the implementation of the Immersed Boundary method, the major challenge faced is the coupling of the 3D fluid flow equation to the moving boundary. Here, the moving boundary is the ventricular surface.

The cardiac dynamic simulation involves solving a number of complex mathematical equations in real time in order to simulate the dynamic heart model. The solving of these mathematical equations requires high computing resources in order obtain precise results. However, the equations can be more effectively solved by leveraging on the distributed computing technologies available widely nowadays. Our implementation architecture is designed based on clustering for high performance computing.

Virtual reality and visualization are important concepts to simulate results that are to be displayed on a computer screen. There is no significant meaning if the results are represented in a numerical format. Computer graphics technologies are playing an important role in this area. It is required for translating simulated numerical results into complex three-dimensional objects in real time. Interactive computer graphics are also required during the model design and result analysis. Through it, objects can be animated, manipulated, displayed in any point of view and magnified into any region of interest as stated in [15].

Figure 1 outlines the virtual heart model research undertaken at University Malaya:

Cardiac cell model

The elastic fibers are made up of cells that expand and contract. The heart is made up of billions of cells, which make up the heart fibers. The heartbeat is actually controlled by the flow of ions in the cardiac cells. There are several types of ion activities such as ion current, pumps and exchanges at the cardiac cell level that can be represented with a number of cellular models. The modeling is based on the knowledge from standard chemical reactions and electrophysiology. With these models, it will be possible to predict the outcome of a diseased heart due to its abnormal ion activities. This type of cell model can be easily extended to incorporate genetic information. This allow us to model the impact of the environment (e.g. pollution), life style (e.g. smoking, stress) and hereditary (e.g. hypertension). If it is known a gene causes a specific heart disease, then it will be possible to model this disease by turning on the gene and simulating the development of the disease in the heart. This process will be useful for drug discovery, where drugs that influence genetic processes can be tested virtually in the computer before being tested on actual humans.

Determination of material property

Stochastic finite element method was used to estimate cardiac kinematics functions and material model parameters. The current implementation assumes constant linear elasticity of the heart muscle with varying distribution of Young Modulus and the Poisson Ratio [18]. The myocardial dynamics are [19]:

$$M\ddot{U} + C\dot{U} + KU = R$$

where ,

C = Dampening factor
R = load vector
U = displacement vector
M = material density

K = function of strain-stress relationship and is related to Young Modulus, E and Poisson ratio, $\acute{o}$ which can vary spatially.

From the above equation, suitable discretization of the spatial distribution of Young Modulus and Poisson Ratio can be determined. It is important that the material characteristics of the myocardium measured by the Young Modulus (E) and Poisson Ratio ($\acute{o}$) are taken from an actual human heart. Thus, the model although virtual, should behave physiologically and mechanically as a real heart.

Heart structure reconstruction

The virtual heart model used in this paper was derived from Diffused Tensor MR images [21]. Diffusion

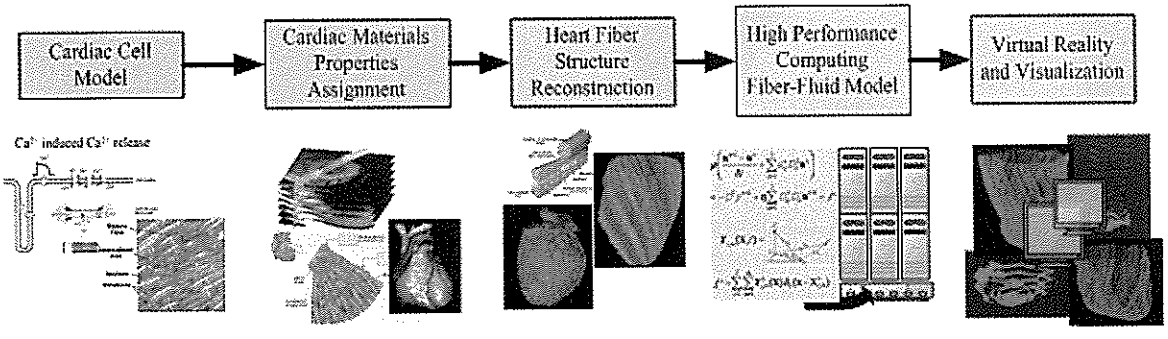

Figure 1. Research framework for virtual heart modeling carried out at University Malaya.

properties allow modeling of fiber orientation in the ventricular myocardium. By using the Moving Least Square (MLS) fiber tracing algorithm [17], the fiber can be traced along the principal eigenvector direction. The method used to reconstruct the fibers for our heart model is described in detail in [34]. In establishing the virtual heart model, the following concepts should be in place before the model can be used to predict its behavior.

1. The geometry of the model should approximately be the same as an actual heart. The parameters like elasticity, Young Modulus, Poisson Ratio should also be identical to that of a real heart.
2. The number of layers of muscle fiber and the fiber orientation should be identical to that of an actual heart.
3. The correct sequence of propagation electrical activation.

So far we have addressed (1) by obtaining the geometry from MR images of the heart and through segmentation of these images. The segmentation will lead to a three dimensional geometry of the heart. Refer to the figure below for the steps taken to construct a 3D geometry model of the heart [34].

Item (2) is also addressed through the use of the fiber orientation algorithm. Refer to Figure 10 in section 3.1 for the constructed fiber model of left ventricle epicardium. The heartbeat is triggered by electrical activation that originates at the sinoatrial node (located at the upper portion of the right atrium) and then spreads to the rest of the heart tissues. In our implementation, since we are only modeling the left ventricle, we assume the propagation starts at the apex and then proceeds sequentially towards the base of the heart (Item (3) above).

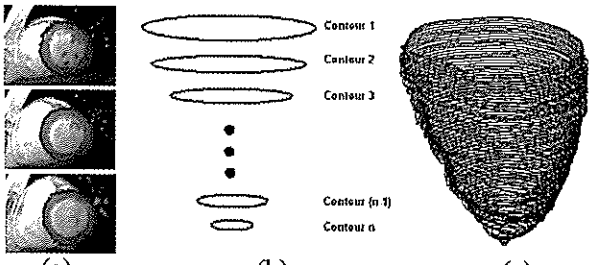

Figure 2. (a) Some selected result of epicardium segmentation process on MR images. (b) Shows schematic diagram of how we stack the contours from segmentation. (c) The three dimensional geometry of left ventricle formed by two dimensional contours obtained from the segmentation process.

Immersed boundary method

The Immersed boundary method (IB method) had been proposed and developed by Charles Peskin and David McQueen of the Courant Institute of Mathematical Sciences (CIMS). This numerical method is an efficient way to simulate systems where elastic fibers are immersed in an incompressible fluid (described extensively in [14]). The IB Method is applicable to problems where a fluid interacts with an elastic material, cardiac fiber in our case. In this method, the elastic material is treated as a part of the fluid in which additional forces (arising from the elastic stresses) are applied [14]. Studies of computational method for blood flow in the heart had been done using this method where the details are presented in [23-26].

The fibers are represented as geometric points and are placed in the fluid. A three-dimension rectangular lattice is used to represent the fluid, as shown in Figure 3.

After every time step, each fiber point obtains a force value (resulting from heart contraction) that is calculated by the following algorithm. Each fiber points needs to know the coordinates of its neighbors in order to calculate the force (Figure 4a). These forces are called Immersed Boundary elastic forces. The amount of force generated is according to the derivation from an energy function created for each entity. The entity is a set of connected immersed boundary points. The energy function has three contributions: energy from stretching springs, energy from bending the entity and energy from moving the entity away from a specified location [22]. The produced fiber forces will now act on the fluid lattice at certain selected points (Figure 4b). For simplicity, the figure shown here is in two dimensions

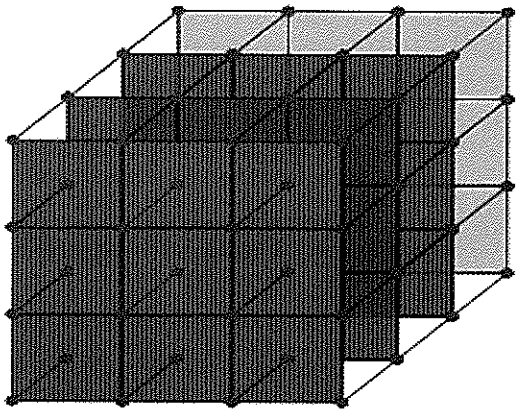

Figure 3. Three-dimension cubic lattices in representing the fluid simulation experimental space. The fluid grid points are represented as dots.

only. The mathematical function known as Dirac delta function, which has a value at each point, is used to selectively exert the fiber forces onto the fluid lattice. The Dirac δ-function is defined as:

$\delta(\mathbf{X}) = 1$; where $\mathbf{X}$ is surrounded by 4x4x4 fluid cells

$\delta(\mathbf{X}) = 0$; otherwise

$\mathbf{X}$ represents the fiber point location in three-dimension geometry. Any fluid cell that is more than 4 units away from a fiber point will not experience the force generated from that fiber point.

The velocity is then calculated for the fluid lattices using the Navier-Stokes equation. Solving this equation produces the velocity and pressure in each fluid lattice (Figure 5a). Once again, via Dirac delta function, the velocities of the fiber points are updated. Each of the fiber point is then moved to new location based on its velocity (Figure 5b). In the next time step, based on the new position of the fiber, the forces are recalculated and the entire operation is repeated. Figure 6 summarize the 4 major steps in Immersed Boundary Method.

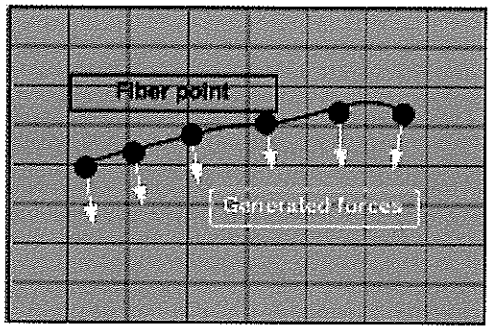

(a)

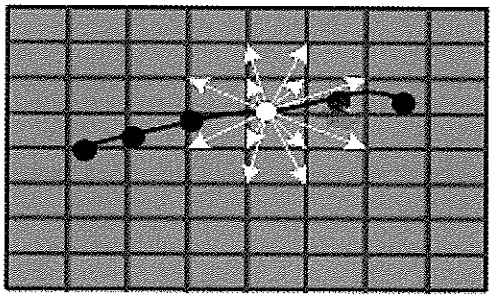

(b)

Figure 4. (a) The forces generated from the each fiber point. (b) The fiber points, represented in black color, carry forces (white arrows) to be exerted onto the fluid lattice.

A data structure is defined to store all the fiber points' coordinates as well as its parameters. The parameters are: contraction factor, the stiffness value and the initial distance between two adjacent fiber points. The contraction factor is determined based on the cardiac cell model. The higher the contraction factor means the larger the force produced by the fiber point during its contraction phase. The material properties

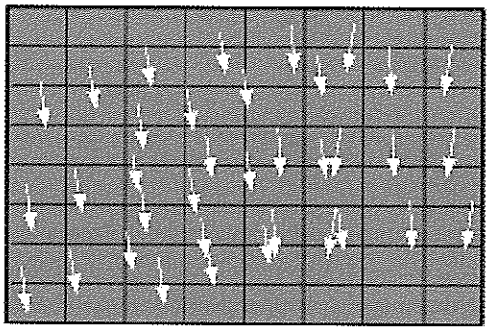

(a)

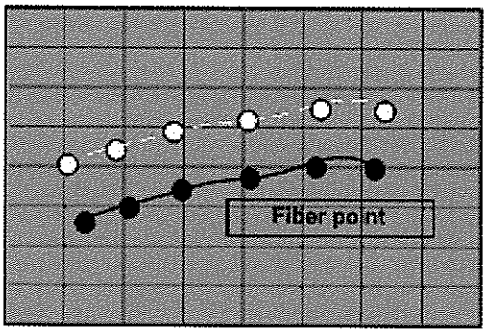

(b)

Figure 5. (a) Each fluid lattice undergoes different velocity that is obtained by solving the NS equation. (b) Fiber points are moved to new locations after updating their velocities. The old positions of fiber points are represented in yellow color.

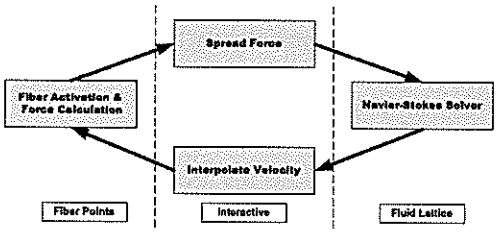

Figure 6. The 4 major tasks in the IB Method in each time step.

carried by a specified type of cell play a role in determining their stiffness value. At the beginning of each time step, if the distance between two consecutive fiber points is different from the initial defined value, the force generated is calculated using Hooke's Law.

The implementation algorithm is as follows:

1. Input the dimension of the fluid space as well as the fiber data.
2. Parameters to be read:
   (a)Parameters of fiber points.
   (b)Viscosity of the fluid.
   (c)Number of time step to simulate.
   (d)Duration of each time step.
3. Input fluid markers' geometry: The structure of fluid markers is similar to fiber points but does not contain any parameters that influences force generation. They are moved at the local fluid velocity by the same algorithm that is used to move the fiber points. (Full details provided in 2.5)
4. The program creates objects that will manipulate the immersed fluid lattice and fiber information. The fluid lattice data structure contains the fiber point objects.
5. Program will then rearrange the fiber points (coordinates) into a list of fiber fragments and registers it with the fluid lattice object.
6. The force produced by each fiber point is calculated and the corresponding fields (e.g. velocity, 3D coordinates) for each fiber object are updated.
7. The fluid lattice object is advanced by one time step by executing the following tasks:
   (a)Forces calculated in (4) are spread onto the fluid lattice.
   (b)Solve the Navier Stokes equation for the fluid velocity.
   (c)Interpolate the velocity back to the fiber points.
8. Repeat steps (6) and (7).

The coordinates and force values of the fiber points are the "in-parameters" to the fluid lattice while the fiber object and the velocity vector are the "out-parameters".

For the purpose of visualization, after a predefined number of time-steps, the numerical results for the fluid grid as well as the velocity and pressure field are dumped to an output file. The fiber coordinates of a specified time step is also available. To visualize the fluid, the fluid marker data at a specified time step is also output as a file. These numerical data are then loaded into a visualization program for further processing in order to display three-dimensional animated model on a computer screen.

Fluid marker

Fluid markers are a set of fibers that do not contribute any force into the fluid experimental space during simulation. However, the surrounding fluid influences their movement. Hence, the movement for the fluid markers can be used to analyze the fluid mechanics. In other words, the markers are used to analyze the blood movement inside the LV chamber during ejection. For this reason the geometry representation of the fluid marker needs to conform in terms of physical location within our fiber model. Specifically, the fluid marker geometry needs to be generated in such a way that they are inside the left ventricle chamber. The figure below shows the layout of the fluid markers as well as its relationship within the LV. The fluid markers are generated at multiple horizontal layers where each layer consists of multiple rings. The reason the fluid markers are generated with multiples layers and rings in the LV is to analyze the fluid dynamics at different locations in the LV chamber (Figure 7b). The outermost ring in each layer is used to observe the fluid mechanics near the endocardium. The lowest horizontal marker layer is used to analyze the fluid dynamics near the heart's apex.

Computing architecture of the IB Method

Our algorithm also works in a distributed computing architecture by taking the processes of the fiber-fluid model and distributing it across all the available processors. The data structure and classes are optimally designed so as to maximize the resources made available through distributed computing. Due to the high computational requirement of the Immersed Boundary method, it is important that it is executed either in a multiprocessor or a distributed environment.

For the purpose of parallelization, the fluid lattice should be partitioned into slabs. Each of the fluid slabs is distributed to a single processor. The fiber points are also distributed into different processors in order to perform the simulation simultaneously (Figure 8a). To calculate the force, each fiber point should know the coordinates of its neighbors. If the neighboring fiber point is stored in another processor (i.e. fiber cut by boundary), the fiber point will send a message to the

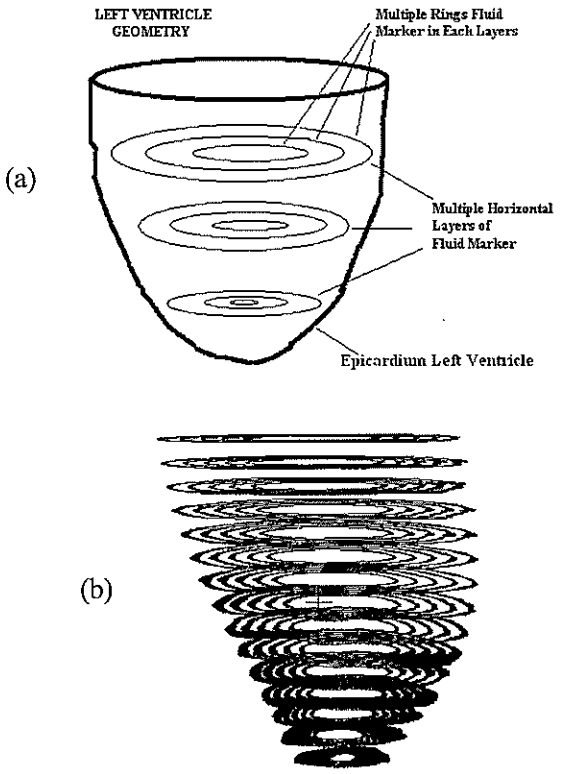

Figure 7. (a) The layout of the fluid markers and its relationship within the LV. (b) Multiple horizontal layers and rings of fluid marker generated to analyze the fluid mechanic in the left ventricle cavity.

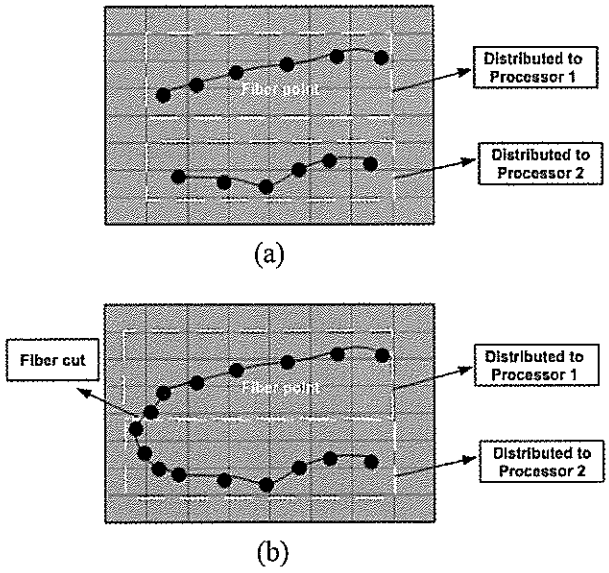

Figure 8. (a) A pair of fiber distributed into different processors. (b) Partitioning strategy on a two-processor distributed system results in the single fiber being cut into two segments.

other processor to get the neighbor's coordinate. In order to minimize communication, the number of fiber cuts must be reduced. Figure 8(b) shows how a fiber is cut in a distributed environment. The amount of computation is proportionate to the number of fiber points within the boundary of a processor. Hence, a partitioning strategy is required that can optimally balance computational load across the processors. Typically, we are dealing with more than 1000 fibers with an average of 300 points per fiber.

Each fiber point is assumed to affect 4 x 4 x 4 fluid cells surrounding it. A Dirac delta function is used to evaluate the force at a particular cell. If a fiber point is spreading the force to a fluid cell owned by another processor, then there is considerable communication cost. Ideally, the fluid cells for which force should be spread should belong to the same processor as the fiber. Also, in order to have a proper load balancing, each processor should own the same number of fiber points. In order to reduce the communication cost, each processor can bundle up the force updates to fluid cells on the same processor into one large data structure and transfer it to another processor as a single message.

The velocity of the fiber points are obtained by interpolating the velocity on the 4 x 4 x 4 fluid grid surrounding the fiber point. The Dirac delta function is used again to evaluate the sum of fluid velocity grid acting on the fiber point. The fiber points are then updated and their new location is based on their velocity. Hence, this phase has the same communication issue as the distributed force phase. When the fluid grid acts on a specified fiber point that is not located in a same processor, it will need to communicate through the network. Partition strategies are employed in order to group the fluid cells and the related fiber points into a same processor. The purpose is to minimize the communication overhead among processors during the simulation process.

Two types of partitioning strategy:

1. Fiber points are partitioned to the processor that contains the fluid cell that it is interacting with. Thus, this processor has to calculate both the force on the fiber and the velocity of the fluid cell. In cases where a fluid cell that does not contain any fiber points in it, the load experienced by it is much lower (i.e. its only need to calculate the velocities of the fluid cells). Hence, there is an imbalance in load distribution among the processors.

Journal of Science and Technology in the Tropics (2005) 1: 67-77

2. For the second strategy, the fibers are partitioned independently from the fluid cells and some of the fiber points may have to interact with fluid cells not in the same processor.

VISUALIZATION AND RESULTS

We have developed a suite of visualization programs that translates sets of numerical simulated results into 3D objects. These programs are equipped with interactive computer graphics features, whereby a user is able to toggle the appearance of the fiber in our heart model in real time. We can also interactively change our point of view and magnify any region of interest. Furthermore, these programs allow for the rearrangement of the simulated data sets and display them in a frame-by-frame manner in order to produce a smooth animation. Moreover, the programs are flexible enough to enable the display of the fluid markers along with the fibers. The programs are also used to view and verify the cardiac fiber model during the preparation stage before proceeding with the actual cardiac simulation.

We leverage the implementation of our programs on OpenGL technology that includes the OpenGL Utility Toolkit (GLUT) 3.6. C programming language has been used extensively to develop these programs. They are compiled into several executable programs which are able to run in different OS platforms such as Window XP, Linux Red Hat 9.0 and IRIX 6.5.13. However, most of our programs are implemented on a SGI workstation (2.4 MHZ Processor speed, 2GB of memory space) because of its high performance in real time graphic visualization tasks.

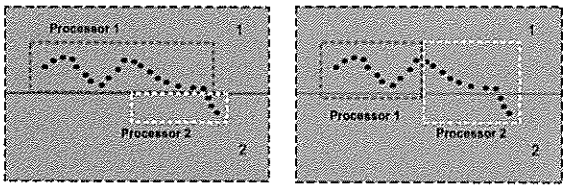

Figure 9. (a) The fluid lattice slab is distributed to two processors, numbered 1 and 2. Fiber points located in their fluid slab are also partitioned to the processor that owns the fluid lattice. In this case, processor number 1 contains 19 fiber points while processor number 2 only contains 3 points. (b) Shows fiber points are distributed equally to two processors independently from fluid cells. Each processor consists of 11 fiber points.

Cardiac fiber reconstruction

Figure 10 shows the results of constructing 1,200 fibers that is made up of 584,589 fiber points. The original epicardium material points extracted from MR images (see Figure 2c). Figure 10a and 10b shows the reconstructed fiber points from different points of view. The system consumed around 21 CPU hours in order to produce a complete fiber model.

Cardiac dynamic simulation

Each of the fiber point contains parameters that are needed for the Immersed Boundary method simulation (as described in Section 2.4). We simulated the heart dynamic for the systolic stage. We assigned our fiber contraction mechanism in such a way that its contraction begins at the base and then proceeds to the apex. The contraction factor at the apex is assigned to be greater than the factor at the base. Furthermore, we assume that the materials properties of the fibers cells at the LV epicardium layer are identical. Thus, we apply a unique stiffness values for all the fiber points. A refined fiber model with 1,038 fibers and 371,658 fiber points incorporated with the above mentioned parameters are provided as input for the cardiac simulation. The simulation consumed about 11 CPU hours to complete a total of 1024 time steps simulation.

After a predefined number of time-steps, simulated numerical results for the fiber model and fluid marker points are dumped to an output file. For cardiac and blood dynamic analysis purpose, the results are fed into our visualization programs (see Figure 11 and 12).

We generated the output data at every 8 time steps as a frame in order to obtain 128 frames in total. Some of the selected results are shown. Figure 11(a) to 11(d) shows the dynamics of the LV cardiac fiber from early ejection stage.

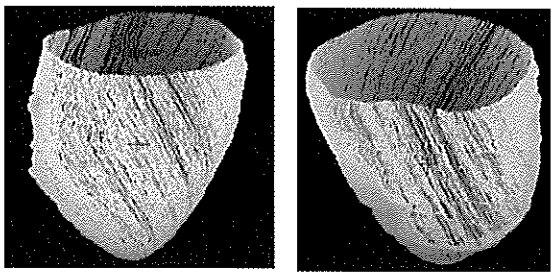

(a) (b)

Figure 10. Reconstructed fibers from different points of view.

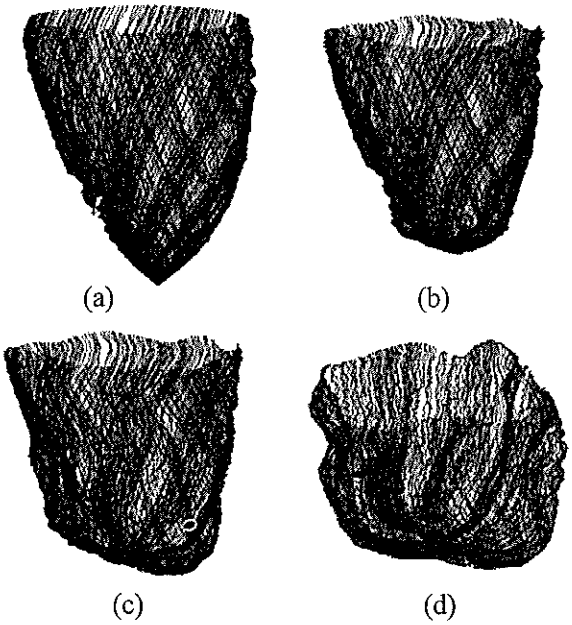

Figure 11. The results of the simulated LV cardiac muscle from early ejection stage. 0ms is the reference time for the start of ejection in this simulation. (a) Shows the simulated cardiac muscles at 0.05ms. (b) Shows result at 0.2ms. (c) Shows the fiber dynamics at 0.35ms and (d) shows result at 0.5ms.

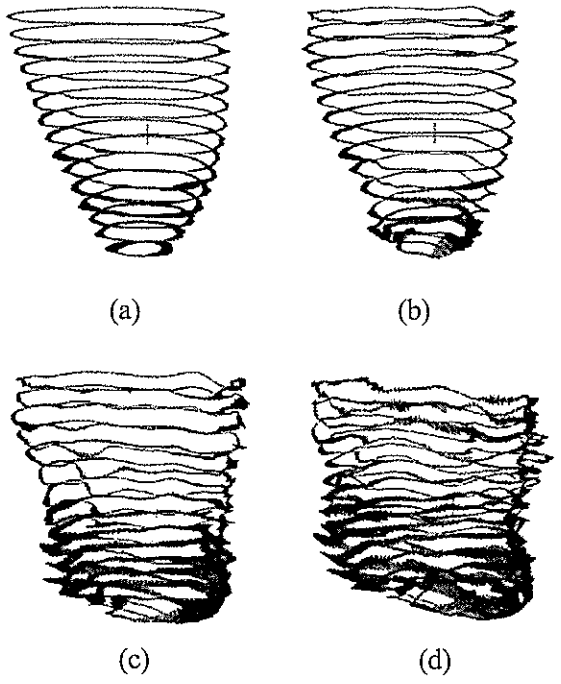

Figure 12. The results of simulated blood flow in LV cavity (based on Figure 11) from early ejection. (a) Shows the blood flow at 0.05ms. (b) Shows result at 0.2ms. (c) and (d) shows results at 0.35ms and 0.5ms respectively.

Blood flow mechanics

A series of outermost ring markers from each horizontal layer are shown in Figure 12 (a) to (d). The simulated fluid markers results are mapped (in term of physical time) with the cardiac fiber movement shown in Figure 11.

By allowing the visualization program to turn on the innermost fluid marker rings on all the horizontal layers, the blood flow mechanics at the centre of LV cavity (see Figure 13(a)) are captured. By turning on only certain horizontal layers of fluid markers, blood flow around the apex can be captured as well. In addition, by manipulating the appearance of ring markers and horizontal layer markers, the blood flow mechanics at different location in LV chamber can be visualized (see Figure 13(b) to (c)). As such, we are able to study a specific patient's blood flow using these simulated results and our visualization program.

CONCLUSION

In this paper we have discussed computer models of the heart in terms of ventricular anatomy structure and material properties. This study is in no way complete and there are researchers studying on the membrane ion channels, calcium handling and myofilament mechanics of cardiac myocytes. The models have established the computational framework linking cells to tissues and to the organ, but more aspects of physiological functions need to be included before one can understand the cardiac disease processes.

The fiber-fluid model represents a compromise between simpler two-dimensional (2D) models (models with predetermined geometric wall movement) and complex 3D models (both fluid flow and movement of the boundary of the myocardium). The fluid lattice, which is often described as a mesh for the Immersed

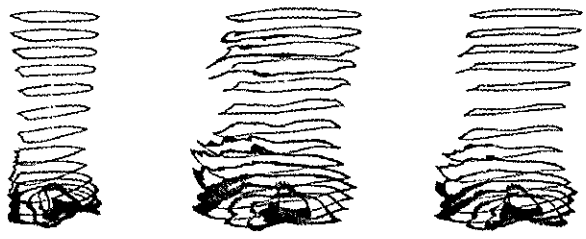

Figure 13. (a) shows the innermost fluid marker rings from each horizontal layers at 0.5ms, (b) and (c) show 2nd and 4th layers of fluid marker rings from each horizontal layer at 0.5ms respectively.

Boundary method, has been the subject of several studies [32,33].

The cardiac models described in the paper can be utilized to provide the structural properties of the heart. Physical properties such as stress, strain, flow and deformation can be used for diagnosis and surgery planning. However, other useful models incorporating electrical function of the heart, coronary circulation and, particularly, cell models are useful for drug testing and diagnosis of gene related diseases.

The major challenges for the heart modeling work are to extend the model to include the heart valves, to extend the tissue level so as to include the cell structure and to extend the cellular level models so as to incorporate signal transduction and metabolic pathways.

REFERENCES

1. Guccionne J.M., MCCulloch A.D. and Waldman L.K. (1991) Passive material properties of intact ventricle determined from a cylindrical model. *ASME J. Biomech. Eng.* **113**: 42-55.
2. Arts T., Veenstra P.C. and Reneman R.S. (1982) Epicardial deformation and left ventricular wall mechanics during ejection in the dog. *Am. J. Physiol. Heart Circ. Physiol.* **243**: H379-90.
3. Bovendeerd P.H.M., Huyghe J.M., Arts T., van Campen D.H. and Reneman R.S. (1994) Influence of endocardial-epicardial crossover of muscle fibres on ventricular wall mechanics. *J. Biomech.* **27**: 941-51.
4. Omens J.H., May K.D. and McCulloch A.D. (1991) Transmural distribution of three-dimensional strain in the isolated arrested canine left ventricle. AM. *J. Physiol. Heart Circ. Physiol.* **261**:H918-28.
5. Waldman L.K., Nossan D., Villarreal F.P. and Covell J.W. (1998) Relation between transmural deformation and local myofiber direction in canine left ventricle. *Circ. Res.* **63**: 550-62.
6. Usky T.P., Mazhari R. and McCulloch A.D. (2000) Effect of laminar orthotropic myofiber architecture on regional stress and strain in the canine left ventricle. *J. Elast.* **61**: 143-64.
7. Vetter F.J. and McCulloch A.D. (2000) Three dimensional stress and strain in passive rabbit left ventricle: a model study. *Ann. Bio. Eng.* **28**: 781-92.
8. Nash M. and Hunter P. (2000) Computational mechanics of the heart. *J. Elast.* **61**: 113-41.
9. Stevens C., Remme E., LeGrice I.J. and Hunter P.J. (2003) Ventricular mechanics in diastole: material parameter sensitivity. *J. Physiol. Heart. Circ. Physiol.* **271**: H2689-700.
10. ter Kerus H.E.D.J., Rijnsburger W.H., Van Heuningen R. and Nagelsmit M.J. (1980) Tension development and sarcomere length in rat cardiac trabeculae: evidence for lenth-dependent activation. *Circ. Res.* **46**: 703-14.
11. Costa K.D., Holmes J.W. and McCulloch A.D. (2001) Modeling cardiac mechanical properties in three dimensions. *Phil. Trans. R. Soc.* London **A359**: 1233-50.
12. McQueen D.M. and Peskin C.S. (2000) A three-dimensional computer model of the human heart for studying cardiac fluid dynamics. *Comput. Graph.* **34**: 56-60.
13. Xu X.Y. and Collins M.W., eds. (1999) *Haemodynamics of Arterial Organs – Comparison of Computational Predictions with In Vitro and In Vivo Data.* Southamptom, UK: WIT.
14. Verdonck P. and Perktold K., eds. (2000) *Intra and Extracorporeal Cardiovascular Fluid Dynamics*, Vols. I, II. Southampton, UK: WIT
15. McQueen D.M and Peskin C.S. (2000) A Three-Dimensional Computer Model of the Human Heart for Studying Cardiac Fluid Dynamics. *ACM Siggraph*, Vol. 34 No 1.
16. Duell J., Montgomery W., Yau S. and Yelick K. (Dec 2001) Cochlea Simulation using Titanium Generic Immersed Boundary Software (TiGIBS). *Class Project.*
17. Zhukov L. and Barr A.H. (2003) Heart-muscle fiber reconstruction from diffusion tensor MRI. In *Proceedings of IEEE Visualization '03*, pages 597-602.
18. Liu H. and June P.S. (2003) Simultaneous Estimation of Left Ventricular Motion and Material Properties with Maximum a Posteriori Strategy. *IEEE Computer Vision and Pattern Recognition* **1**: 161-169.
19. Bathe K. and Wilson E. (1976) *Numerical Methods in Finite Element Analysis.* Prentice-Hall, New Jersey.
20. Roach P.J. (1998) *Verification and Validation in Computational Science and Engineering.* Albuquerque, NM: Hermosa.
21. Hsu E.W. and Henriquez C.S. (2001) Myocardial fiber orientation mapping using reduced encoding diffusion tensor imaging. *J Cardiovasc Magn Reson.* **3**(4): 339-47.
22. Software for Immersed Boundary & Interface

Simulation homepage: http://www.math.utah.edu/IBIS/man/node6.html

23. Peskin C.S. and McQueen D.M. (1989) A three-dimensional computational method for blood flow in the heart: (I) immersed elastic fibers in a viscous incompressible fluid. *J. Comput. Phys.* **81**: 372-405.
24. McQueen D.M. and Peskin C.S. (1989) A three-dimensional computational method for blood flow in the heart: (II) contractile fibers. *J. Comput. Phys.* **82**: 289-297.
25. McCracken M.F. and Peskin C.S. (1980) A vortex method for blood flow through heart valves. *J. Comput. Phys.* **35**: 183-205.
26. Hunter P.J. and Smaill B.H. (1989) The analysis of cardiac function: a continuum approach. *Prog. Biophys. Molec. Biol.* **52**: 101-64.
27. Glass L., Hunter P. and McCulloch A., eds. (1991) *Theory of Heart: Biomechanics, Biophysics, and Nonlinear Dynamics of Cardiac Function.* Springer Verlag, New York.
28. Guccione J.M. and McCulloch A.D. (1991) Finite element modelling of ventricular mechanics. See Ref. 27, pp. 121-44.
29. Omens J.H., Mackenna D.A. and McCulloch A.D. (1991) Measurement of strain and analysis of stress in resting rat left ventricular myocardium. *J. Biomech.* **26**: 665-76.
30. Emery J.L. and Omens J.H. (1997) Mechanical regulation pf myocardial growth during volume-overload hypertrophy in the rat. *Am. J. Physiol. Heart. Circ. Physiol.* **273**: H1198-204.
31. Emery J., Omens J. and McCulloch A. (1997) Biaxial mechanics of passively overstretched left ventricle. Am. *J. Physiol. Heart. Circ. Physiol.* **272**: H2299-305.
32. Denaro F.M. and Sarghini F. (2002) 2-D transmitral flows simulation by means of the immersed boundary method on unstructured grids. *Ini. J. Num. Methods Fluids* **38**(12): 1133-58.
33. Roma A.M., Peskin C.S. and Berger M.J. (1999) An adaptive version of the immersed boundary method. *J. Comput. Phys.* **153**: 509-34.

Remarks – Diamond [6] and several other authors including Miyata [7] have pointed out that *T. chattoni* might be separated from the genus *Trypanosoma* because of the absence of trypomastigote stage with undulating membrane in the blood of the veretebrate host. Two species of similar trypanosomes, viz. *T. celastinai* [7] and *T. tsunezomiyatai* [9] have also been reported from Brazil and Japan, respectively. The discovery of seven more species that share common morphology with these forms enables us to propose a new genus *Diamondtrypanum* for them. The genus is very common in *Rana* spp., *Amolops larutensis*, *Staurois natator*, and *Bufo* spp. in South-east Asian countries.

Diamondtrypanum chattoni (Mathis & Léger, 1911), new combination

(Figs. 3, 6, 9, 12-18)

Redescription – Longest diameter of body 32.3~63.0μm (41.94±7.34μm); shortest diameter of body 25.1~41.3μm (32.19±5.10μm); longest diameter of nucleus 6.6~9.9μm (8.07±0.81μm); shortest diameter of nucleus 5.6~8.6μm (7.0±0.72μm); flagellum 2.0~5.0μm (3.47±0.67μm); shortest distance of kinetoplast to nuclear membrane -3.6~-2.0μm (-2.60±0.42μm); in many individuals, body margin wrinkled and pleats present.

Host – *Bufo melanostictus* (Amphibia; Bufonidae).

Locality – Kuala Lumpur: Merdeka Stadium, Desa Pahlawan and Campus of University of Malaya; Selangor: near Salak Selatan; Penang: Botanical Garden.

Slides – Nos. 89-09-07-08, 89-09-07-06 and 89-10-17-28 from *B. melanostictus* captured at Desa Pahlawan are preserved for reference.

Remarks – Because the original description based on examples from *Bufo melanostictus* (type host) in Tonkin, Vietnam (type locality) is quite brief, the above redescription is given based on the Malaysian material. This species is characterized by the position of the kinetoplast which is always situated around the centre of the nucleus. According to the original description by Mathis and Léger (1911), the longest diameter of the body is 31-38μm and the diameter of the nucleus is 7.5μm which fall within the range for the present material.

Diamondtrypanum kodok new species

(Figs. 19-25)

Description – Longest diameter of body 34.3~62.6μm (41.76±7.28μm); shortest diameter of body 25.1~53.5μm (34.45±5.79μm); longest diameter of nucleus 5.3~9.6μm (7.37±1.03μm); shortest diameter of nucleus 5.0~8.6μm (6.45±082μm); flagellum 1.7~5.0μm (3.44±0.86μm); shortest distance of kinetoplast to nuclear membrane -4.0~0μm (-1.74±0.83μm).

Type Host – *Bufo asper* (Amphibia: Bufonidae).

Type locality – Gombak, Selangor, Peninsular Malaysia.

Type smears – Holotype smear: Slide No. 90-01-21-08 from Gombak Field Study Centre of University of Malaya, Selangor. Paratype smears: Slide No. 90-01-11-52 from Gombak area near Hindu Temple, Selangor; No. 89-09-19-03 from Ulu Langat, Selangor; No. 90-01-08-58 from Ampang Forest Park, Selangor.

Etymology – The species name is derived from the Malay word '*kodok*' meaning toad.

Remarks – *D. kodok* is distinguished from *D. chattoni* by the eccentric position of the kinetoplast and the appearance of the peripheral part of the body. In *D. kodok*, the position of the kinetoplast is always eccentric, and usually pleats are absent except in the rare case shown in Figure 25. The host toad, *B. asper* prefers quite different habitat from that of *B. melanostictus*, the host of *D. chattoni*, in Malaysia. The former is a forest living toad and usually seen near streams, while the latter is an open land species and seen near small ponds or lawns in parks or private gardens.

Diamondtrypanum bungateratai new species

(Figs. 10, 26-35)

Description – Longest diameter of body 28.7~84.5μm (41.29±9.07μm); shortest diameter of body 24.1~45.9μm (31.81±5.14μm); longest diameter of nucleus 4.3~7.9μm (5.96±0.90μm); shortest diameter of nucleus 3.6~7.3μm (4.96±0.74μm); flagellum 2.3~9.6μm (4.68±1.69μm); shortest distance of kinetoplast to nuclear membrane -3.0~0μm (-1.14±0.76μm).

Journal of Science and Technology in the Tropics (2005) **1**: 79-81

Crystal structure of bis(2,2'-bipyridine)copper(I) trihydrogen dodecamolybdophosphate trihydrate

Zhang Xian-Ming[a] and Ng Seik Weng[b]
[a]School of Chemistry and Materials Science, Shanxi Normal University, Linfen 041004, P. R. China
[b]Department of Chemistry, University of Malaya, 50603 Kuala Lumpur, Malaysia

Received 3 March 2005; accepted 12 April 2005

Abstract The hydrothermal reaction of $Mo^{VI}O_3$, $Cu^{II}O$, 2,2'-bipyridine and phosphoric acid yields crystalline $[(C_{10}H_8N_2)_2Cu^{I}]$ $[H_3O_{36}(PO_4)Mo^{V}Mo^{VI}_{11}]\cdot 3H_2O$ [*P*-1, a = 11.7046(5), b = 13.1276(6), c =17.3721(7) Å, α = 94.749(1),), β = 94.452(1), γ = 111.116(1)°]. The structure was refined to R = 0.030 for 8392 $I>2\sigma(I)$ reflections. The cation has the copper atom in a four-coordinate geometry that is intermediate between a square plane and a tetrahedron; the β-Keggin anion has a PO_4 unit encapsulated by the $H_3O_{36}Mo_{12}$ framework. Each oxygen atom of the PO_4 unit interacts with three molybdenum atoms; all molybdenum atoms exist in octahedral environments.

Keywords Decamolybdophosphate – Keggin – crystal structure

INTRODUCTION

A number of dodecamolybdophosphates, $\{Mo_{12}[\mu_{12}\text{-}O_4P][\mu_2\text{-}O]_{24}[O]_{12}\}^{n-}$ anions have been reported; among these are a few having hydrogen atoms within the Keggin core, e.g., two in the 18-crown-6 oxonium clathrate monohydrate [1], two in the hexamethylenediammonium acetaldehyde dimethylformamide trihydrate [2], three in pentakis(diethylammonium) monohydrate [3,4] and four in the diisopropylammonium dehydrate [5]. The cations are typically organic cations; in fact, a metal salt of a dodecamolybdophosphate has not been crystallographically authenticated although the copper complex of $\{Mo_6W_6[\mu_{12}\text{-}O_4P][\mu_2\text{-}OH]_{23}[O]_{12}\}^{2-}$ has been described [6]. The title compound constitutes a contribution to the studies dodecamolybdophosphates having a metal-bearing cation.

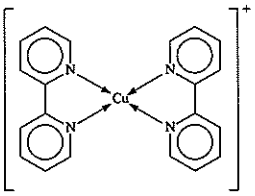

$[H_3PO_{40}Mo_{12}]\cdot 3H_2O$

EXPERIMENTAL

A mixture of molybdenum(VI) trioxide (0.214 g), copper(II) oxide (0.040 g), 2,2'-bipyridine (0.078), 85% phosphoric acid (0.115 g) and water (7 ml) in a molar ratio of 3:1:1:2:770 was sealed in a 15-ml Teflon-lined stainless bomb. The bomb was heated at 433K for 120 h. Dark, almost black, crystals were isolated from the cool mixture. The Mo(V):Mo(VI) ratio of 1:11 was determined from cerimetric titration of a DMSO–H_2O solution of the compound. Room-temperature diffraction measurements [7] were carried out on 0.32 x 0.31 x 0.15 mm prism with a Bruker APEX area-detector diffractometer (Mo-$K\lambda$ = 0.71073 Å) up to 2θ = 52°; 18410 reflections were collected of which 8392 were unique reflections that satisfied the $I > 2\sigma(I)$ criterion. The structure was refined on 730 parameters to R = 0.030 [8]. The structure is depicted as *ORTEP* [9] plots.

A dimensionless μ*2r value of 1.0 was used in the multi-scan absorption step. The carbon-bound hydrogen atoms were placed at calculated positions (C–H = 0.93 Å) and were included in the refinements in the riding model approximation; U(H) = 1.2U_{eq}(C).

The water H-atoms were placed in chemically sensible positions on the basis of hydrogen bonds but there were not refined; $U(H) = 1.2U_{eq}(O)$. The three belonging to the Keggin anion could not be placed in any chemically sensible positions. The final difference Fourier map had a large peak at about 1 Å from Mo4, but when the 2θ limit was lowered, the peak was of a smaller magnitude. The diffraction measurements were carried up to a 2θ limit of 56° but the reflections beyond 52° were not used in the refinements. The crystallographic-information-file has been deposited at the Cambridge Crystallographic Database Centre as CCDC 265280.

Crystal data $C_{20}H_{25}CuMo_{12}N4O_{43}P$, *fw* = 2255.23, triclinic, *P*-1, *a* = 11.7046(5), *b* = 13.1276(6), *c* = 17.3721(7) Å, α = 94.749(1),), β = 94.452(1), γ = 111.116(1)°; *V* = 2464.9(2) Å^3, r = 3.039 g cm^{-3}, *F*(000) = 2130, μ = 3.514 mm^{-1} for *Z* = 2.

RESULTS AND DISCUSSION

The hydrothermal reaction of molybdenum(IV) trioxide, copper(II) oxide, 2,2'-bipyridine and phosphoric acid under hydrothermal conditions yields $[(C_{10}H_8N_2)_2Cu^{I}]$ $[H_3O_{36}(PO_4)Mo^{V}Mo^{VI}_{11}]\cdot 3H_2O$. The dodecamolybdophosphate anion has one Mo(V) and eleven Mo(VI) atoms, the negative charge of the Keggin anion being implied along with the presence of three hydrogen atoms as the copper(II) ion in the reaction would have undergone reduction under the hydrothermal conditions to furnish the black colored compound. In the cation, the Cu(I) atom exists in a four-coordinate geometry that is intermediate between a square plane and a tetrahedron (Fig. 1); the geometry is disorted owing to the presence of two Cu···O contacts [3.006(3), 3.198(4) Å]. Bond lengths and angles compare well with those found in bis(6,6'-dimethyl-2,2'-bipyridine)copper(I) perchlorate [11], which has the bis-chelated metal atom in a similar four-coordinate environment.

The Keggin anion has its PO_4 unit encapsulated by the $H_3O_{36}Mo_{12}$ framework (Fig. 2), a feature that is common to such molybdophosphates, a noted from a cursory search through the Cambridge Structural Database (Version 5.26) [11]; all molybdenum atoms exist in octahedral environments. The sole molybdenum(V) atom cannot be differentiated from the other eleven molybdenum(VI) atoms from the crystal structure; this is common feature of heteropolyanions [12]; the compound is an example of a mixed valence system. Probably because both the cation and anion are sterically crowded, water molecules occupy the small spaces in the crystal structure; these serve to stabilize the crystal structure through hydrogen bonds.

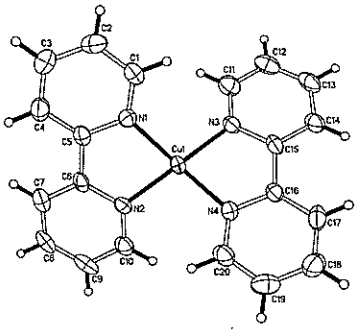

Figure 1. *ORTEP* plot of the $[(C_{10}H_8N_2)_2Cu]^+$ cation at the 50% probability level. Hydrogen atoms are drawn as spheres of arbitrary radii. Selected bond distances and angles: Cu1–N1 = 1.968(4), Cu1–N2 = 1.964(4), Cu1–N3 = 1.969(4), Cu1–N4 = 1.958(4) Å; N1–Cu1–N2 = 83.2(2), N1–Cu1–N3 = 103.6(2), N1–Cu1–N4 = 146.5(2), N2–Cu1–N3 = 155.4(2), N2–Cu1–N4 = 104.1(2), N3–Cu1–N4 = 83.4(2)°.

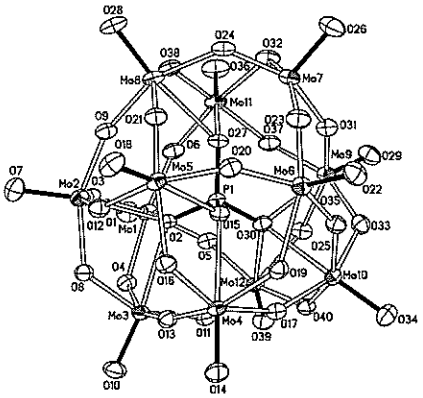

Figure 2. *ORTEP* (Johnson, 1976) plot of the $[H_3O_{36}(PO_4)Mo_{12}]^-$ anion at the 50% probability level. The H atoms are not shown they could not be placed in any chemically sensible positions. Selected bond distances and angles: P1–O2 = 1.537(3), P1–O15 = 1.537(3), P1–O27 = 1.535(3), P1–O30 = 1.533(3) Å; O2–P1–O15 = 110.1(2), O2–P1–O27 = 109.8(2), O2–P1–O30 = 108.8(2), O15–P1–O27 109.5(2), O15–P1–O30 = 109.0(2), O27–P1–O30 = 109.6(2), P1–O2–Mo1 = 125.0(1), P1–O2–Mo2 = 126.8(2), P1–O2–Mo3 = 126.2(2), P1–O15–Mo4 = 125.3(2), P1–O15–Mo5 = 127.56(2), P1–O15–Mo6 = 125.0(2), P1–O27–Mo7 = 126.3(2), P1–O27–Mo8 = 125.5(2), P1–O27–Mo11 = 125.5(2), P1–O30–Mo9 = 123.4(2), P1–O30–Mo10 = 125.3(2), P1–O30–Mo12 = 124.9(2)

Acknowledgements – We thank Shanxi Normal University and the University of Malaya for supporting this work.

REFERENCES

1. You W.-S., Wang E.-B., He Q.-L., Xu L., Xing Y. and Jia J.-P. (2000) Synthesis and crystal structure of a new supermolecular compound: $[C_{12}H_{24}O_6][H_3PMo_{12}O_{40}]\cdot 22H_2O$ ($C_{12}H_{24}O_6$ = 18- crown-6). *J. Mol. Struct.* **524**: 133-139.
2. Liu S.-Z., Li J.-P., Zhang Z.-W. Chen J.-Y., Xing Y., Jin, H.-Q. and Lin Y.-H. (2001) Photochemical synthesis and crystal structure of a charge transfer salt $[HMDH_2][H_2PMo^{V}Mo_{11}O_{40}]\cdot 2AA\cdot 3H_2O\cdot DMF$. *Chin. J. Struct. Chem.* **20**: 221-225.
3. Niu J.-Y., Wang J.-P., Yan B., Dang D.-B. and Zhou Z.-Y. (2000) Preparation, characterization and crystal structure of an intermolecular compound based on $H_3PMo_{12}O_{40}\cdot nH_2O$ and diethylamine. *J. Chem. Cryst.* **30**: 43-48.
4. Clemente D.A. and Marzotto A. (2003) The *P*-1 space group changes in *Journal of Crystallographic and Spectroscopic Research* and in *Journal of Chemical Crystallography*. *J. Chem. Cryst.* **33**: 933-945.
5. Ishikawa E. and Yamase T. (2000) Photoreduction processes of a-dodecamolybdophosphate in aqueous solutions: Electrical conductivity, ^{31}P NMR, and crystallographic studies. *Bull. Chem. Soc. Jpn.* **73**: 641-649.
6. Yang L., Naruke H. and Yamase T. (2003) A novel organic /inorganic hybrid nanoporous material incorporating Keggin-type polyoxometalates. *Inorg. Chem. Commun.* **6**: 1020-1024.
7. Bruker AXS Inc. (2002) *SADABS*, *SAINT* and *SMART*.
8. Sheldrick G.M. (1997) *SHELXS*-97 and *SHELXL*-97. University of Göttingen, Germany.
9. Johnson C.K. (1976) *ORTEP*-II. Report ORNL-5138. Oak Ridge National Laboratory, Oak Ridge, Tennessee, USA.
10. Cui G.H., Li J.-R., Gao D. and Ng S.W. (2005) Bis(6,6'-dimethyl-2,2'-bipyridine)copper(I) perchlorate. *Acta Cryst.* **E61**: m72-m73.
11. Allen F H (2002) The Cambridge Structural Database: A quarter of a million crystal structures and rising. *Acta Cryst.* B**58**: 380-388.
12. Baker L.C.W. and Glick D.C. (1998) Present general status of understanding of heteropoly electrolytes and a tracing of some major highlights in the history of their elucidation. Chem. Rev. **98**: 3-50.

Journal of Science and Technology in the Tropics (2005) **1**: 83 - 85

An extension of the numerical solution of the time-dependent Schrödinger equation

Bernardine R. Wong
Quantum Scattering Theory Group, Institute of Mathematical Sciences, University of Malaya, 50603 Kuala Lumpur, Malaysia. Email: bernardr@um.edu.my

Received 4 March 2005; accepted 24 March 2005

Abstract We extend a numerical method to solve the time-dependent Schrödinger equation in one dimension. The algorithm uses the Crank-Nicholson approximation for the time dependence together with a Numerov approximation for the spatial variation. Further, the algorithm employs discrete transparent boundary conditions, under the assumption that the exterior regions are force-free. We describe an extension to the method so that it remains applicable when the exterior regions are under a constant force.

Keywords TDSE – transparent boundary conditions – Numerov method – Crank-Nicholson

INTRODUCTION

The simulation of a wave-packet propagating, in one dimension, according to the time-dependent Schrodinger equation (TDSE) has been described by Goldberg *et.al* [1]. Here, the simulation was carried out using the Crank-Nicholson method [2] for the time-variable, which is accurate to second order in the time increment. The space-variable was generated by means of the usual centred-difference formula, which is accurate to third order in the spatial stepsize. The simulation is carried out within a spatial region, say $x_L \le x \le x_R$, bounded by rigid walls. These rigid-wall boundary conditions were alright for the simulation of bound states. However, the need to simulate the propagation of scattering wave-packets requires the use of discrete transparent boundary conditions [3]. This permits the propagation to proceed through the boundaries at x_L and x_R without any spurious reflections or transmissions. Recently, Moyer [4] has improved the method of generating the spatial profile of the wave-function by use of the Numerov approximation, which is accurate to fifth order in the spatial stepsize. This algorithm has been used, for example, to model electron transport across semiconductor superlattices [5]. However, the use of the discrete transparent boundary conditions still requires that the exterior regions be force-free, i.e. at constant potential energy. There are some applications for which the exterior regions are better modelled by a constant force, e.g. the potential energy profile of a resonant tunnelling diode [6]. In this case, it would be useful if one could relax the requirement for force-free exterior region.

In this paper we show, through a detailed derivation, how the transparent boundary condition algorithm can be extended to include the situation of a linear potential-energy term in the exterior regions. The computations arising from this derivation, for particular potential-energy functions, will be presented elsewhere.

EXTENSION OF A METHOD TO SOLVE THE TDSE

In one dimension, the propagation in space x and time t of a wave-packet $\Psi(x,t)$ for a particle of mass m satisfies the time-independent Schrödinger equation

$$-\frac{\hbar^2}{2m}\frac{\partial^2\Psi(x,t)}{\partial x^2}+[V(x)-fx]\Psi(x,t)=i\hbar\frac{\partial\Psi(x,t)}{\partial t} \qquad (1)$$

Journal of Science and Technology in the Tropics (2005) 1: 83-85

Here, $\hbar$ denotes the Planck constant divided by 2π. In the potential energy, the constant force term has been written explicitly; the parameter $f > 0$ $(f < 0)$ represents a constant force in the positive (negative) x-direction. The remaining potential term $V(x)$ may have any reasonable form but must be constant in the exterior regions. Following Bernardini [6], let us define the transformation variables ξ and τ such that

$$\xi = x - \frac{f}{2m}t^2 \qquad (2)$$
$$\tau = t$$

Using these variables, one may write the required solution as a product of two functions, viz.

$$\Psi(x,t) = \Phi(\xi,\tau)\,F(x,t) \qquad (3)$$

Here, the functions $\Phi(\xi, \tau)$ and $F(x,t)$ are defined to be solutions of the following time-dependent Schrödinger equations

$$-\frac{\hbar^2}{2m}\frac{\partial^2\Phi}{\partial\xi^2} + V(\xi,\tau)\Phi = i\hbar\frac{\partial\Phi}{\partial\tau} \qquad (4)$$

and

$$-\frac{\hbar^2}{2m}\frac{\partial^2 F}{\partial x^2} - fxF = i\hbar\frac{\partial F}{\partial t} \qquad (5)$$

We note that (5) is the TDSE for a purely linear potential energy, while (4) applies to an arbitrary short-ranged force. Substituting (3) into (1) and eliminating terms using (4) and (5), we obtain

$$\left(-\frac{\hbar^2}{m}\frac{\partial F}{\partial x} + \frac{i\hbar}{m}ftF\right)\frac{\partial\Phi}{\partial\xi} = 0 \qquad (6)$$

which yields

$$F(x,t) = \exp\left[\frac{i}{\hbar}ftx + g(t)\right] \qquad (7)$$

In order to further specify the arbitrary function $g(t)$, we substitute (7) into (5) and obtain

$$\frac{dg}{dt} = -\frac{i}{\hbar}\frac{f^2t^2}{2m} \qquad (8)$$

Hence, $F(x,t)$ becomes

$$F(x,t) = \exp\left[\frac{i}{\hbar}\left(fxt - \frac{f^2t^3}{6m}\right)\right] \qquad (9)$$

Here, the arbitrary (unobservable) initial term $g(0)$ has been set to zero for convenience. Finally, we obtain the wave-packet solution to (1) which may be written in terms of the variables x and t as

$$\Psi(x,t) = \Phi\left(x - \frac{ft^2}{2m}, t\right)\exp\left[\frac{i}{\hbar}\left(ftx - \frac{f^2t^3}{6m}\right)\right] \qquad (10)$$

Equation (10) becomes identical to equation (3.8) of Bernardini [7] for the case of a free particle, i.e. if in $V(\xi, \tau) = 0$ in (4). From (10) we see that the constant force term introduces the phase shift $F(x,t)$. In addition, the force-free (i.e. $f = 0$) wave-packet profile $\Phi(x,t)$ is translated by an amount $ft^2/(2m)$ in the x-direction. Hence, at any given time t, one may use the discrete transparent boundary condition method, as outlined by Moyer [4], to solve (4) numerically. Substitution of Φ into (10) then enables us to evaluate the wave-packet profile Ψ at that time t.

CONCLUSION

In this paper, we have extended a numerical method to solve the time-dependent Schrödinger equation in one dimension. This method, which employs discrete transparent boundary conditions under the assumption that the exterior regions are force-free, was extended to be applicable when the exterior regions are under a constant force term.

Acknowledgements – The support of the Ministry of Science, Technology and the Environment, Malaysia, via IRPA Grant No. 09-02-03-1011 is gratefully acknowledged.

REFERENCES

1. Goldberg A., Schey H.M. and Schwartz J.L. (1967) Computer-generated motion pictures of one- dimensional quantum-mechanical transmission and reflection phenomena. *Am. J. Phys.* **35**: 177-186.
2. Crank J. and Nicolson P. (1947) A practical method for numerical evaluation of solutions of partial differential equations of the heat-conduction type. *Proc. Cambridge Philos. Soc.* **43**: 50-67.
3. Ehrhardt M. (1999) Discrete transparent boundary conditions for general Schrödinger-type equations. *VLSI Design* **9**: 325-338.
4. Moyer, C.A. (2004) Numerov extension of transparent boundary conditions for the Schrödinger equation in one dimension. *Am. J. Phys.* **72**: 351-358.
5. Veenstra C.N., van Dijk W., Sprung D.W.L. and Martorell J. (2004) Time dependence of transmission in semiconductor superlattices. Preprint arXiv:cond-mat/0411118.
6. Ferry, D.K. (2001) *Quantum Mechanics: An introduction for device physicists and electrical engineers*. Institute of Physics Publishing (2nd ed.), Bristol.
7. Bernardini C., Gori F. and Santarsiero M. (1995) Converting states of a particle under uniform or elastic forces into free particle states. *Eur. J. Phys.* **16**: 58-62.

Journal of Science and Technology in the Tropics (2005) **1**: 87-91

Discriminant analysis involving dependence and censoring: Trace and minor elemental concentrations of normal and malignant breast tissues

S. H. Ong[1], B. W. Yap[2], K. H. Ng[3] and D. A. Bradley[4]

[1]Institute of Mathematical Sciences, University of Malaya, 50603 Kuala Lumpur, Malaysia
[2]Faculty of Information Technology & Quantitative Science, University of Technology MARA, 40450 Shah Alam, Malaysia
[3]Department of Radiology, University of Malaya Medical Centre, 50603 Kuala Lumpur, Malaysia
[4]School of Physics, University of Exeter, Exeter EX4 4QL, United Kingdom

Abstract In a recent study involving Instrumental Neutron Activation Analysis (INAA) concerning trace and minor elemental concentrations in normal and malignant breast tissues, because the determination capability of the particular irradiation-measurement arrangement it was found necessary to impute (complete) the data set in order to perform the discriminant analysis. In addition, since use was made of pairings of normal and malignant breast tissues from each of the 26 patients whose biopsies were included in the study, it was also apparent that the data were not independent. In the present work, involving Monte Carlo simulation, investigation has been made of data representing such features. A number of commonly used methods of completing data have been considered. Results from the study indicate that the method of pseudo-completion gives an error rate of classification close to actual values. The findings of the study have then been applied to analysis of the trace and minor element concentration data set.

Keywords imputation – classification – Monte Carlo simulation – pseudo-completion

INTRODUCTION

The particular issue with which this paper is concerned is discriminant analysis of elemental concentrations in paired samples of involved and healthy (normal histology) tissues, the latter being taken from the periphery of sites of tumour tissue. Ng *et al.*[1] have reported data from Instrumental Neutron Activation Analysis (INNA) of breast biopsy samples taken from twenty-six female patients. The data set involved censoring, with a number of readings being below the minimum determination limits (DL) for the particular irradiation-measurement arrangement. Ng *et al* [1] set these readings at DL before performing a discriminant analysis. An additional feature of this data set is dependence between the two groups of normal and involved tissues, use being made of pairings of normal and involved breast tissues from each of the 26 patients whose biopsies were included in the study

The intent of the present study has been to revisit the evaluations in [1], examining the effect of non-independence of data and the action of setting readings at DL. In particular the object is to consider the error rate of classification for two dependent populations, examining the effects of some common methods of data completion. The work is carried out via a Monte Carlo simulation allowing, in the light of present findings, an examination of the error rate of the discriminant analysis given in [1].

Since preliminary data analysis shows that the covariance matrices are unequal, quadratic discriminant analysis is considered in the simulation study. In the present investigations a multivariate normal (MVN) distribution is assumed for each population.

A brief literature review concerning handling of values below DL, involving discriminant analysis and statistical models for two dependent populations, is given in the next section. The simulation procedure, summary of simulation results, statistical analysis of the trace and minor element concentrations and concluding remarks are given in subsequent sections.

Type host – *Rana blythi* (Amphibia: Ranidae).
Type locality – Gombak Field Study Centre of University of Malaya, Selangor.
Type smears – Holotype slide: Am-450 collected in 1988 at Gombak Field Study Centre, University of Malaya, Selangor. Paratype slides: Am-428 collected in 1988 at Gombak Field Study Centre ; No. 89-10-18-28 from Gombak area near Hindu Temple; No. 89-11-08-11 and 89-11-08-18 from Ampang Forest Park, Selangor.
Etymology – The species name, *bungateratai*, is derived from the lotus flower in Malay.
Remarks – *D. bungateratai* somewhat resembles *D. chattoni* in the position of the kinetoplast and the general appearance of the pleats. However, in *D. bungateratai* the position of the kinetoplast is rather eccentric, and

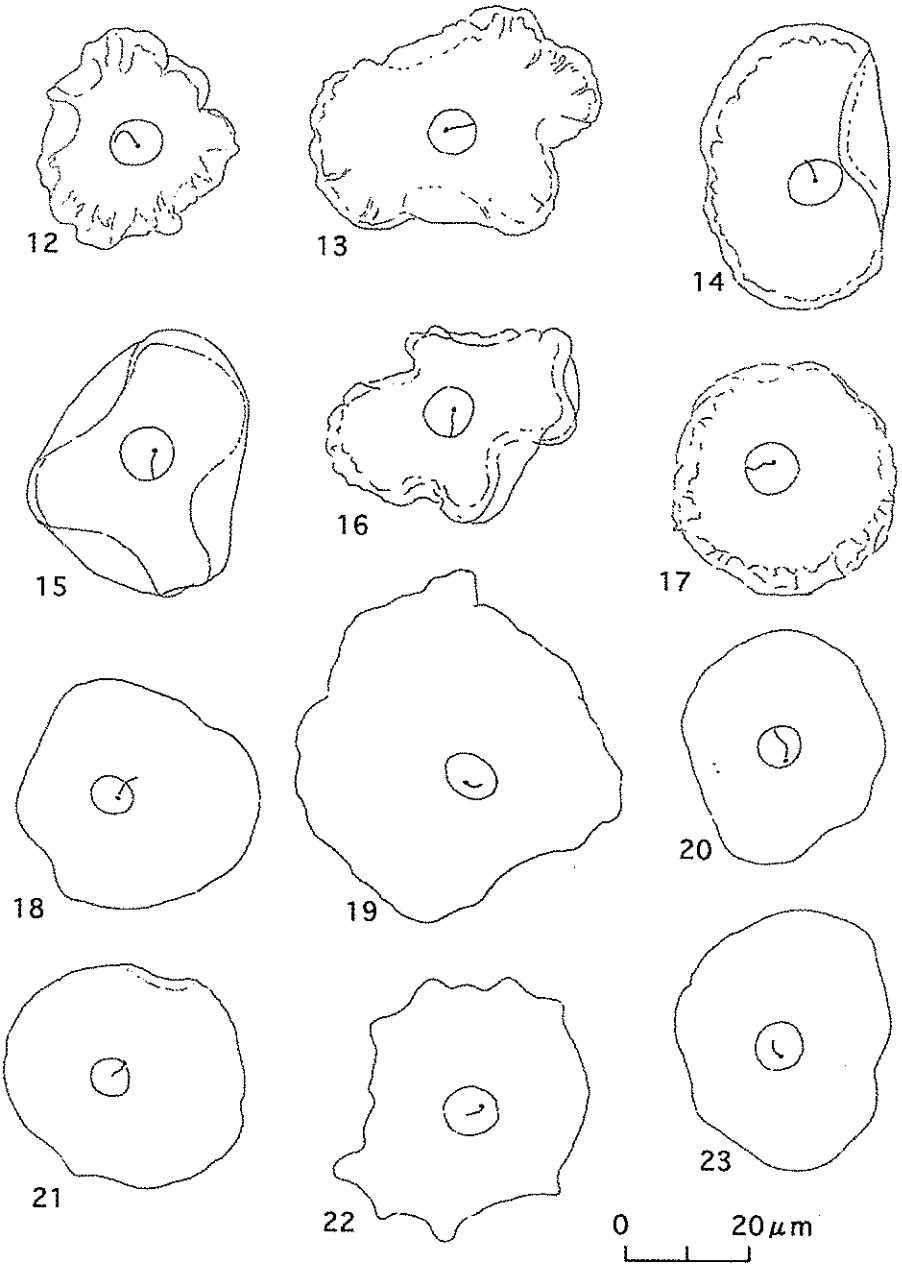

Figures 12-23. 12-18: *Diamondtrypanum chattoni* (Mathis & Léger, 1911), new combination, in *Bufo melanostictus*. **19-23**: *Diamondtrypanum kodok* new species, in *Bufo asper*.

Journal of Science and Technology in the Tropics (2005) 1: 87-91

BRIEF LITERATURE REVIEW

Handling observations below determination limits
For the one-sample case a number of methods have been established for dealing with values below DL. In [3] these have been classified into three broad areas as follows:

(a) Simple substitution; typically the censored value is substituted with 0, DL/2, or DL.
(b) Parametric methods, with maximum likelihood estimation being used to fill-in the missing values.
(c) Robust parametric methods. An example of such an approach is the probability-plot regression, where regression, based on the ranks of the observations, is used to extrapolate censored values.

In considering statistical analysis of censored environmental data, Akrtitas *et al.* [4] have included a comprehensive review of the methods outlined above (including the nonparametric Buckley-James regression). The one-sample and k-samples situations have been considered. While the simple substitution methods are popular it is to be noted, perhaps unsurprisingly, that these lead to biased estimates of summary statistics such as the mean and variance.

Discriminant analysis in two dependent populations
Discriminant analysis for two jointly distributed (dependent) MVN populations has been considered [5-8]. These authors gave asymptotic results for the error rates of classification. For two independent populations with missing observations, a number of simulations [9-11] that have been conducted, allow study of the effects on the error rates of classification. The present authors are not aware of any published reports concerning probabilities of misclassification which result from censoring of dependent populations. Indeed, for this latter situation, a mathematical derivation of the error rate, asymptotic or otherwise, appears to be extremely complicated (see [5-6]; [12-13]).

In the present study the probability of correct classification (PCC) is defined as

$$PCC = 0.5(p^{(1)} + p^{(2)})$$

where $p^{(i)}$ is the probability of correct classification for an observation from population i. The expected PCC, average of the PCC's , is used as a measure of performance of the classification in the Monte Carlo simulation.

THE STATISTICAL MODEL AND CLASSIFICAION STATISTIC FOR TWO DEPENDENT POPULATIONS

For a sample size of N, consideration is made of the joint distribution of two p-variate MVN populations $\pi_1$and π_2,

$$\begin{bmatrix} \underset{\sim}{x} \\ \underset{\sim}{y} \end{bmatrix} \sim N_{2p}(\theta, R) \qquad (1)$$

where

$$\theta = \begin{bmatrix} \theta_1 \\ \theta_2 \end{bmatrix} \quad R = \begin{bmatrix} \Sigma_1 & \varsigma \\ \varsigma' & \Sigma_2 \end{bmatrix} \qquad (2)$$

are the mean vector and covariance matrix respectively. Σ is the covariance matrix for each population and ζ is such that R is positive definite. Note that if ζ=0, then $\pi_1$and π_2 are independent. Due to invariance under canonical transformation, it can be assumed, without loss of generality, that θ_1=0 and θ_2=(Δ,0,....,0), where the Mahalanobis distance Δ^2 (see, for instance, [13]) represents the separation between the two populations, and R has diagonal elements 1.

It is to be noted that the form of the linear (quadratic) discriminant function is the same, regardless of whether the two populations are dependent or independent [7]. In consequence, statistical computer programs for discriminant analysis of independent populations can also be used for dependent populations. However, the probability of correct classification (or equivalently probability of misclassification) will depend on ζ (equation (2)), which reflects the dependence between two populations (see, for instance, [7] p. 235).

MONTE CARLO SIMULATION PROCEDURE AND RESULTS

In simulation studies that consider various values of the parameters p, N and Δ, it is usual for a simple factorial design to be employed. In order to make the simulation experiment computationally tractable, the number of parameters to be considered is reduced by using the covariance matrix derived from the trace and minor element concentration data. This also has the advantage that a realistic covariance matrix may be

used. In the present study the number of variables (the dimensionality) has been chosen to be six (for further justification of this see the section 'Statistical Analysis and Results' below). For each variable, values at or below the specified DL are deleted to form the incomplete sample. Actual DL's from the trace and minor element concentrations study [1] have been chosen for this purpose.

MVN samples are generated by means of the subroutine MVNORM [14] in accord with relation (1), with the covariance matrix R given by relation (2) such that R is positive definite. The following popular methods of dealing with observations below DL are considered:

1. Replacing censored values with zero (RZERO)
2. Replacing censored values with DL (RDL)
3. Replacing censored values with lognormal probability regression (EXTP)
4. Pseudo-completion ([15]; [16]) (PSEUDO).

where each of the methods is applied to each marginal variable in order to 'complete' the data. Note that such a step is equivalent to regarding the marginal variables as independent. The missing observations examined here are missing at random (MAR) as defined by [17]. At a later date it is intended that other multivariate methods will be examined.

SUMMARY OF SIMULATION RESULTS

Results of the simulation study, summarized in Table 1 and Figure 1, support an intuitive expectation of the PCC's:

1. increasing dramatically as separation between populations (D) increases,
2. increasing as the sample size N increases.

All four methods, PSEUDO, EXTP, RDL and RZERO, underestimate the actual PCC. Of these methods, PSEUDO consistently provides values of PCC's closest to actual values, while RZERO grossly underestimate the PCC's. When the distance Δ^2 between the populations is large, as exemplified by $\Delta = 4$, there is not much difference between the three methods PSEUDO, EXTP and RDL. Obviously, a simple method like RDL will be adequate.

In the next section, results of the simulation study are used in revisiting the reported discriminant analysis of trace and minor element concentrations in normal and involved breast tissues in [1] and [2].

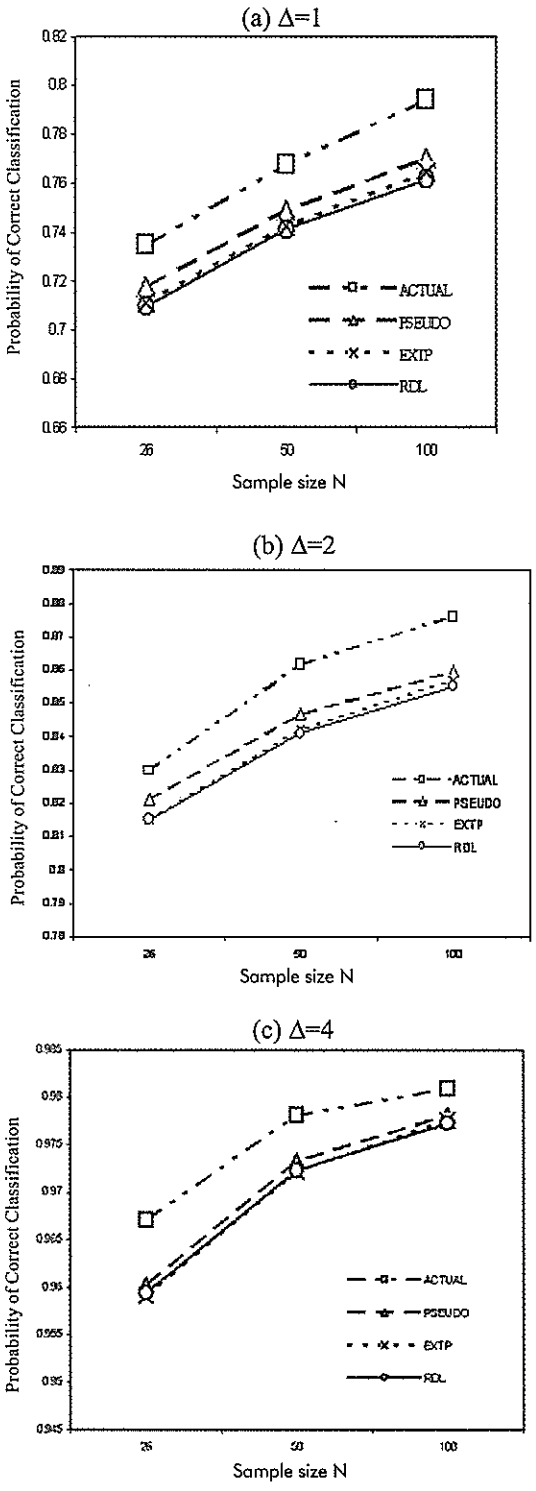

Figure 1. Plot of the Probability of Correct Classification (PCC) as a function of sample size, N, for (a) $\Delta=1$ (where Δ^2 represents the separation between the two populations), (b) $\Delta = 2$, and (c) $\Delta = 4$.

Journal of Science and Technology in the Tropics (2005) 1: 87-91

Table 1. PCC and standard error (in brackets) using QDF ACTUAL= PCC for original data (before censoring).

	ACTUAL	PSEUDO	EXTP	RDL	RZERO
N\Δ = 1					
26	0.7346	0.7175	0.7113	0.7096	0.5911
	(0.0744)	(0.0787)	(0.0823)	(0.0836)	(0.0786)
50	0.7675	0.7484	0.7424	0.7413	0.6045
	(0.0460)	(0.0429)	(0.0452)	(0.0435)	(0.0489)
100	0.7941	0.7701	0.7645	0.7616	0.6110
	(0.0301)	(0.0278)	(0.0286)	(0.0284)	(0.0389)
N\Δ = 2					
26	0.8298	0.8211	0.8150	0.8152	0.6875
	(0.0612)	(0.0634)	(0.0642)	(0.0634)	(0.0808)
50	0.8617	0.8467	0.8421	0.8412	0.7080
	(0.0385)	(0.0407)	(0.0451)	(0.0410)	(0.0583)
100	0.8762	0.8596	0.8569	0.8551	0.7190
	(0.0225)	(0.0257)	(0.0260)	(0.0260)	(0.0393)
N\Δ = 4					
26	0.9671	0.9603	0.9590	0.9594	0.8755
	(0.0267)	(0.0278)	(0.0288)	(0.0283)	(0.0443)
50	0.9781	0.9733	0.9722	0.9723	0.9156
	(0.0143)	(0.0174)	(0.0172)	(0.0174)	(0.0259)
100	0.89809	0.9781	0.9776	0.9773	0.9356
	(0.0094)	(0.0093)	(0.0999)	(0.0103)	(0.0147)

STATISTICAL ANALYSIS AND RESULTS

Ng *et al.* [2] have provided details of their INAA method, resulting data and their interpretation of these data in respect of the biological role of trace and minor elements in breast cancer. Six of the trace and minor elements reported in that citation have been chosen for the purposes of present analysis, these being considered to be of particular interest in application to discrimination of involved and histologically normal breast tissues. The particular elements are Ca, Rb, Br, Zn, Mn, and Fe. Based upon simulation results and, for the purposes of comparison with the results of the RDL method [1], the method of pseudo-completion has been chosen for completion of values below DL. The completed data set has been tested for multivariate normality and found to be approximately normal. A quadratic discriminant analysis with SAS DISCRIM gives the output. Results are summarized in Table 2. An inspection of the generalized squared distances shows that both groups (viz. trace and minor element concentrations in normal and involved tissues) are well separated; in particular a value of 3.78 ($\Delta \approx 2$) is found. Based upon present simulation results, a high probability of correct classification (or low error rate) is predicted, with very little difference in performance of the classification for any of the three methods of completion, EXTP, RDL or PSEUDO. Table 3 summarizes the cross-validation error rates for the two particular methods RDL and PSEUDO, showing no discernible difference between results obtained using these methods.

DISCUSSION AND CONCLUDING REMARKS

Estimating the censored values by setting at DL has been found effective in discriminating between the two groups considered here since they are well separated. As an aside, it should be noted that the imputation program, NORM, of [18] (Chapter 5) does not work for the data set examined here since the censoring mechanism being considered is different.

Table 2. Summary of results from SAS DISCRIM for quadratic discrimination.

Cross-validation Summary using Quadratic Discriminant Function Number of Observations and Percent Classified into GROUP:

From GROUP	1	2	Total
1	18	8	26
	69.23	30.77	100.00
2	5	21	26
	19.23	80.77	100.00
Total	23	29	52
Percent	44.23	55.77	100.00
Priors	0.5000	0.5000	

Error Count Estimates for GROUP:

	1	2	Total
Rate	0.3077	0.1923	0.2500
Priors	0.5000	0.5000	

Table 3. Comparison of error rate for RDL and PSEUDO.

Method	Cross-validation error rates (QDF)
RDL	0.2500
PSEUDO	0.2500

The Monte Carlo simulation results for the case of quadratic discrimination with two multivariate normal populations has been found useful in allowing selection of a particular method of completing data for a given set of parameters. In general for all separations of the populations, the PSEUDO completion method is preferred. However, if the populations are well separated, the simpler method of replacing censored values with DL (RDL) would suffice. It is apparent that the method of setting censored values at zero (RZERO) is not a good choice in all cases.

REFERENCES

1. Ng K.H., Ong S.H., Bradley D. and Looi L.M. (1997) Discriminant analysis of normal and malignant breast tissue based upon INAA investigation of elemental concentration. *Applied Radiation and Isotopes* **48**: 105-109.
2. Ng K.H., Bradley D.A. and Looi L.M. (1997) Elevated trace element concentration in malignant breast tissue. *British Journal of Radiology* **70**: 375-382.
3. Helsel D. (1990) Less than obvious: Statistical treatment of data below the detection limit, *Environmental Science and Technology* **24**:1767-1774.
4. Akritas M.G., Ruscitti T.F. and Patil G.P. (1994) Statistical Analysis of Censored Environmental Data. *Handbook of Statistics*. Vol. 12.
5. Bandyopadhyay S. (1979) Two population classification in Gaussian process. *Journal of Statistical Planning & Inference* **3**: 225-233.
6. Bandyopadhyay S. (1982) Covariate classification using dependent samples. *Australian Journal of Statistics* **24**(3): 309-317.
7. Leung C.Y. and Srivastava M.S. (1983) Covariate classification for two correlated populations. *Communication in Statistics – Theory and Methods* **12**: 223-241.
8. Bandyopadhyay S. and Bandyopadhyay S. (2000) Exact density of W classification statistic based on unmatched training sample from correlated populations. Technical report No. ASD/2000/25, Indian Statistical Institute.
9. Chan L.S. and Dunn O.J. (1972) The Treatment of Missing Values in Discriminant Analysis I-The Sampling Experiment. *Journal American Statistical Association* **67:** 473-477.
10. Chan L.S. and Dunn O.J. (1974) A Note on the Asymptotic Aspect of the Treatment of Missing Values in Discriminant Analysis. *Journal American Statistical Association* **69**: 672-673.
11. Bello A.L. (1993) A Simulation Study of Imputation Techniques in Linear, Quadratic and Kernel Discriminant Analysis. *Journal of Statistical Computation & Simulation* **48**: 167-180.
12. Das Gupta S. and Bandyopadhyay S. (1977) Asymptotic expansions of the distributions of some classification statistics and the probabilities of misclassification when the training samples are dependent. *Sankhya Series B.* **39**: 12-25.
13. McLachlan G.J. (1992) *Discriminant Analysis and Statistical Pattern Recognition.* New York: Wiley.
14. Dagpunar J. (1988) *Principles of Random Variate Generation.* Oxford: Clarendon Press.
15. Whitten B.J. and Cohen A.C. (1988) A Pseudo-Complete Sample Technique for Estimation from Censored Samples. *Communications in Statistics-Theory and Methods* **17**(7): 2239-2258.
16. Cohen A.C. (1991) *Truncated and Censored Samples: Theory and Applications.* New York: Marcel Dekker.
17. Rubin D.B. (1976) Inference and missing data. *Biometrika* **63**: 581-592.
18. Schafer J.L. (1997) *Analysis of Incomplete Multivariate Data.* London: Chapman and Hall.

JOURNAL OF SCIENCE AND TECHNOLOGY OF THE TROPICS

NOTICE TO CONTRIBUTORS

JOSTT is a multi-disciplinary journal. It publishes original research articles and reviews on all aspects of science and technology relating to the tropics. All manuscripts are reviewed by at least two referees, and the editorial decision is based on their evaluations.

Manuscripts are considered on the understanding that their contents have not been previously published, and they are not being considered for publication elsewhere. The authors are presumed to have obtained approval from the responsible authorities, and agreement from all parties involved, for the work to be published.

Submission of a manuscript to JOSTT carries with it the assignment of rights to publish the work. Upon publication, the Publisher (COSTAM) retains the copyright of the paper.

Manuscript preparation

Manuscripts must be in English, normally not exceeding 3500 words. Type double spaced, using *MS Word*, on one side only of A4 size with at least 2.5 cm margins all round. Number the pages consecutively and arrange the items in the following order: title page, abstract, key words, text, acknowledgements, references, tables, figure legends.

Title page

Include (i) title, (ii) names, affiliations and addresses of all authors, (iii) running title not exceeding five words, and (iv) email of corresponding author.

Abstract and key words

The abstract, not more than 250 words, should be concise and informative of the contents and conclusions of the work. A list of not more than five key words must immediately follow the abstract.

Text

Original research articles should be organized as follows: Introduction, Materials and Methods, Results, Discussion, Acknowledgements, References. The International System of Units (SI) should be used. Scientific names and mathematical parameters should be in italics.

References

References should be cited in the text as numbers enclosed with square [ ] brackets. The use of names in the text is discouraged. In the reference section, the following examples should be followed:

1 Yong H.S., Dhaliwal S.S. and Teh K.L. (1989) A female Norway rat, *Rattus norvegicus*, with XO sex chromosome constitution. *Naturwissenchaften* **76:** 387-388.

2 Beveridge W.I.B. (1961) *The Art of Scientific Investigation*. Mercury Book, London.

3 Berryman A.A. (1987) The theory and classification of outbreaks. *In* Barbosa P. and Schultz J.C. (eds.) *Insect outbreaks* pp. 3-30. Academic Press, San Diego.

Tables

Tables should be typed on separate sheets with short, informative captions, double spacing, numbered consecutively with Arabic numerals, and do not contain any vertical lines. A table should be set up to fit into the text area of at most the entire page of the Journal.

Illustrations

Black-and-white figures (line drawings, graphs and photographs) must be suitable for high-quality reproduction. They must be no bigger than the printed page, kept to a minimum, and numbered consecutively with Arabic numerals. Legends to figures must be typed on a separate sheet. Colour illustrations can only be included at the author's expense.

Proofs and reprints

Authors will receive proofs of their papers before publication. Ten reprints of each paper will be provided free of charge.

Submission

Manuscripts should be submitted in triplicate (including all figures but not original artwork), together with a floppy diskette version of the text, to:

The Managing Editor
JOSTT
C-3A-10, 4th Floor Block C
No. 1 Jalan SS20/27
47400 Petaling Jaya
Selangor Darul Ehsan
Malaysia